POLITECNICO DI MILANO

School of Industrial and Information Engineering
Master Degree in Materials Engineering and Nanotechnology

Carbon atomic wires-based nanocomposites:
Single step synthesis from polymeric solutions and in situ Raman characterization

Supervisor: Prof. Carlo S. Casari
Co-supervisor: Dr. Sonia Peggiani
Dr. Anna Facibeni

Master Thesis of:
Anna Sacchi
Matr. 919609

Academic Year 2019-2020

” Chi pianta tamarindi, non raccoglie tamarindi”

Proverbio indiano

Abstract

Carbon nanostructures are in the frontline for nanoengineered applications thanks to the wide range of properties achievable according to the different structure involved. Carbon atomic wires (CAWs) are the most promising in terms of properties but the most difficult to apply due to their instability. CAWs are linear structures of carbon atoms sp-hybridized that tend to aggregate and move to sp^2 hybridization. CAWs show two different structures: cumulenic with only double bonds and polyynic with alternation of single and triple bonds. This work deals with stability issue of polyynic structures and is focused into developing an effective method to obtain CAWs-polymer nanocomposites. A single step production process is implemented: laser ablation of a metal target in polymeric solutions produces linear carbon chains and metal NPs directly in a polymeric matrix. Metal NPs are exploited to obtain surface enhanced Raman spectroscopy (SERS) signal evolution of polyynes during ablation process in order to conduct an *in situ* SERS analysis. This is done to better understand CAWs formation mechanism and polymer role in the process. This is applied to ablations in polyvinyl alcohol (PVA)/organic solvent solutions; it results not efficient for CAWs SERS signal detection during ablations. Data are available only for post-ablation behaviour. A comparison is then made between the different systems to understand what are the parameters more affecting detection of CAWs SERS signal. In terms of nanocomposite films synthesis, single step process results to be effective; CAWs SERS signal is detected in films coming from different polymeric solutions. The *in situ* SERS analysis results to be successful when a new configuration is applied: NPs are anchored on a polymer pellet inserted in the ablation system, not participating to ablation; they are effective for detection of SERS signal with ongoing ablation. This new configuration is applied to ablation in PVA/water solutions to understand if polymer is playing an active role into CAWs production. Polymer is varying the dynamic of CAWs SERS signal evolution but whether is playing an active role is yet to be determined.

Sommario

Le nanostrutture di carbonio sono tra le più utilizzate in applicazioni ingegneristiche. Pur essendo costituite di solo carbonio, presentano una grande varietà di proprietà a seconda dell'ibridazione del carbonio. Le strutture lineari di carbonio (CAWs) sono le più promettenti dal punto di vista delle proprietà; la loro applicazione su larga scala è però ostacolata dalla loro instabilità. Si tratta di strutture lineari di carbonio sp-ibridizzato che, se mantenute isolate, tendono allo stato di ibridizzazione sp^2. CAWs presentano due strutture: cumulenica con soli legami doppi e poliinica con alternanza di legami singoli e tripli. Il lavoro qui presentato si occupa della stabilizzazione dei CAWs, tramite sviluppo di un metodo efficace per la realizzazione di nanocompositi a matrice polimerica in cui CAWs siano dispersi. E' stata sviluppata una sintesi tramite singolo step: un target di metallo ablato con laser in una soluzione polimerica permette di produrre CAWs e nanoparticelle (NP) di metallo direttamente in una matrice polimerica; le NP vengono sfruttate nella spettroscopia Raman amplificata da superfici (SERS), necessaria per la rilevazione dei CAWs. L'idea è quella di studiare la formazione dei CAWs tramite segnale SERS durante il processo di ablazione e condurre così un'analisi detta *in situ* SERS. Questo per studiare i meccanismi di formazione dei CAWs e il ruolo ricoperto dal polimero nel processo. Questa analisi è condotta per ablazioni in soluzioni di alcool polivinilico (PVA)/solvente organico; non risulta però efficace nella rilevazione del segnale SERS durante l'ablazione. Le informazioni ottenute riguardano solo gli eventi post-ablazione; i dati vengono analizzati per capire quali parametri influenzIno la comparsa del segnale SERS dei CAWs. Per la realizzazione dei film nanocompositi, il processo tramite singolo step risulta efficace: i film depositati dalle soluzioni ablate presentano il segnale SERS dei CAWs. L'analisi *in situ* SERS ha successo quando una nuova configurazione viene attuata: un pellet di polimero funzionalizzato con NP di argento è inserita nel sistema di ablazione. Le NP sono ora esterne al sistema liquido. Questo permette di ottenere il segnale SERS durante l'ablazione. Questo metodo è applicato per ablazioni in PVA/acqua per capire se il polimero svolga un ruolo attivo nella produzione di CAWs. Si è osservato che il polimero causa una variazione nella dinamica di evoluzione del segnale ma la sua effettiva pertecipazione al processo come sorgente di carbonio deve essere ancora determinata.

Index

List of Figures

List of Tables

Introduction

It was 1970 when Primo Levi wrote: I would love to tell you the story of a specific carbon atom, but nowadays, it is not possible for us to see or to isolate a single atom. Only 20 years later nanostructured world has been disclosed and since then has gained increasingly attention; in 2013 the first atomic movie as been recorded by IBM. The possibility of exploiting peculiar phenomena offered by nano-scaled materials, involving the least amount of matter matches with the desire of developing a sustainable and affordable science. Carbon-based nanostructures are one of the main characters into nanomaterials scenario and researches in this field are dotted with Nobel prize assignments. This is due to the novelty of the topics and to the appeal of the field. Carbon nanostructures are indeed versatile and can show a wide variety of properties according to the different hybridization of their constituents atoms. Their study has begun in the 80s when discovery of carbon nanotubes happened during analysis of interstellar medium. Since then new structures such as fullerenes and graphene have been discovered, studied and exploited in a huge amount of fields. Being carbon sp^2 and sp^3 hybridized structures high-performing, efforts have been put into discovery of the missing sp linear configuration. This was encouraged also by outstanding mechanical and physical properties that have been modeled on ideal linear structure. Even if the natural carbon linear compound is not found yet, linear carbon chains have been synthesized artificially following several different routes. Carbon atomic wires (CAWs) occur in theory in two different structures distinguished by the bonding between carbon atoms. A cumulenic structure, characterized by only double bonds and a polyynic conformations constituted by alternation of single and triple bond. This latter results to be the most stable and the one more easily synthesized in laboratory and based on this is the most studied and the main character in this experimental work. CAWs present wide variety of properties according to bonding structure, length of chains and end groups properties. This feature makes these structures even more appealing given the possibility of tailoring properties according to the desired application. However CAWs show a main issue that has prevented till now their deeper characterization and application on industrial scale. These structures are highly unstable being non energetically favoured and indeed produce in non-equilibrium conditions. When isolated sp linear chains tend to degrade and sp-to-sp^2 transformation happens via crosslinking mechanisms. One big part of research on linear carbon chains is indeed focused on stabilization mechanisms. Some works have been successful in this optic when CAWs are combined with other materials such as metal nanoparticles, dispersed in liquids or embedded in solid matrices of various kind. This experimental work takes place in the branch of polyynes stabilization by development of nanocomposite materials. For this specific study polymeric matrix is involved due to high performance of polymer as supporting matrix for nanostructured material and for

the versatility of the polymer itself. Moreover, having polyynes stabilized in a solid state film, it may allows further studies of mechanical and transport properties of CAWs. Till now lot of models have been developed and theoretical values are given but there is still lack of experimental measurements. The aim of this work is to obtain a nanocomposite film constituted by carbon linear nanostructures embedded in a polymer matrix. Realization of the nanocomposite material is not the only purpose. Optimization of the production process will be attempted by developing a single step technique in which ablation of a target in a polymeric solution will allow to have the final product by a single ablation in a liquid medium where all the materials are already present both for production and detection of linear carbon structures. Polyynes production process here involved is pulsed laser ablation in liquid (PLAL): ablation is performed on a metal target to obtain metal nanoparticles useful to perform surface enhanced Raman spectroscopy (SERS) measurement to detect polyynes produced in solution. Liquid medium for ablation process will be a polymeric solution of polyvinyl alcohol (PVA) dispersed into organic solvent. These two elements will work as carbon sources for polyynes production and as mother solution to have polymeric film deposition with dispersed polyynes. Development of this single process will be accompanied by implementation of a *in situ* SERS analysis in order to visualize polyynes signal while they are produced. This thesis work is organized as follows:

Chapter 1: overview on carbon nanostructures and introduction to CAWs; their properties together with characterization and production methods are described.

Chapter 2: overview on polymer-nanocomposite materials and state of art of CAWs-polymer nanocomposites.

Chapter 3: materials and methods used to synthesize nanocomposite films and develop *in situ* SERS analysis are shown.

Chapter 4: experimental results are reported and discussed, organized in three main parts: optimization of laser parameters, ablations in PVA/organic solvents and *in situ* SERS study.

Chapter 1

Carbon Atomic Wires

Carbon is romantically defined the element of life. It is indeed present in the majority of organic structures, bound to other elements. Carbon versatility is due to its peculiar electron configuration. Carbon has 6 electrons arranged as follows: $1s^2 2s^2 2p^2$. According to valence electron theory, carbon is expected to form 2 bonds. Experimental evidences have shown that C is prone to form 4 bonds. This is justified by hybridization theory according to which energy difference between 2s-state and 2p-state is really low and easily overtaken when C is affected by a perturbation such as proximity of an other atom. This effect brings to linear combinations of the atomic orbitals s and p known as hybridization. According to the combination between the atomic orbitals, three main hybridization states are obtained: sp^3, sp^2 and sp. Depending on the different hybridization, a different geometry is conferred to the molecules involved. This has been seen in organic molecules where different spatial configurations are assumed by alkanes, alkenes and alkynes compounds. Theirs constituents carbon atoms show sp^3, sp^2 and sp hybridization, respectively. The molecules adopt as consequence a 3D tetrahedral, 2D planar and 1D linear structure. The same is observed in pure carbon compounds. Graphite and diamond are well-known carbon allotropic forms that show opposite mechanical and physical properties due to the different hybridization of their C atoms; presence of such diversity between structures made of the same element, catches attention of researcher since centuries. The matter becomes even more interesting when studies are brought to nanoscale level. Carbon-nanostructures, schematically plotted in fig. 1.1 according to the different hybridization, show a wide variety of geometries as well as properties. sp^3 hybridization is the one shown by diamond; it confers tetrahedral geometry and strong bonds between atoms obtaining the peculiar hardness of diamond. Nanodiamonds are enumerated among carbon-nanostructures and well studied and described [13, 22]. Graphite planar structure is conferred by sp^2 hybridization which implies presence of strong in-plane σ bonds and weak van der Waals interplanar bonding, making graphite one of the softest 2D material even used as solid lubricant in mechanical applications [83]. The related nanostructure is graphene. It consists into a single layer of graphite and it represents a one-atom thickness sheet. Besides these structures, many others are present with intermediate levels of hybridization. The most studied ones are carbon nanotubes (CNTs), fullerens and carbon fibers.

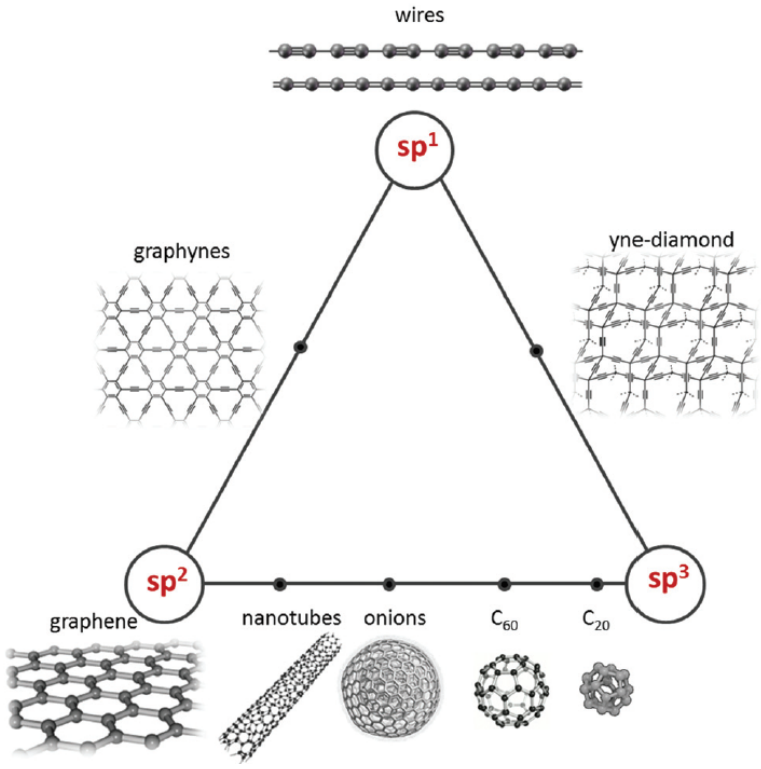

Figure 1.1: *Carbon nanostructures formed according to the different hybridization adopted [8].*

1.1 Overview on carbon nanostructures

A common way to introduce carbon-nanostructures geometries and properties is starting from graphene. Graphene is indeed call "the mother of all graphitic forms of carbon" [20]. This comes from the fact that all the carbon nanostructures can be modeled starting from a graphene sheet as depicted in fig. 1.2. Graphene is known as "the strongest material ever measured" to report the words of Lee at al. [43] that were studying mechanical properties of graphene. Reported value for tensile strength is of 130 GPa while for Young Modulus is 1.0 $\pm$ 0.1 TPa [67]. This is ascribed to the stability and strength of σ bonds characterizing in-plane hexagonal structure of graphene. From the point of view also of transport properties this material shows outstanding properties thanks to its peculiar electronic configuration, Castro et al. have performed a deep analysis of graphene electronic properties [9], that results to be a zero-gap semiconductor. When the material sheet is defect-free, high values of electrical and thermal conductivity are reported allowing application of these structures for electronic devices and wherever thermal management issues are present. Electrical conductivity values are assessed around 10^8 S/m while thermal conductivity ranges from 3000 to 5000 W/mK, according to the measurement technique involved [14]. Huge efforts are put in developing then effective synthesis technique to obtain defect-free graphene layers. Both bottom-up and top-down techniques are applied. The former method involves carbon sources modification by chemical vapour deposition or epitaxial growth that leads to graphene sheet formation from a chemical generated carbonaceous vapour or by thermal decomposition of a carbon substrate; top-down technique are based on deconstruction of precursors such as mechanical exfoliation of graphite or unzipping of CNTs etc. [45].

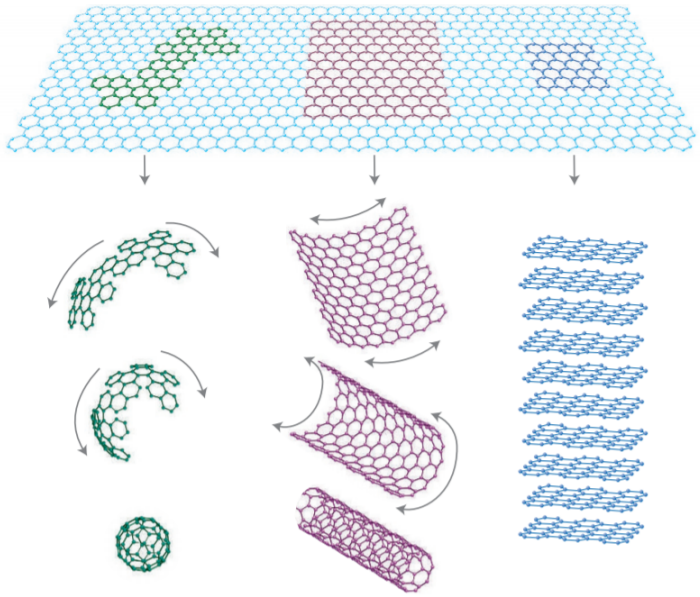

Figure 1.2: *Carbon nanostructures obtained from a graphene sheet [20].*

CNTs are one of the other interesting carbon-nanostructures. Their official discovery is attributed to Iijima in 1991 that defines them as "helical microtubules of graphitic carbon" [27]. He synthesizes CNTs by arc evaporation process and basically pulls the trigger to years of analysis, characterization and application studies for these new structures. Their appealing nature is due to the possibility of tuning properties by changing their geometry. CNTs are classified as multi-walled (MWCNTs) or single-wall (SWCNTs) according to the number of graphene rolled-up. In order to describe CNTs properties, geometry elements are defined. Chirality is the first element evaluated: when an object is chiral, is not superposable with its mirror image. For CNTs chirality or achirality determines metallic or semiconductor behaviour [26]. Properties of CNTs are described by geometrical parameters:

Chiral vector $\mathbf{C}_H$ defined as the vector connecting two primitive lattice points of graphene that, once folded, will be coincident. It is defined usually as

$$C_H = n\mathbf{a_1} + m\mathbf{a_2} = (n, m)$$

Translation vector T is the smallest graphene lattice vector perpendicular to C_H.

Chiral angle θ identified as the angle between C_H and the primitive vector $\mathbf{a}_1$.

$\mathbf{C}_H$ allows to identify univocally a CNT that is reffered to as (n,m) CNT. According to the values of n and m coefficients, chirality and hence physical properties of CNTs are defined. (n,n) CNTs are armchair; (n,0) or (0,m) CNTs are zig-zag. The names armchair and zig-zag represent the profile followed by carbon atom on the circumference of the CNTs. Both these structures are achiral; moreover (n,0)CNTs show metallic behaviour when n is multiple of 3, otherwise semiconducting while (n,n)CNTs are metallic. Generic (n,m) CNTs are chiral and metallic when

(2n+m)/3 is an integer [64]. In fig. 1.3 geometrical parameters just described are drawn on a graphene sheet.

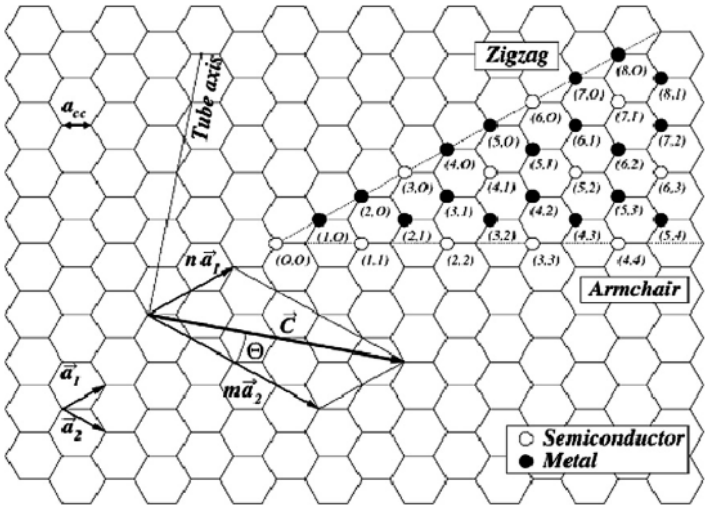

Figure 1.3: *CNTs geometry parameters useful to characterize physical properties [15]*

For CNTs as well, lot of synthesis methods have been developed. Arc-discharge, laser ablation and chemical vapour deposition are applied at industrial scale. By varying parameters of production processes and involving catalyst in the reactions, characteristic of CNTs are tuned [34]. In general these structures show good mechanical properties due to, as seen in graphene, strong σ bonds. Tensile strength values are in the range of 11-63 GPa and recorded Young's modulus ranges from 270 to 950 GPa [26]. It is also demonstrated by Gao et al. that mechanical properties of SWCNTs are directly proportional to the tube diameter [19], while they are not changing from chiral to achiral structures. The main issue with this tubular structure is given by the radial direction along which softer behaviour is registered; this behaviour is ascribed to Van der Waal's forces that tend to gather tube walls. Transport properties are affected by several parameters such as defects, chirality and geometrical parameters, e.g. thermal conductivity values vary from 6600 W/mK for individual SWCNTs to 0.1 MWCNTs [42]. This allows to have diametrically opposite properties by tuning specific parameters and this opens wide possibilities of application [24].

Fullerenes are also noteworthy among carbon-nanostructures for their peculiar structure. Discovered in 1985 by Kroto et al. [40] while studying carbon molecules in interstellar matter, they represent a class of closed-cage carbon molecules, C_n. Their structure contains at least 12 pentagon rings a variable number of hexagonal rings. The pedex n indicates the number of carbon atoms involved in the structure. Each carbon atom is sp^2 hybridized and bounded to other three carbon atoms. C_60 is the most stable among fullerenes structures and it is composed by 20 hexagons and 12 pentagons [86]. High surface area shown by these structures confers high reactivity and possibility of functionalization and combination with other materials. Transport properties, for instance, can be totally varied from insulating to conducting or even superconducting conditions when fullerenes are combined with alkali metals. Ways of synthesis of fullerenes foresee laser ablation of carbon material such as graphite,

arc discharge between graphite electrodes or pyrolisis of aromatic hydrocarbons. Fullerenes are nowadays largely involved in energy conversion devices as n-type conductors [47].

1.2 Carbon atomic wires

Carbon nanostructures just described are characterized by sp^3 or sp^2 hybridization or even an intermediate configuration, as shown in fig. 1.1. However carbon atoms can be arranged also in sp-hybridization forming linear structures. If this configuration is detected and well-known for organic molecules, existence in nature of a linear carbon compound has been subject of controversy and still not demonstrated. Evidences of linear carbon structure presence were detected while analyzing matter on a meteor crater [21]. Researchers tried then to replicate conditions and reactions happening in a star environment to synthesize the linear structure. However researches on linear structures were damped by discoveries of nanotubes and fullerenes [27, 40]; Kroto et al. were actually trying to synthesize linear carbon structures by laser vaporization when they proved the existence of fullerenes structures. Anyway, stimulated also by the incredible mechanical and physical properties calculated considering an ideal infinite carbon chain [46], researches on sp linear structures have been developed in the last decades.

1.2.1 Structural, physical and vibrational properties

Carbyne model, as it is called the suggested carbon linear compound, is a infinite carbon chain sp-hybridized. Constituents carbon atoms can be arranged following two structures namely: cumulene, where only double bonds exist between C atoms and polyynes in which alternation of single and triple bonds are present. The two structures are reported in fig. 1.4a and 1.4b. A fundamental parameter to characterize the two structures is the Bond Alternation Length (BLA) [38, 87]. It represents the mean difference of length between two adjacent bonds in the chain. BLA is ideally equal to zero for cumulenic structure while different from zero for polyynic structure. The presence of cumulenic or polyynic structure affects the electronic configuration of the chain, hence the transport properties. It can be explained both with orbitals theory as well as solid-state approach. Starting with the orbitals, each C atom of the chain has free p atomic orbitals that, linearly combined, will form π orbitals. In cumulenic structure the presence of π orbitals along the whole chain will result in the so called conjugation effect, seen also on polymer chains, while in polyynic structure, due to presence of single bonds, conjugation effect is hindered and π orbitals are localized in specific chain points [5]. This results in a different behaviour of the two structures when dealing with transport properties. This is highlighted also by quantum physic approach. As can been seen in fig. 1.4a, cumulenic unit cell is constituted by one single atom; each atom is contributing with 2 electrons in the 2 π orbitals obtaining a half filled conduction band. Cumulene results indeed to have a metallic behaviour. Polyynic structure on the other hand, as depicted in fig. 1.4b presents two carbon atoms per unit cell. This means availability of 4 total electrons that filled completly the valence band. Polyynic structure results then as a semiconductive material. The difference in unit cell occupation has effect on vibrational properties as well. Cumulene has only acoustic phonons while

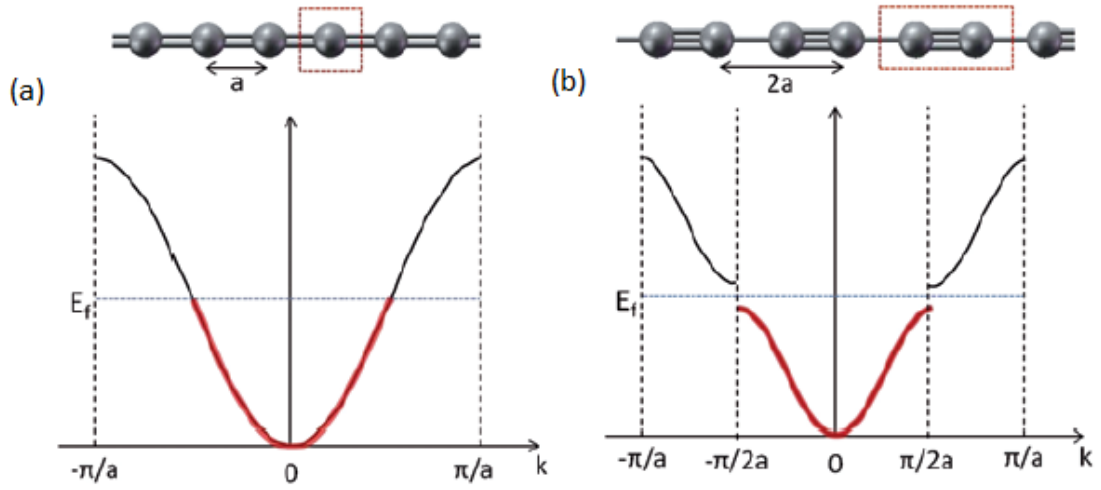

Figure 1.4: *Schematic electronic geometrical and band structures for (a) infinite cumulene and (b) polyyne explaining conductive and semiconductive behaviour [8].*

polyynic structure has acoustic as well as optical phonons.

The link between the two structures is given by Peierl's distortion theory [71], suitable when dealing with infinite chains model. It affirms that the dimerized structure, where alternation of bonds is present, is energetically favoured. Then cumulenic chains tend to rearrange assuming polyynic structure. This is valid for infinite chains while, when dealing to real structures, it has less influence. Indeed real structures show finite length and termination groups. These two elements have higher impact of real linear structures and affect BLA as well as electronic and optical properties [1]. It is then considered that Peierl's distortion effect rules for long chains, approaching the infinite model; a limit is given by S. Yang et al. for application of Peierl's theory to chains with n $>$ 52. While on finite chains, with n $<$ 52, end group effects are predominant. End group effects are also more influent on shorter chains [57].

The strong affection of end groups on chains behaviour is thus exploited to tailor specific properties of the chains by modification of their termination groups. Carbon chains are usually terminated with hydrogen (-H) groups and they are referred to as C_nH_2 wires with n is number of carbon atoms involved in the chain; other end groups such as methylic (-CH_3) or cyano (-N) can be found as well, according to synthesis process. Modification of end groups covers a huge part of research mainly on chemical ways of production since according to end groups, not only properties are varied, but stability of the structures can be reached. Stability is the main issue when dealing with carbon linear structures. Their configuration is indeed not favoured, it is formed in non equilibrium conditions, and they tend to degrade by crosslinking effects that bring them to switch to sp^2 hybridized structures, loosing their linearity. To overcome stability problem several ways are studied: by tailoring end group termination is possible to prevent crosslinking, this is achieved with bulky molecules that provide steric hindrance [12, 30, 29]. Moreover polyynes are more stable in liquid so, if kept in solutions they degrade less rapidly. Last approach that will be investigated deeply in the next chapter, is the possibility to embed these

structures into solid matrices.

1.3 Characterization methods

Several analysis techniques are applied to characterize CAWs. Some of them exploit light-matter interaction such as Raman and UV-Vis absorption technique. Others operate selection of CAWs based on material properties such as polarity, as in the case of high performance liquid chromatography (HPLC) or mass as in mass spectroscopy. For the purpose of this work, only Raman and UV-Vis absorption technique have been applied as characterization methods. Furthermore, as will be explained later, UV-Vis absorption technique is not used to investigate CAWs structures but metal nanoparticles.

1.3.1 Raman analysis

Raman vibrational analysis is certainly one of the most useful characterization technique and the one mostly exploited in this experimental work. According to the different arrangement and hybridization of atoms in a defined structure, vibrational states are changing; hence, a vibrational sensitive technique is a useful instrument to analyze these compounds.
Raman technique exploits inelastic scattering of light. A monochromatic laser beam with defined wavelength (λ) is used to investigate the sample. The photon absorption by the material will cause excitation of electrons to a higher vibrational state. Relaxation then happens resulting into a higher or lower vibrational state with respect to the initial one. These are accompanied by emission of a photon with higher or lower energy if compared to the incident one. These two mechanisms are known as Stokes and Anti-Stokes processes and leave the molecules in a lower or higher vibrational state. The energy difference, from initial and final state, is connected to a specific vibrational state, that differs from molecule to molecule and is used as fingerprint materials. The information acquired is then visualized as a spectrum where Raman shifts (cm^{-1}) vs. Raman intensities are plotted.

As depicted in fig. 1.5a, the different allotropic forms of carbon show peculiar Raman signals at different wavenumbers. This allows to distinguish them and detect their presence in samples. As it can be seen, signals of CAWs cover a region from 1800 to 2200 cm^{-1} where no other carbon structures have signals. Moreover, as shown in fig. 1.5b, spectrum of CAWs is changed by variation of end groups. Raman analysis appears then to be a valid technique to identify specific CAWs structures.

CAWs Raman signal has been accurately studied with both computational techniques, such as Density functional theory (DFT), and experimental observation. Raman signal of carbon linear structures is given by stretching of C≡C bonds, called ECC mode, coming from Effective Conjugation Coordinate model; this signal is constituted by two main bands called α and β mode; α contribution is located at higher Raman shift (2000-2200 cm^{-1}), shows higher intensities and it is attributed to shorter chain vibration [56]. This because π conjugation is lower and chain vibration are stronger. β mode, on the other hand, is located at lower wavelength (1800-2000cm^{-1}) and with lower intensities [54, 57]. It is given by longer chains contributions. Frequencies of the signal is determined also by BLA parameter. In

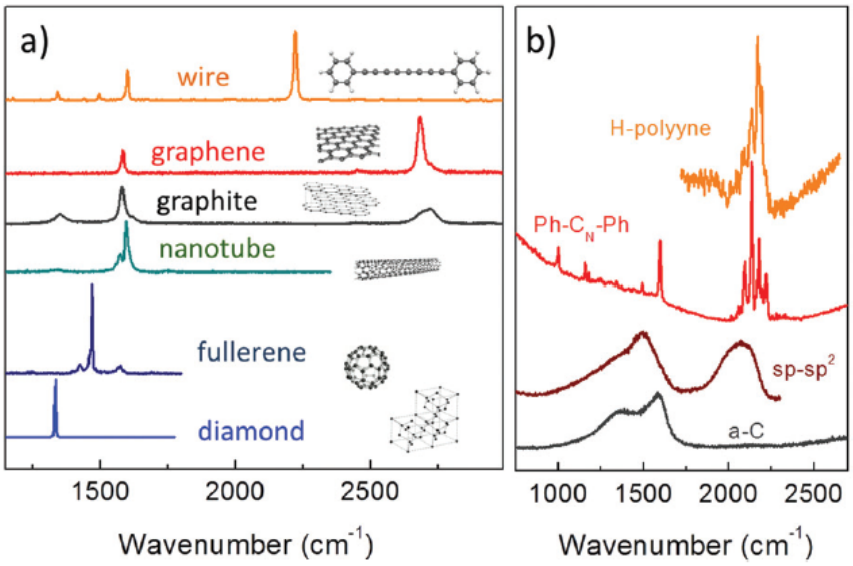

Figure 1.5: *(a) Raman signals for various carbon allotropes and (b) variation of CAWs Raman signal according to different end groups [57]*

theory cumulenes structure are not supposed to give Raman signal since their absence of optical phonons, but this is valid for infinite chain model. Actually they show Raman signal since, cumulene of finite length have not BLA = 0 due to chain length and end group effects [28].

The main drawback and limitation for this technique is the fact that, for low concentration of molecules, i.e. $< 10^{-3}$M, Raman signal is not detected. CAWs concentration, obtained with the physical generation process here involved, is around 10^{-6}M, too low to be detected with Raman technique. This problem is overtaken by exploitation of surface enhanced Raman spectroscopy (SERS) effect, described in the following section.

SERS

SERS effect is a signal amplification method obtained when metal nanoparticles are interacting with the analyzed molecules. It exploits excitations of the surface conduction electrons of metal nanoparticles known as surface plasmons. When laser wavelength matches surface plasmons absorption wavelength, local enhancement of electric field is obtained together with intensification of Raman signal up to 10^6 times. This effect is due to two different mechanisms: an electrical one and a chemical one. The former is given by the local enhancement of the electric field while the second comes from chemical reactions and interactions happening between metal nanoparticles and analyzed molecules. In order to have the best effect in terms of Raman signal amplification, a good match must be found between metal NPs absorption and Raman laser wavelength. In theory the closer they are, the better the amplification. In order to do so, UV-Vis absorption spectra of NPs are studied and Raman laser wavelength is tuned on the basis of that.

Furthermore it has been noted that SERS signal of CAWs shows different features, in terms of peaks shape and location, with respect to Raman signal. This is justified by a different vibrational states when carbon chains are interacting with

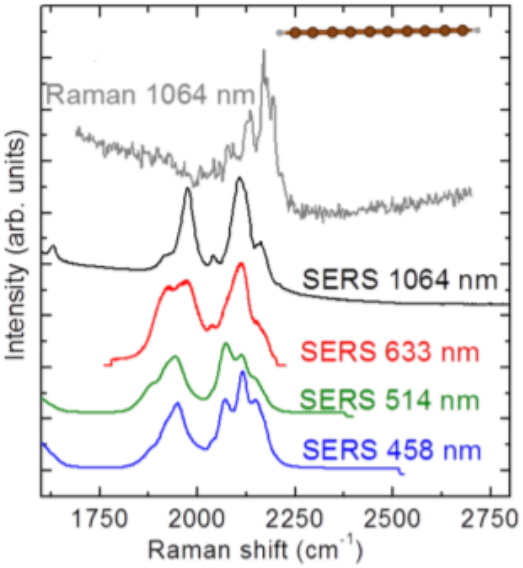

Figure 1.6: *SERS spectra acquired at different Raman λ of H-capped polyynes in solutions compared with Raman signal acquired with 1064 nm Raman wavelength [57]*

NPs; this has resulted in a peak red shift and appearance of a new band at lower wavelength assigned to CAWs-NPs interaction. Moreover, when metal NPs and CAWs are interacting, charge transfer happens between them affecting BLA values [58]. All these elements need to be considered when interpreting the information obtained with this characterization method. In fig. 1.6 SERS spectra are reported for H-capped polyynes in solution investigated by different Raman λ; variation of intensity among the various SERS spectra and red shift with respect to Raman spectrum is highlighted.

1.3.2 UV-Vis absorbance

UV-Vis absorbance technique exploits light-matter interaction to acquire information on investigated molecules. A light beam with energies from UV-visible to infrared wavelengths impinges on the sample. Light-matter interaction causes electron promotion to higher energy states. The energy difference between the ground and excited states represents a specific absorbed energy wavelength. Looking at the absorption profile is possible to identify specific molecules according to location of absorption peak. Anyways different molecules can have same absorption peak. The information on CAWs given by their UV-Vis spectra are: concentration and chain length.

The first information is deducible from absorbance values A (adimensional); on spectra are given by intensity of the peaks. By application of Lambert-Beer law it is possible to define the concentration of the species:

$$A = log_{10}(I_0/I) = \epsilon L c$$

where A is the absorbance, I_0 and I are the transmitted and incident light, ϵ is the molar extinction coefficient(cm^2 mol^{-1}), L the optical path (cm) and c the molar concentration (mol cm^{-3}) to be determined.

Chain length is deducted by observing absorption peak location. It is verified that for higher π conjugation effect, the energy gap between HOMO and LUMO

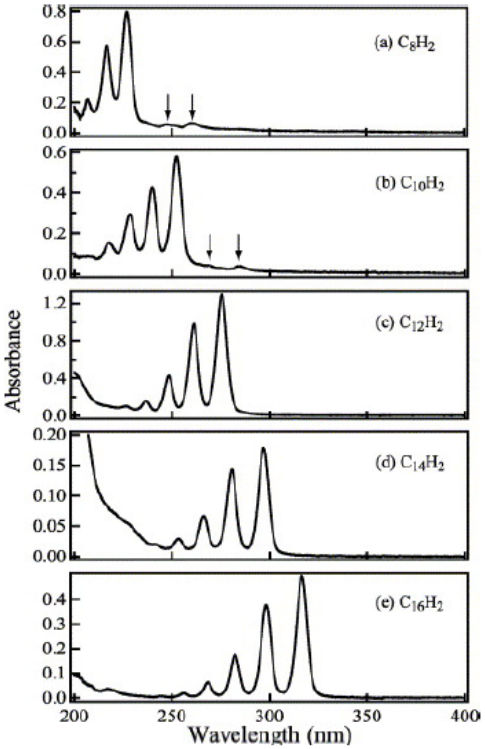

Figure 1.7: *UV-Vis absorption spectra of separated H-capped polyynes [77].*

levels decreases making electron promotion easier at lower energies. From Plank-Einstein relation, lower energies are given at longer wavelength. This means that longer chains, for which π conjugation effect is higher, will absorb at longer wavelength [55]. Each CAWs absorption profile is characterized by one main peak and two secondary peaks; CAWs absorption region is in the range of 200-350 nm. These features have been verified by performing UV-Vis absorption acquisitions on size selected CAWs. This is possible thanks to application of chromatographic technique such as HPLC; indeed, in fig. 1.7, absorption spectra for HPLC size selected polyynes are reported. Shape of the peak and relative shift positions when moving from short to long chains are visible.

1.4 Overview on production methods

Different methods have been successfully developed to obtain polyynic structures. The methods are classified as physical and chemical production and they deal with bottom-up approach. Top-down processes exist as well but they are not in frontline.

Chemical ways can follow two different approaches to obtain linear carbon chain. The first one involves a polymerization method that starting from polymer molecules or hydrocarbon compounds brings to synthesis of linear carbon chains [11, 41]. The second one exploits dimerization reaction of the ethynyl group from molecules with defined length and end groups [31]. Top-down technique, on the other end, starts from a graphene layer and by laser action act a selective removal of carbon atom till wires realization [32].

1.4.1 Physical way

There exist many physical processes that allow linear structure production. The techniques deals with generation of a carbon vapour, in different environments, that is then quenched in order to have a non equilibrium condition. In this way CAWs, that are not energetically favoured, can be formed. Among the physical ways of polyynes production the two most common are submerged arc discharge in liquid (SADL), developed by F. Cataldo [10] and pulsed laser ablation in liquid (PLAL) [70, 25, 52]. Arc discharge process allows to produce polyynes by applying an electric arc between two graphite electrodes. The electrodes are submerged in a dielectric solvent that can be water as well as an organic solvent. A DC electric arc is then produced and electrodes are kept almost in contact and in continuous movement in order to produce a very bright light. This generated a plasma in which radicals are present. After already 1 minute of arcing, a sample of solution is analyzed, and polyynes presence is detected by UV-Vis absorption technique. Arc discharge in gas was already knew as a valid technique to produce carbon nanostructures such as fullerenes. It is probable that also polyynes were produced, being also precursors for other nanostructures formations. Anyway their instability will lead to crosslinking reactions and they were not detected as independent and isolated structures. When the process is run in a liquid environment, the quenching effect given by the liquid allows to stabilization and detection of out of equilibrium linear structures.

PLAL

A deeper description is given for laser ablation production process, since it is the production technique applied in this thesis project. It allows to obtain isolated CAWs with polyynic structure in a liquid medium [77]. Even if the mechanism of CAWs formation is not yet fully described and understood, Amendola et al. give a deep explanation of the reactions occurring during laser ablation of a target in a liquid medium. This can shed light on the mechanisms involved and help to understand CAWs formation [2].

PLAL mechanism is described by Amendola's work by dividing it into several stages, as shown in fig. 1.8. In the first stage laser runs through the solvent. The optimization of the process wants the maximum laser energy delivered on target surface. This implies that solvent absorption must be as low as possible at laser wavelength and scattering effect must be avoided as well as solvent breakdown [6, 63]. Second step deals with laser absorption on the target surface. Several processes are then involved in this step according to the duration of the laser pulse. For ns pulse duration, vaporization, boiling, melting and thermionic emission happen. This is due to the fact that nanosecond pulse duration is longer than electron-lattice thermalization time [90]. All these effects are followed by detachment of material from the target. For ns pulse duration detachment of material from the target is described as "explosive boiling" [59]. This implies homogeneous nucleation of vapor and liquid phase of the irradiated material. The presence then of the liquid environment causes a confinement of the plasma plume right above the crater area slowing the cooling rate with respect to ablation performed in gas environment. This generates further heating of the target and thermalization of a larger portion of material due to a double transfer of heat: from laser to target and from plasma plume to

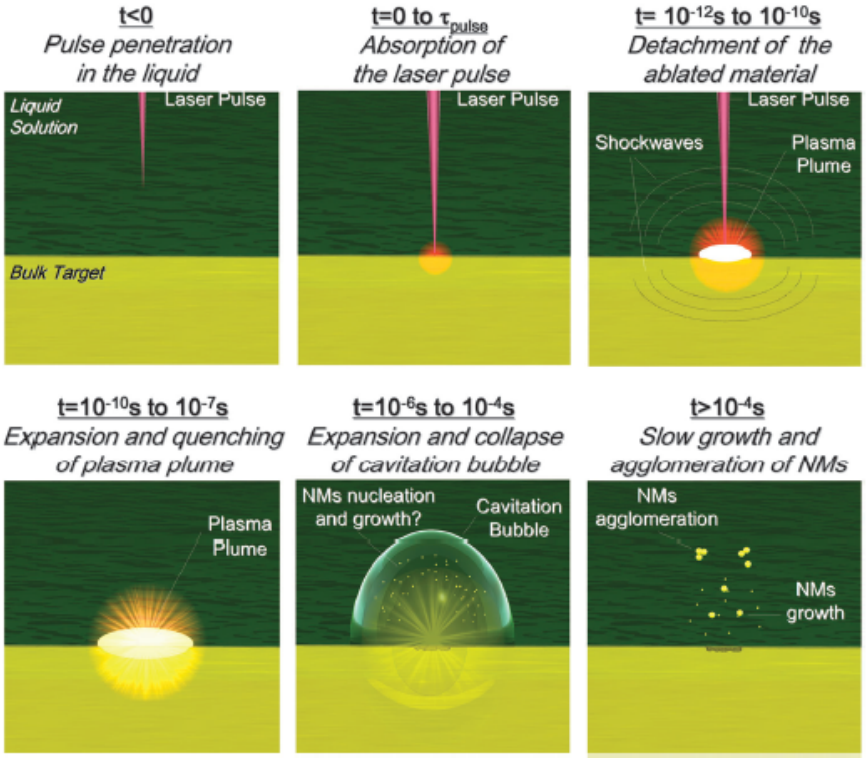

Figure 1.8: *Schematic sketches of mechanisms involved during laser ablation process on a target in a liquid medium [2].*

target. The extinction then of the plasma plume induces generation of cavitation bubbles that further aids material detachment from the crater. Bubbles collapse is accompanied by energy released that can affect species present in solutions by phase transitions, aggregation and, as said, material detachment form the target. After this, physical and chemical steady state is reached. Further modification that can happen are due to nanostructure nature that can lead to aggregation phenomena, precipitation, oxidation etc.

This just described is the general mechanism of laser ablation of a target in a liquid medium. In the specific case of CAWs generation it is believed that two main mechanisms are occurring during their formation: radical polymerization namely consecutive coupling of C_2 radicals and termination of chains by hydrogenation [79]. The predominance of one mechanism or the other implies synthesis of longer or shorter carbon chains. The control of laser parameters is of crucial importance to determine yield of polyynes production. Laser wavelength and energy, focus conditions and spot size, pulse duration and time of ablation are all elements that require proper analysis in order to optimize the production process. Being PLAL a relative new technique for CAWs production, it is still not clear how combination of these parameter affects the final product also because contradictory affirmations are made in literature. For instance optimum laser wavelength for CAWs production is a controversy matter. Matsutani at al. [53] affirmed that production of polyynes increases by increasing λ while the opposite is stated by Tsuji et al. [80]. The difference is then justified by a different system configuration applied for the two researches. In general longer laser wavelength are supposed to deliver more energy

at target surface giving higher yield of production. The same reasons laid under the fact that higher energies brought to higher amount of ablated material [68].

Not only laser parameters are affecting the rate and quality of CAWs but also material parameters are involved. Starting from the choice of target, usually a graphite target is used but several experiment have been made on carbon powder, nanodiamonds dispersion as well as fullerenes and nanotubes [89, 78]. Being then in a liquid environment, the choice of the solvent is of crucial importance as well. Solvent molecular structure and properties affect structure and length of CAWs. This happens because solvent undergoes decomposition process, making radical available as end groups for polyynes. This occurs for examples with acetonitrile: when used as liquid medium polyynes are terminated with cyano end groups [70]. Moreover viscosity of the solvent is a determining parameter. It is believed that higher viscosities favour formation of long chains since mobility of radicals is hindered and crosslinking mechanism prevented, as seen by Matsutani et al. in decalin [53]. All these parameters have to be considered when applying PLAL process and choice of materials is of fundamental importance to determine the final product. According to the final application all these parameters have to be tailored.

Chapter 2

Polymer-carbon nanostructured materials

In this chapter nanocomposite materials will be presented along with their properties. Nanostructured composites or nanocomposites are multiphase materials in which one of the phases, the reinforcement, has at least one dimension of less than 100 nanometers. Reinforcements are classified as particles, wires or sheets, according to their extension along the three directions x, y, z.

Nanostructured materials are increasingly employed in a wide variety of fields carrying out structural as well as functional roles. It is forecast that by 2024 nanocomposites market size will almost double, reaching 8.5 billions U.S dollars with respect to the 4.1 registered for 2019 [39]. This market expansion is due to the wide range of possible applications and properties available once different materials come together. The possibility of tailor desired properties by combining different materials and involving the least amount of them is definitely appealing. On the other hand the complexity of the system, given by the presence of two or more phases, require deep studies in order to predict the properties of the final material. For this purpose, several elements must be taken into account and are described in the following sections. Once the properties and parameters of evaluation are listed, polymer nanocomposites are described, focusing mainly on polymer-CAWs composites state of art, properties and production methods.

2.1 Polymer-based nanocomposites

The structure of composite materials is constituted of a matrix and a reinforcement. They absolve to different roles and their properties influence the whole material performances together with other parameters that will be presented below. The matrix is commonly identified as the continuous phase; its main functions are: to give the physical structure, to bind, protect and stabilize the reinforcement, to transfer the load and to provide the final aspect to the product. Three different typologies of matrix are identified: ceramic, metallic and polymeric. On the other hand, the reinforcement or filler, identified as the discontinuous phase, has the role of improving specific characteristics of the matrix. According with matrix nature, different properties are enhanced by the filler; when ceramic matrices are involved, toughness and hardness are the properties mainly positively affected, while in metal matri-

ces tensile strength, creep and corrosion resistance are interested. For polymeric matrices young modulus, tensile strength, electrical and thermal conductivity are enhanced. In terms of improvement of the performances, polymeric matrices are the ones that give the best results: when used as matrix in nanocomposites, they confer lightweight, flexibility, low cost, gaining at the same time outstanding performances thanks to the reinforcement [17]. These properties bring polymer-based nanocomposites at the forefront in many industries e.g. automotive and packaging [75].

From henceforth, due to the magnitude of the topic, the description will be narrowed down to polymeric matrix combined with carbon-based fillers; this is made in order to deal only with elements strictly related to the work developed by the author.

2.1.1 Structure and properties

Polymer-carbon based nanocomposites are subject of huge investments and research interests among nanostructured materials. This is imputable both to the complexity of the theme, that has to account many variables in order to have a complete understanding, and to the promising properties that can be achieved. At structural level, as aforementioned, nanocomposites are constituted of a matrix and a reinforcement or filler. The interaction between the phases is of crucial importance both in the definition of the properties as well as in their optimization. Proper characterization of this bond happens through study of the so called interphase, conventionally described as an immobilized layer which increases the effective filler volume.

In order to evaluate performances of nanocomposite materials, and in general for every engineered material, their behaviour is assessed when subjected to different kind of stresses i.e. tensile, compressive, shear, static and dynamic load in both normal and adverse test environments. The information obtained is essential to select the proper material combination and to design the suitable structure. According to the behaviour shown under the listed conditions, mechanical properties are estimated.

The description of properties behaviour is led by rules already used for composite materials. It is experimental demonstrated that they work for nanocomposites as well: rule of mixtures (ROMs) e.g. is a well known weighted mean used to predict various properties of composite materials [36]. It supplies a theoretical upper and lower bond on several properties such as elastic modulus, electrical conductivity, ultimate tensile strength etc. Ideally it is designed to define elastic properties of continuous unidirectional fibres reinforced materials; actually it has been demonstrated that is valid also for plastic properties of particles as well as fibers reinforced nanomaterials [37]. Other studies [88] have highlighted how simple rules as ROMs can be applied to complex systems, once some adjustment are made. The main adjustments, when dealing with nanofillers, have to consider the dispersion of the filler inside the matrix, filler alignment along preferred directions, strength of the matrix-filler interaction. These facts gain relevance in particular in nanocomposite due to high aspect ratio and specific surface area. Hence, in order to optimize these features, pre-treatment on the filler are conducted; if properly purified, deagglomerated and functionalized the interaction with matrix can be improved. Weak

matrix-filler interaction is attributed to low dispersion, low affinity and incompatible polarity. These conditions are undesired since they entail bad load transfer among phases thus poor mechanical performances.

Good dispersion of nanofiller in the matrix proves to be a real challenge: intercalation of polymer within the filler happens to be not energetically favoured since a loss of freedom, hence entropy loss, is implied; conversely aggregation is a inherent thermodynamically supported phenomenon [61]. Thus, to make intercalation happens and to obtain a good dispersion, this process must be favoured; this aim is reached via surface modification of the filler: coating with surfactants, coupling agents and other technique have been tested and proved to be effective [49]. Furthermore, having a good dispersion hinders filler reagglomeration that turns out to be one of the major cause of fatigue and creep failure on nanostructured material [17].

Another aspect influenced by reinforcement presence is matrix morphology. Particles, wires and sheets work as heterogeneous nucleation agents. This brings to trans-crystalline growth viz. polymer tends to crystallize perpendicularly to filler surface enhancing matrix-filler stress transfer. In general the presence of nanoparticles increases crystallization rate acting as active nucleation sites; although this stands only for low filler percentage. One of the most crucial aspect that need to be considered is indeed filler content. It could be expected that improvement of mechanical properties goes linearly with filler volume in the matrix; however experimental results have shown that mechanical properties reach the optimum for a specific filler content and then decrease if this latter is heightened, as shown in fig. 2.1. It has been established that the optimal nanofiller content (ONC) is linked to percolation phenomena [62].

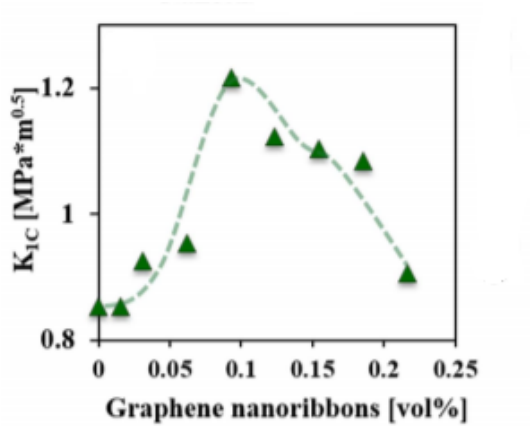

Figure 2.1: *Trend of fracture toughness K_{IC} in epoxy matrix when graphene nanoribbons content is varied [62].*

Percolation theory states that exists a percolation threshold that represents a concentration limit above which a long-range link is established between randomly arranged sub-units. There exist different thresholds according with the interested property, e.g. conductivity percolation which stands for minimum amount of nanofillers in reciprocal contact allowing transport phenomena [18]. According then

with the specific property enhancement desired, the filler content must be adjusted.

2.1.2 Process methods

There exist a huge amount of processing methods to embed carbon nanofillers inside a polymeric matrix and they are in constant evolution and update. However they can be grouped into three main categories, listed as follows:

- *in situ* polymerization
- solvent assisted technique
- melt compounding

In *in situ* polymerization, the filler is dispersed in a liquid monomer or oligomer; polymerization is activated by UV or electron irradiation bringing the polymer formation together with its intercalation within the filler. Indeed this process is also called intercalative polymerization. The final result shows a homogeneous dispersion of the filler and a strong covalent filler-matrix bond [84]. Solvent assisted technique is used for organic solvent soluble polymers. The filler is dispersed in a solution in which polymer is dissolved. To encourage particles dispersion, high- power ultrasonication can be applied. The nanocomposite material is then obtained after solvent evaporation via spin coating or drop casting technique. Spin casting is preferred since it provides, through a rotating support, fast evaporation of the solvent. This is a desired condition to avoid particles reagglomeration that happens with slow solvent evaporation. Melt compounding is the most industrial compatible technique. It consists into high temperature and shear forces application to have nanofiller dispersion in melted polymer. It provides fast dispersion but it is suitable only for low filler volume due to high polymer viscosity. Furthermore the application of harsh conditions arises the problem of filler integrity [61].

All these techniques are already used to encapsulate carbon fillers in polymeric matrix. CNTs, graphene sheets, fullerens, carbon fibers are all widely employed in this field [85, 66, 35]. Conversely CAWs, both for their novelty and their difficult handling, are still not largely employed in nanocomposites material; there is then plenty of room for research and applications.

2.2 CAWs-based nanocomposites

CAWs, described in chapter 1, seem to be promising structures from mechanical and physical point of view. Their main issue remains the instability and tendency to crosslink, forming sp^2 structures. To overcome this problem, embedding them in solid matrices seems to be very appealing. Differently from what has been described before, dispersion in a matrix will represent here firstly a method to preserve the filler and not only matrix properties improvement. Some work has been done involving SiO_2 matrix [52] or even more engineered solutions like encapsulation of CAWs inside CNTs [51] as well as anchoring the wires inside a porous alumina matrix [76]. All these attempts reach the goal of stabilizing the carbon linear structures

while further studies need to be performed in order to understand properties and possible applications. Focusing now on the purpose of this work, state of art of CAWs-polymer nanocomposites will be presented.

2.2.1 State of art

In literature only few works are present regarding these structures and here are shown comparing the different production processes and the results obtained in terms of stability of polyynes and generation of a solid free-standing nanocomposite.

The first publication appears in 2011 based on the work performed by Okada et al [65]. Polyynes are produced using pulsed laser ablation in liquid (PLAL): methanol employed as solvent, graphite powder as carbon source. Second harmonic (532 nm) of Nd:YAG laser beam is used for ablation process, with 20 Hz frequency and 7 ns pulse duration obtaining an estimated fluence of 1.2 J/cm^2 and the beam loosely focused on the side wall of vessel. During ablation the solution is stirred by magnetic agitation. Polyynes so obtained are added to an Ag nanoparticles (NPs) colloid solution in a 1:4 ratio. Ag NPs are produced by laser ablation of a silver plate in water. To complete the process the polymer is added. Here 8 wt% poly-vinyl-alcohol (PVA) is used. The choice fell on PVA due to its well known behavior, cost-effectiveness, compatibility with carbon structures and Ag NPs and transparency down to polyynic absorption region. The role absolved by Ag NPs, in this specific case, deals with stability of polyynes and their detection through SERS effect. A specific section will follow, devoted to explanation of Ag and other metal NPs role for this specific application. After polymer addition, the solution is heated up to 373 K and then deposited on a glass substrate. After solvent evaporation a free-standing film is obtained by peeling it off from the substrate. For characterization purposes the sample is tested with UV-vis and Raman absorption techniques as well as imaging methods i.e. transmission electron microscopy.

A different process is followed by An et al. in 2015 [3]: polyynes are generated by arc discharge: two graphite electrodes constitute the carbon source in methanol liquid medium; 10 A of alternate current are applied for 4 minutes. Another important difference is the addition of gold nanoparticles (GNP) instead of silver ones. GNP here used are obtained by chemical reduction method. Once produced, polyynes are size selected through high performance liquid chromatography (HPLC) method in order to isolate C_8H_2, $C_{10}H_2$ and $C_{12}H_2$. The separated polyynes are then mixed with GNP colloid at 1:4 ratio; afterwards 9 wt% PVA is added and the solution heated up to 373 K. After half an hour heating, the top of the solution is collected and coated on a glass substrate.

Only few years later, in 2019, Sata et al. [73] realize nanocomposite samples following another different route: polyynes are produced by PLAL in methanol, $C_{10}H_2$, $C_{12}H_2$ and $C_{14}H_2$ chains are isolated with HPLC procedure and then absorbed on PVA films by soaking. The goal of this work differs from the previous on the grounds that not only nanostructures stability is pursued but also the study of peculiar properties of polyynes; specifically Sata wants to study the angular dependance of UV absorption spectra of aligned polyynes with linearly polarized incident

light. Alignment of CAWs is obtained by mechanical action through stretching of the PVA films. During stretching action, wires embedded in the interstitial space of polymer chains result to be oriented according to the stretching direction.

The last works are realized in 2020 by Peggiani et al. and Sala S. [69, 72]. They introduce a new production process referred to as *in situ* process or *one step* process that provides for a single step synthesis in which a polymer solution is used as liquid medium in the laser ablation production of polyynes. This new method simplifies and shorten the realization of samples and investigates the effect of the different elements in solution in terms of polyynes production yield, stabilization of the system, interaction matrix-filler via generation of a blend. In the former work, made by Peggiani et al., PVA at different weight percentages dissolved in water is used as polymer solution. The use of water as solvent makes this an environmental sustainable process by avoiding the use of organic solvents. However one side effect is the removal of an additional carbon source represented by the organic solvent. After ablation of graphite target is performed, Ag aqueous colloid is added and then film deposited via drop casting technique. On the other hand Sala S., in his project thesis, uses both a different polymer and a different solvent: polymethylmethacrylate (PMMA) dissolved in acetone. The main carbon source remains a graphite target that is ablated in the polymeric solution though the presence of the organic solvent increases the availability of carbon source. The addition of Ag NPs is here performed in two different ways, explained hereafter, in order to find the best approach. The films are then deposited by drop casting and the solvent is left to dry.

In the following sections a overview about metal nanoparticles integration in the systems will be presented along with results in terms of polyynes stability.

Metal nanoparticles roles

This section covers metal nanoparticles roles in CAWs nanocomposites and describes the different methods used to integrate them in the studied systems. Metal nanoparticles are already known as a method of stabilization of polyynes as investigated by Casari et al. [7]. In their research, Ag NPs aqueous colloid is mixed with a solution of polyynes, produced by SADL in methanol and let dried on a substrate; from surface enhanced Raman scattering investigation, stability of the system up to 3 months is highlighted as shown in fig. 2.2a. This is attributed to Ag NPs-polyynes interaction that stabilizes wires electronic configuration hindering crosslinking reaction.

Polyynes-metal NPs interaction is detected in other works as well [65, 3] where an agglomerative phenomenon is encountered when metal nanoparticles are mixed with polyynes. This feature is proved both with scanning electron microscopy (SEM) images and UV-vis absorbance analysis which show that when put together, polyynes cause agglomeration of NPs. This is visible clearly into TEM images reported in fig. 2.2c and 2.2d and is deducible from UV-vis peak broadening shown in fig. 2.2b. This is precisely the behaviour needed to have a good SERS effect. Agglomerates of NPs represent hot spots at which enhanced local fields are generated having the best SERS performance.

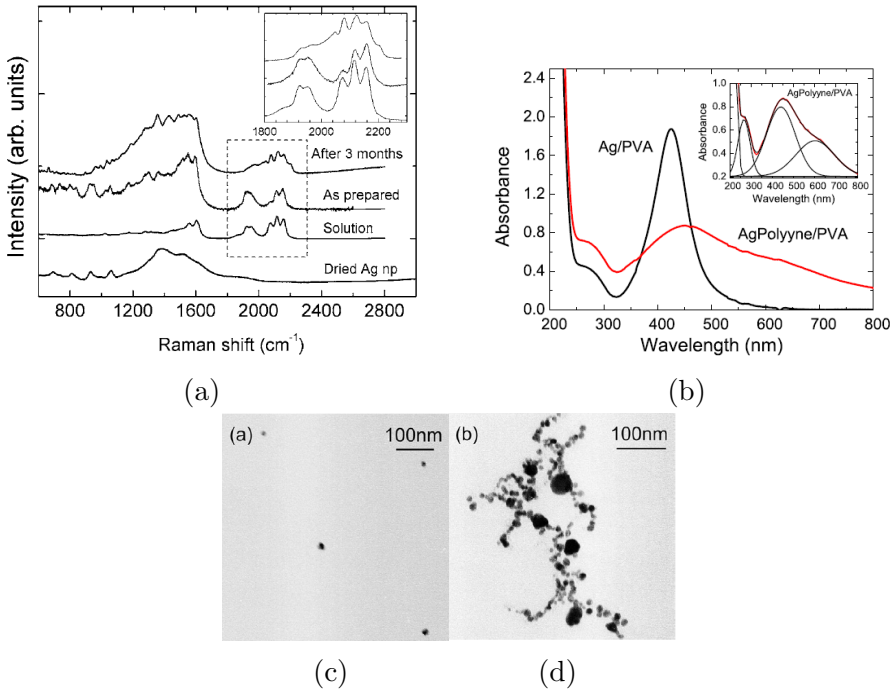

Figure 2.2: *(a) SERS signal of polyynes in solution and deposited with Ag NPs: as prepared and after 3 months. Background signal of dried Ag NPs is provided. In the inset a zoom on the sp region signals[7]; (b) UV-Vis spectra of Ag/PVA and Ag/PVA/polyynes. In the inset the deconvolution of Ag/PVA/polyynes UV-Vis spectrum [65]; (c) TEM image of Ag/PVA film[65]; (d) TEM image of Ag/PVA/polyynes film[65].*

Ag NPs are also combined with polymers i.e. PVA, to achieve better mechanical performances and to provide a high antimicrobial action. On this basis such systems are highly applied in bio engineering [74]. Last role, and in this case the most relevant, is the possibility of perform surface enhanced Raman scattering analysis on samples. SERS, as described in chapter 1, allows to detect really low concentration of materials thanks to surface plasmon resonance given by metal nanoparticles. Based on this both Ag and Au nanoparticles are used for polyynes detection .

Metal nanoparticles can be produced following many different roads; chemical synthesis and physical generation are the ones applied in the works here described. The former avails of reduction processes; Ag NPs are usually generated by Lee-Meisel method [44] while Au NPs are obtained via citrate reduction [82]; both of them results in a colloidal aqueous solution in which nanoparticles are dispersed. Simple addition integrates them in polyynes solutions at specific ratios experimentally optimized [69]. On the other side, via physical way, NPs are generated by laser ablation. The target of the raw material is bombarded with a laser beam causing detachment of metal nanoparticles in liquid environment. Stabilization of NPs remains an open issues and matter of wide research since, according to the solvent they are dispersed in, they show higher tendency to reaggregation. The different stability of Ag NPs in different solvents has been deeply investigated [81], highlighting how organic solvents are not efficient for NPs stabilization while water appears to have the best behaviour. Another crucial aspect that is considered when physical particles are realized concerns laser parameters. From several works arises the fact that, according to the different laser parameters, different average size of NPs is

obtained; it is also well known that to have a good SERS effect, a specific range of NPs average size is required. In light of this and by comparing several researches it appears that the best conditions of ablation are: low laser energies, beam focused on the target surface, implying high fluences, and optimum laser wavelength of 532 nm for silver and gold nanoparticles [23, 33, 16].

There is one more technique used to perform SERS analysis, which regards functionalization of surfaces with metal nanoparticles; in doing so Ag NPs are somehow external elements with respect to the system hence not involved in the occurring reactions or subjected to laser action or polymer interaction. This issue is the main object of study in Sala's thesis project [72]. Here realization of PMMA/polyynes films from PMMA/acetone solutions via one step process is conducted. The will of verify polyynes time stability requires presence of metal nanoparticles. Their integration appears to be a non trivial issue given the incompatibility of PMMA towards water, the latter present in the colloidal suspension of Ag NPs. This fact challenges the author into finding new ways to add Ag NPs to the system. The first attempt foresees physical generation via silver target ablation. The *one step process* technique is still on thus the total process involves a first ablation of Ag target in the polymeric solution. After that a graphite target is ablated for polyynes production. Even opposite order of ablation has been tried but it results in a lower amount of polyynes due to degradation for prolonged laser action. The results of this process, given in terms of polyynes signal in films, are shown in fig. 2.3 where SERS spectra of Ag NPs/PMMA and Ag NPs/PMMA/polyynes are plotted.

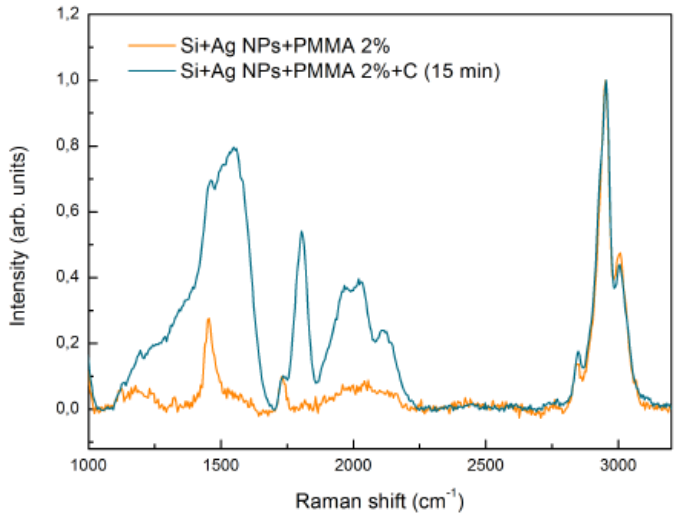

Figure 2.3: *SERS spectra of PMMA/polyynes films with Ag NPs ablation generated [72].*

The second route deals with deposition of Ag NPs colloid on a Si substrate. This will lead to formation of a solid film of Ag NPs on the top of which is then deposited a PMMA/polyynes film. Results obtained in terms of SERS signal acquired are promising and showed in fig. 2.4. In the picture SERS spectra of PMMA/polyynes film casted onto a Ag NPs film are plotted. Two samples are analyzed for different times of graphite target ablation, 5 and 15 min, in the polymeric solution of PMMA 2wt% in acetone. As reference, spectrum of Ag NPs film on Si substrate is plotted

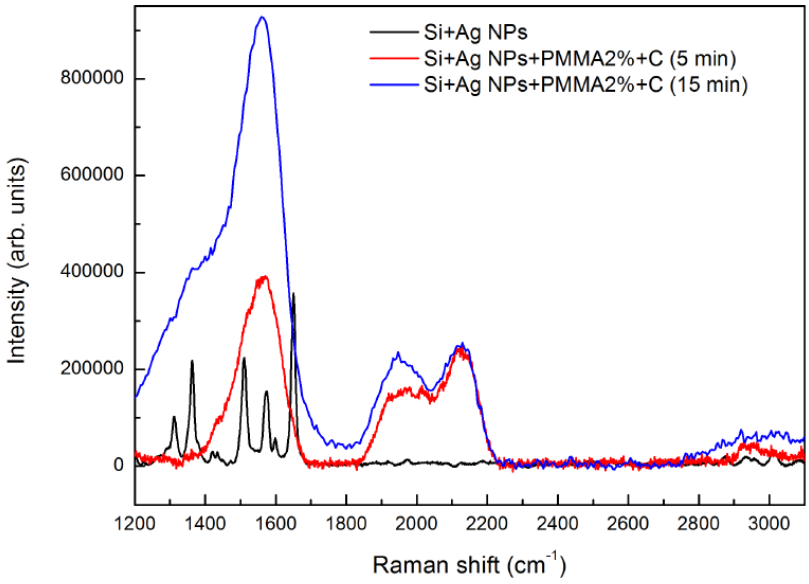

Figure 2.4: *SERS signal of PMMA/polyynes film deposited over Ag NPs film from colloidal solution [72].*

as well. The sp signal of polyynes clearly appears in the 1880-2200 cm^{-1} region. However it is noted that, compared to the previous technique, the polyynic signal shows a different shape probably due to a different interaction Ag NPs-polyynes. This will be described more accurately in the following section.

Polyynes stability

Once the production processes have been described and roles of the various elements involved in the samples have been listed, results obtained in terms of polyynes stability are shown hereafter. In order to evaluate polyynes presence and stability, their SERS signal evolution in time is studied. As depicted in chapter 1, carbon linear structures show a peculiar Raman spectra, with presence of a signal in the region from 1800 to 2200 cm^{-1}, indeed the detection of this signal implies presence of polyynes. All the works aforementioned succeeded in stabilizing polyynes proving that embedding in polymer matrix is a successful way to protect CAWs from environmental and heat damages and hinder crosslinking. Okada et al. [65] have success in polyynes stabilization. In fig. 2.5 A, B, C curves represent SERS spectra of Ag/polyynes/PVA samples acquired as prepared, after 1 week and after 1 month. The presence of P1 and P2 broad Raman bands in the polyynic region points out polyynes stabilization. This result is confirmed also by steadiness of the UV-vis absorption spectra in time. This is shown in the inset in fig. 2.5: A', B', C' correspond respectively to A, B, C curves. Considering that polyynes are not size selected in this research, it is not possible to assign the individual chain lengths contribution to the signal.

An et al.[3] obtain similar results compared to Okada's group in terms of polyynes

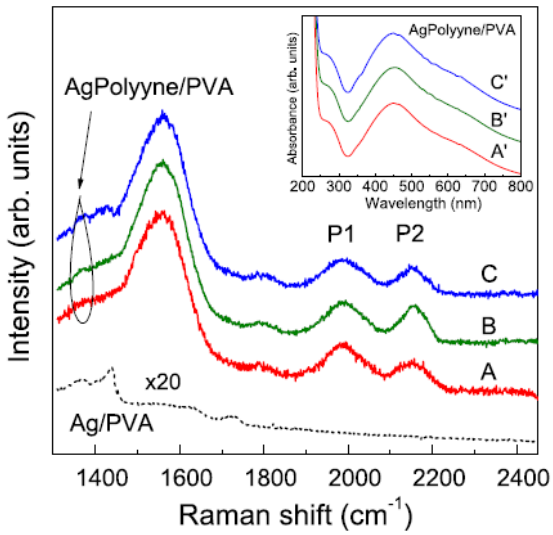

Figure 2.5: *SERS spectra of PVA/Ag/polyynes films as prepared A, after one week B and after 1 month C. In the inset the evolution in time of UV-Vis absorption spectra is shown. UV absorption spectra A', B', C' correspond to A, B, C Raman spectra,respectively [65].*

stability. SERS signal evolution is studied up to six months, as can be seen in fig. 2.6a. It can be noted that, when phase change occurs from solution (Au/polyynes) to film, a shape change in polyynic signal is detected: from a resolved signal with defined peaks to a broader band. This can be attributed to a higher stability of polyynes in films, hence the broad band is given by overlapped signals of several polyynes.

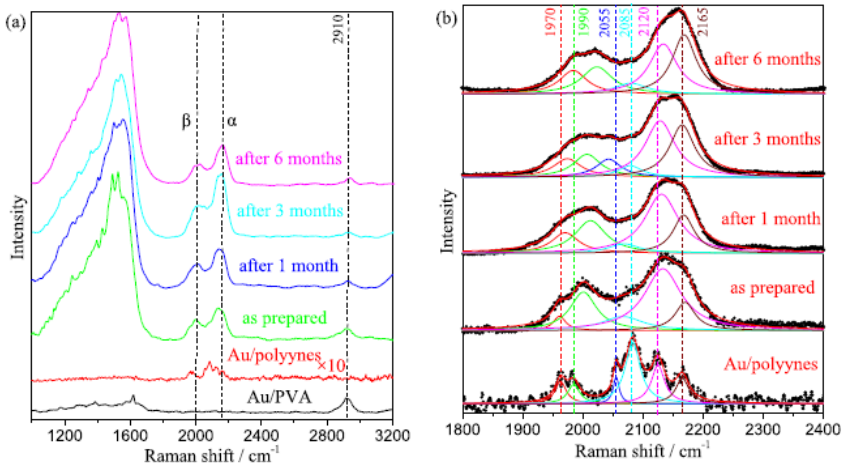

Figure 2.6: *(a) Evolution in time of SERS spectra of PVA/Au/polyynes films up to six months, (b) Lorentz fits for α and β mode in PVA/Au/polyynes[3].*

Furthermore the deconvolution of signal via Lorentz fit, shown in fig. 2.6b, highlights a red shift of signals from solution to film and in the films itself when time is passing; a higher polyynes-GNPs interaction, happening when the structures are anchored in a solid state, can be responsible of this effect. Even an increase of intensity of the peaks in α mode range is encountered. Being α mode range, the region

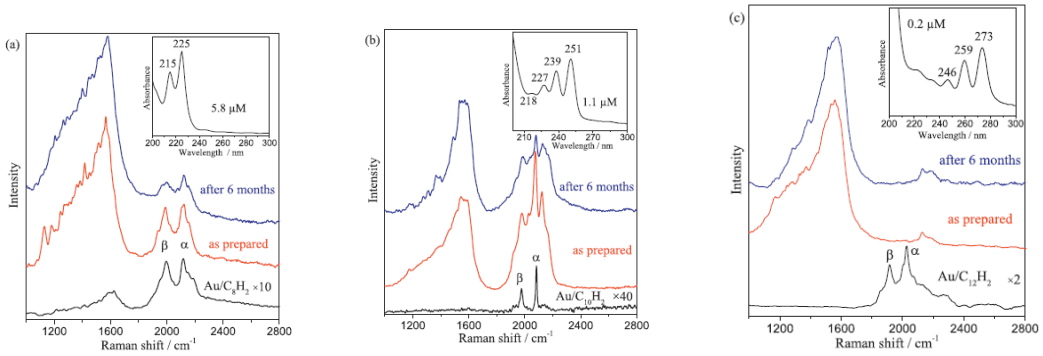

(a) (b) (c)

Figure 2.7: *SERS spectra of (a) C_8H_2, (b) $C_{10}H_2$, (c) $C_{12}H_2$ separated polyynes in solution with Au, in PVA films as prepared and after six months. In the insets UV-vis absorption spectra of each chain are depicted [3].*

attributed to short chain contributions, this implies different stability from short to long chains; these latter have lower stability and tend to degrade into shorter ones. This is also confirmed by SERS spectra of separated polyynes reported in fig. 2.7a, 2.7b and 2.7c. Here SERS spectra of C_8H_2, $C_{10}H_2$, $C_{12}H_2$ are reported and their variation from solution to films firstly and then in time is observed. Higher stability of C_8H_2 with respect to $C_{10}H_2$, $C_{12}H_2$ is registered; longer chains SERS signals exhibit higher variation. The trend is again characterized by the decrease of signal intensity in β mode region in favour of α mode.

As last, the results obtained from *in situ* generation process are described. The work of Peggiani et al., besides the introduction of the innovative synthesis route, tries to understand the mechanism of encapsulation of polyynes in the matrix, in order to optimize it [69]. Studying the variation of PVA SERS signal from pristine material, to aqueous solutions at different percentages and to films deposited from solutions after addition of Ag NPs and polyynes, it highlights that the characteristic peak of the polymer undergoes a shift and a shape change in the case of solutions and for films at low concentration, i.e. PVA 1 wt%. The position of the peak and the shift with respect to the raw material signal corresponds to presence of a less ordered structure; hence the presence of Ag NPs and polyynes seems to hinder the crystallization of the polymer bringing to life samples with higher blending. This means better polyynes encapsulation and higher interaction between the phases. This effect is not shown for systems at higher PVA concentration, i.e. PVA 10 wt%, suggesting a more crystalline configuration probably due to higher connection among polymer chains. Furthermore, it is investigated the uniformity of solid samples. Their aspect at naked eye appears not uniform showing the so called "coffee-ring" effect that means darker edges with respect to the center. Via SEM images it is confirmed that Ag NPs distribution is not homogeneous and NPs are more abundant at the edges of the films. To investigate the implication of this, SERS spectra are acquired along a line crossing the sample from center to edge. It emerges that where presence of Ag NPs is lower, polyynes signal is more intense and conversely for higher Ag NPs concentration. This fact is crucial to shed light on the importance of homogeneity for properties optimization. In this research stability of polyynes is reached up to

11 months. The stability study in time is carried on for solutions and films samples in parallel; after 1 week polyynes signal of solutions is already highly decreased and it totally disappears after just 2 months.

The other work involving *in situ* process, conducted by Sala S. and already presented in the previous section, deals with different ways to add Ag NPs to the nanocomposites. Deposition of a Ag NPs film under the PMMA/polyynes film results in a double layer structure that, as already shown in fig. 2.4, allows to detect polyynic signal with a broad band shape typical of polymer-encapsulated polyynes. Here two main peaks are distinguished. An interesting thing is that PMMA C-H stretching peak usually located around 2951 cm^{-1} is not visible in the reported spectra. This fact is attributed to a scarce interaction between PMMA and Ag NPs due both to high molecular chains nature and solidification process. On the other hand the physical production of Ag NPs by PLAL gave a different films spectra, reported in fig. 2.3. PMMA peak here is clearly defined implying a higher interaction with Ag NPs and the polyynes signal shows three main peaks. A new feature is also detected around 1800 cm^{-1}. This peak covers the C=O vibration region and, even if this specific bond is present in acetone as well as PMMA, it does not match with their Raman spectra. It is then assigned to some possible byproducts formed during ablation due to oxygen presence in the environment.

Both the routes result to be successful to obtain polyynes SERS signal for a prolonged time even though a different SERS mechanism is clearly happening; thus, a deeper study need to be conducted in order to properly described polyynes-Ag NPs interaction. SERS signal, for both cases, is studied in time up to 21 weeks and it is reported in fig. 2.8a and 2.8b. Polyynes signal is still visible for either but a different evolution of the respective shapes in time can be detected. This is probably due to the different SERS mechanism and a possible change of Ag NPs-polyynes interaction in time.

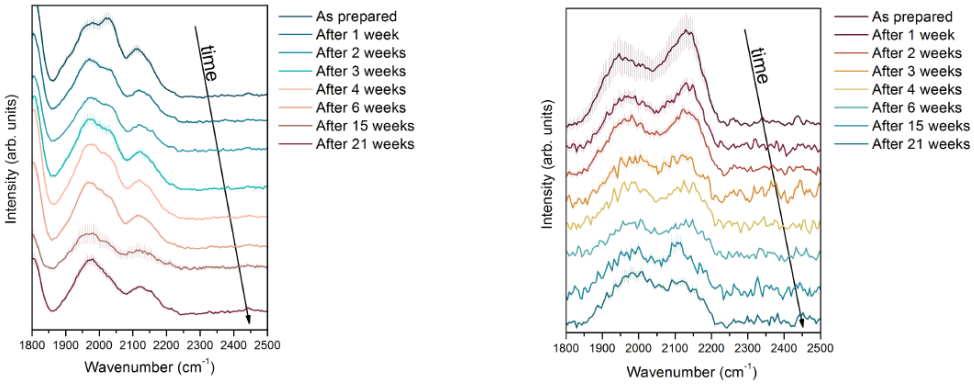

(a) (b)

Figure 2.8: *Evolution in time of SERS spectra for PMMA/polyynes films with Ag NPs from aqueous colloid (a) and ablation generation (b) [72].*

Chapter 3

Materials and methods

In this chapter, synthesis and characterization methods of samples are described: polyynes are produced via laser ablation hence PLAL apparatus will be described; since a *one step* process is applied, ablations are performed in polymeric solutions thus choice of polymer-solvent combinations and the motivations behind them are presented. Moreover this work has been focused on developing simultaneous production and detection process for polyynes. In order to do so metal nanoparticles, responsible of SERS effect mechanism, have to be present in the solution. Three different ways are then experimented to reach this goal and described in SERS enhancers section. After the description of samples realization, methods for their characterization are introduced: UV-Vis absorption technique and Raman vibrational spectroscopy. The latter is used in two different configurations: *in situ* to acquire spectra of solutions during ablation process and *ex situ* to study effective stabilization of polyynes in deposited nanocomposite films. In the following sections the author present all the materials involved and the steps followed to obtain the final nanocomposite materials.

3.1 Materials

The whole process followed to obtain the final product consists in two steps: ablation of a target in a polymeric solution and subsequent deposition of films. In previous works, described in chapter 2, ablations were performed on a carbon material, i.e. carbon powder or graphite target, to obtain polyynes production; here ablation happens mainly on a metal target. Both gold and silver have been tested. The targets have a disk-like shape with 8 mm diameter and 2 mm thickness. The purpose of this particular ablation is to generate metal NPs essential to perform SERS measurement. Hence, source of carbon to have polyynes production is found in other elements of the system: organic solvent and polymer. It has already been demonstrated by Peggiani et al. that organic solvents dissociation occurs during ablation process, contributing to polyynes production [70]; while the active role of polymer into polyynes formation must be demonstrated. Indeed bonds between carbon atoms of polymer chains are stronger with respect to the ones involved in organic solvent molecules.

3.1.1 Polymeric solutions

The first step is the choice of the proper solvent-polymer combination. Some guidelines drive the selection both on polymer and solvent, i.e. compatibility with metal nanoparticles and carbon nanostructures, non toxicity or flammability to reduce risk in production process, polymer filmability and water compatibility is a desirable property; water is present in some elements that could be involved in the systems, e.g. in Ag NPs colloid. Other aspects that need to be considered regard the characterization methods: ideally the materials involved must not interfere in polyynes detection. This means that both solvent and polymer must be transparent in UV-Vis polyynic region and SERS sp region. However the parameters to be satisfied are many and added to these, solubility of the polymer in the selected solvent must be considered as well. In the following sections polymeric solutions choices are shown highlighting properties of the materials involved and method of synthesis. It must be said that not all the selection parameters aforementioned have been satisfied; however these polymeric solutions represent a good trade-off and seem to be promising in terms of polyynes production and detection.

PMMA/acetonitrile

The first choice falls on polymethyl methacrylate (PMMA) combined with acetonitrile. PMMA has been already used as polymer in Sala's work [72]. It shows good mechanical properties and high filmability; like most polymers, it does not show any Raman signal in the sp region, as shown in fig. 3.1. Instead, the ideal behaviour is not followed for UV-Vis absorption. PMMA absorbs in the polyynic region, at 250 nm, and for this reason it is not possible to investigate polyynes presence and concentration in the polymeric solutions. Anyway UV-Vis absorption technique is used in this work to study metal NPs, whose region is not covered by polymer and solvent. PMMA is combined with acetonitrile (ACN) which shows the highest yield in terms of polyynes production among the different organic solvents. This fact is highlighted by the aforementioned research conducted on organic solvents by Peggiani et al.[70]. ACN Raman spectrum is reported in fig. 3.2c. Peaks are not present in the polyynic region. For what it concerns UV-Vis absorption, ACN shows its cut-off, minimum wavelength of absorption, at 190 nm. This value is really valid, interfering neither with polyynes nor with metal nanoparticles signal. Molecular structure of PMMA and ACN are shown in fig. 3.2a and 3.2b.

Dissolution of PMMA in ACN was actually a non trivial issue since it emerges from literature that acetonitrile is not a good solvent for PMMA; indeed it is defined as θ solvent [50]. The condition of θ solvent represents the limit between good and poor solvent. In a good solvent polymer coils expand due to favoured interaction polymer/solvent while in a poor solvent polymer coils contract being the interaction polymer/polymer promoted. In θ solvent condition, volume effect is canceled. Despite what is claimed in literature, an attempt is made to dissolve 10wt.% PMMA in ACN. The solution is kept under magnetic agitation at room temperature for 4 hours. The process brings to complete dissolution of the polymer in the solvent. In order to assess the polymer integrity and that no degradation phenomena have occurred, 10 wt.% PMMA film is deposited via spin coating technique and Raman spectrum are acquired, reported in fig. 3.1. No variation with respect to pristine

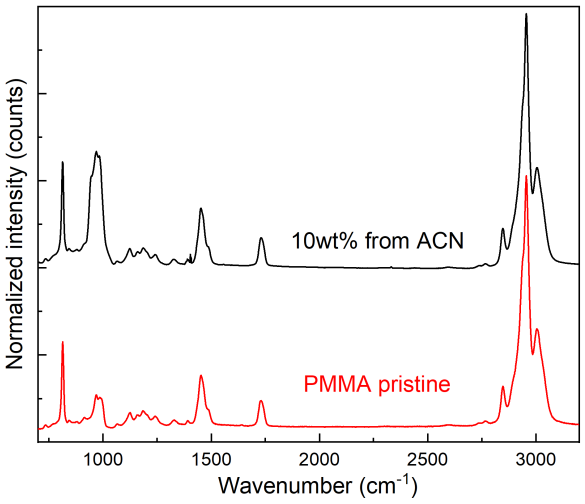

Figure 3.1: *Raman spectra of PMMA pristine material (red) and 10 wt.% PMMA film deposited from PMMA/ACN solution (black).*

PMMA powder is detected. Hence this polymeric solution is used to perform ablations of Ag and Au targets with PMMA at 1, 2 and 3 wt.%.

The main drawback shown by this system is the incompatibility with water. PMMA undergoes instantaneous aggregation in contact with water molecules so other polymeric solutions have been tested. The following combinations involve a different polymer, polyvinyl alcohol (PVA), and the use of three organic solvents: acetonitrile, methanol and ethanol. The choice of organic solvents is made according to: availability of product, well-known and studied behaviour in ablation process, suitable UV-Vis and Raman absorption. Indeed, for methanol and ethanol, UV-Vis cut-off is located at 205 nm and they are silent in Raman sp region, as already seen for ACN. The open issue remains compatibility with PVA.

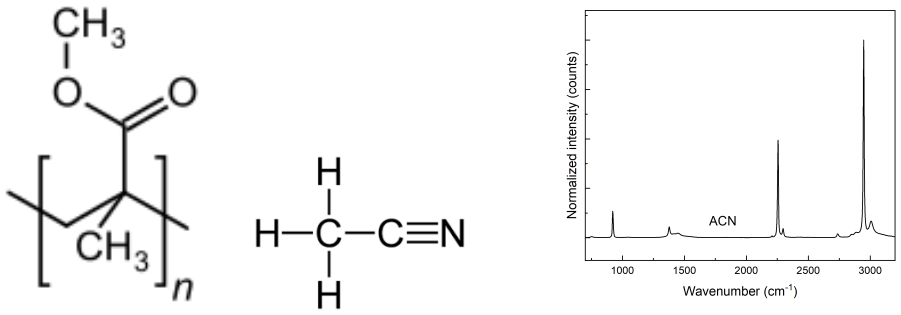

(a) (b) (c)

Figure 3.2: *(a) PMMA and (b) acetonitrile molecular structures. (c) Acetonitrile Raman spectrum.*

PVA/acetonitrile

Polyvinyl alcohol is the main character in the majority of the works presented in chapter 2. It has been effective for polyynes stabilization. PVA is water compatible while it seems not to be soluble in organic solvent. Solubility tests were anyway attempted. Starting from a solution of 5 wt.% PVA in water, by addition of small quantities of acetonitrile, it was possible to reach up to 42%vol of ACN without having PVA aggregation phenomena. Once solubility has been tested, solutions are generated at different PVA percentages: 0.5, 1, 1.5 and 2 wt.% and with fixed ACN volume fraction at 42%vol. Ablations of Ag target are then performed with 30 mJ laser energy at focal length distance for 15 minutes. These parameters, which have shown to be the optima in terms of NPs generation, are kept for all the subsequent ablations. After ablations, films are deposited on Si substrates by spin coating and drop casting technique.

PVA/methanol

The process seen for PVA/ACN system is applied to PVA/methanol system. Addition of methanol (me-OH) to 5 wt.% PVA/water solution is performed up to 75%vol of organic solvent. Then 0.5, 1, 1.5 and 2 wt.% PVA/me-OH solutions are synthesized. In these solutions Ag target is ablated and films deposited by drop casting technique. For PVA/methanol systems, graphite target ablation is also performed. Thus, double ablation is occurring: 15 min ablation of Ag target followed by 15 min ablation of C target. This is done in order to ensure the presence of polyynes, fact that was not take for granted given the lower yield of polyynes production of methanol with respect to acetonitrile, as stated in Peggiani's work [70]. After double ablation process films are deposited by drop casting technique.

PVA/ethanol

The last polymeric solution foresees PVA combined with ethanol (et-OH). Ethanol volume fraction added to aqueous PVA solution is equal to 50 %vol. The ablations performed for these solutions are the same made in methanol. Hence Ag target and also C target are ablated in solutions with PVA content equal to 0.5, 1, 1.5 and 2 wt.%. Films are then deposited by drop casting technique from single Ag target ablations as well as double Ag-C ablations.

In fig. 3.3, molecular structures of PVA, me-OH and et-OH are provided.

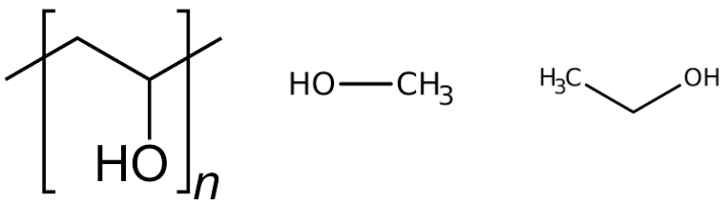

(a) (b) (c)

Figure 3.3: *Molecular structure of (a) PVA, (b) me-OH and (c) et-OH.*

With the aim of verifying the integrity of PVA after dissolution in the different organic solvents, films with 1 wt.% PVA are deposited on a Si substrate from the three different systems by drop casting technique. Raman spectra are acquired and compared with pristine material. As shown for PMMA, even PVA does not undergo any modification. The spectra are reported in fig. 3.4 and they match with the pristine material. The only difference is given in the region of 1000 cm^{-1} where a wide peak appears for films spectra. This peak is given by the silicon substrate, not present for the raw material.

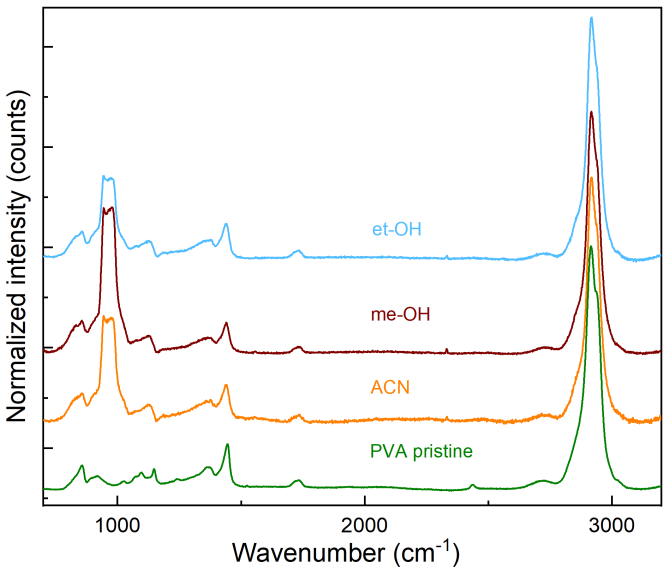

Figure 3.4: *Raman spectra of 1wt.% PVA films deposited by drop casting from the different polymeric solutions. Raman spectrum of pristine PVA is given as reference.*

In table 3.1 properties of PVA polymeric solutions are summarized. Volume fractions of organic solvents, ablated target, refractive index (n) of the solutions, fluences for the different systems are there listed. Refractive indexes are calculated considering molar fractions of the elements in solution. They remains equal for the different polymeric solutions when PVA percentages are varied since the molar fraction of the polymer is not incisive. Refractive index is needed to calculate the effective fluence on the target surface together with the volume of the solvent and the distance lens-target. All the ablations in polymeric solutions with organic solvents were performed in 1.5 ml volume and at focal distance of 200 mm. The target is allocated on the bottom of a glass vial that is fixed on the movable stage. To avoid solvent evaporation during ablation process, the vial is inserted in a beaker filled with distilled water. This provides a cooling system for the ablated solutions. All solvents and polymer here described are purchased by Sigma Aldrich. Organic solvents are characterized by purity degree higher than 99.9%.

Organic solvent	%vol	Target ablated	n	fluence (J/cm^2)
ACN	42	Ag	1.334	10.06
me-OH	75	Ag; Ag + C	1.327	10.15
et-OH	50	Ag; Ag + C	1.345	9.93

Table 3.1: *Properties of PVA polymeric solutions.*

3.1.2 SERS enhancers

In order to detect polyynes presence, Raman signal is acquired exploiting SERS effect. The physics behind this analysis technique has already been explained in chapter 1. In the following section methods for metal nanoparticles integration in the systems are explained.

Physical Au and Ag NPs

The first method applied to have metal nanoparticles is physical generation. NPs are obtained via ablation of a metal target located at the bottom of the glass vial. The metals used are gold and silver. Several ablations have been performed firstly in PMMA/acetonitrile to tune the laser parameters. Laser energy, lens-target distance, liquid volume and ablation time are varied; UV-Vis spectra are acquired after every ablation and absorption peaks of metal NPs are observed. It results that Ag NPs show the best absorbance profile when low energies, low solvent volumes and high fluences are employed. Au NPs, on the other side, exhibit lower absorption values and will be discarded. Thus, all ablations are performed at 30 mJ, 200 mm target-lens distance, 1.5 ml solution volume for 15 minutes on Ag target.

Ag colloid

Another route that was followed involves addition of Ag NPs aqueous colloid inside the solution. The colloid was already available, realized following the Lee-Meisel chemical method [44]. It was added to the PVA/ACN solution before ablation, covering one fourth of the total water volume fraction. Then ablation of graphite target was performed. SERS analysis and UV-Vis acquisitions are performed before and after ablation, results are given in chapter 4.

PE functionalized

This technique foresees functionalization of an element, external to the system, with metal NPs, as already seen in Sala's thesis [72] and also presented in Lucotti's work, described afterward[48]. In Sala's work a film of Ag NPs, deposited under the investigated films, is exploited; while Lucotti uses an optical fibre Raman probe over which Ag NPs are anchored.

In the present work, pellets of polyethylene functionalized with Ag NPs (PE_func_Ag) are used. Their synthesis occurs by immersion of the pristine polymeric material into the system in which generation of Ag NPs is happening via chemical reduction method. Thanks to the porous surface of the polymer pellets, Ag NPs will be absorbed. In order to verify the efficiency of the pellet for polyynes detection, a

drop of polyynes is deposited on a pellet of PE_func_Ag and SERS signal is detected as shown in fig. 3.5a. The technique results to be effective thus a new ablation configuration is implemented. A technique is developed to bind the PE_func_Ag on the inner wall of the glass vial. The bond is realized thanks to a polymeric film. The new configuration is shown in fig. 3.5b.

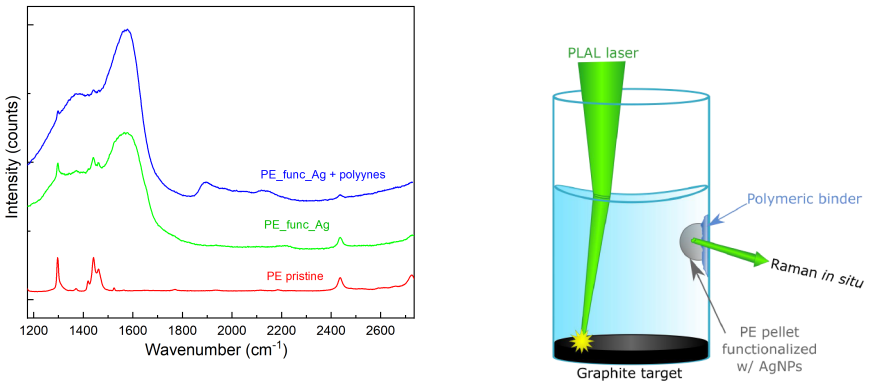

(a) (b)

Figure 3.5: *(a) SERS spectra of polyynes deposited on a pellet of PE_func_Ag. Reference spectra of PE_func_Ag and pristine PE pellet are given as well.(b) Ablation and Raman configuration with pellet attached inside the vial.*

It must be specified that, due to the complexity of the system, and the hard interpretation of the results obtained in the first part of the work, PE_func_Ag configuration technique is applied only for ablations performed in PVA/water solutions. Organic solvents are indeed not involved; this part of the research is focused only in polyynes production mechanism and in understanding polymer role. Furthermore no films are deposited after ablations performed with this configuration since no metal NPs are present in the solution and no polyynes signal will be detected.

3.2 Methods

3.2.1 Pulsed laser ablation in liquid

Pulsed laser ablation in liquid (PLAL) is the technique used for polyynes production in the current work. PLAL apparatus available in the laboratory is equipped with a Quantel Q-Smart 850 Nd:YAG (neodymium-doped yttrium aluminum garnet) solid-state nanosecond pulsed laser. The whole system is shown in fig. 3.6.

Laser beam, once generated, passes through a beam attenuator and a second harmonic generation module; the former is used to tune the energy per laser pulse while the second allows to select the output laser wavelength of 532 nm; this laser device fundamental wavelength is of 1064 nm, however for this work only laser wavelength of 532 nm has been used. Energy tuning happens thanks to the beam attenuator and a power meter is employed to measure the energy. Fixed laser parameters are frequency at 10 Hz and pulse duration of 5 ns. Once the proper laser wavelength at a tuned energy is obtained, it is deviated thanks to a 45° oriented

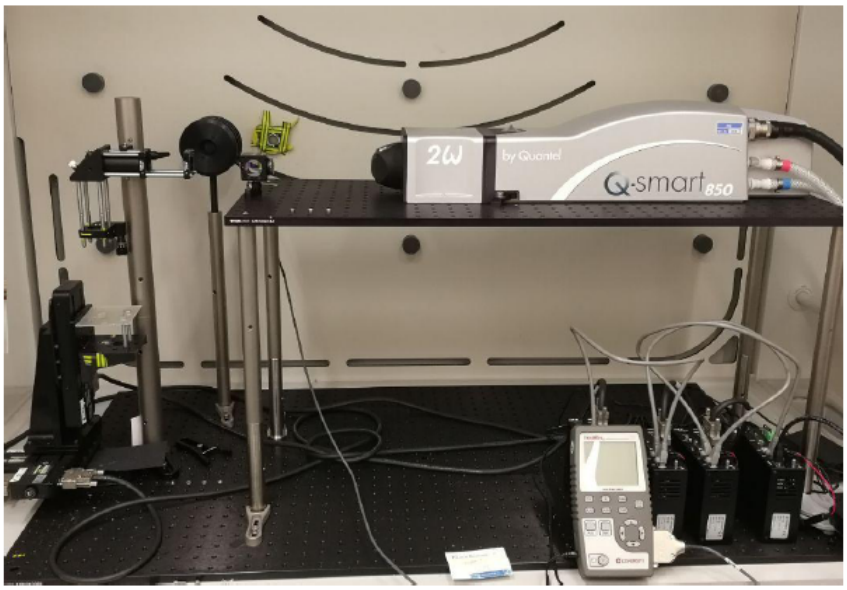

Figure 3.6: *Pulsed laser ablation in liquid apparatus.*

mirror in order to be focused on the ablation target. The target is fixed on a mobile stage. Stage movements can be remotely controlled by software and x, y, z coordinates can be imparted in order to put the samples in the desired position. Along the z direction samples are maintained at lens focus length equal to 200 mm. In this configuration, laser results to be focused on the target surface and this results in high fluence, expressed as energy per surface unit (J/cm^2). This parameter is calculated considering also the volume of the solvent and refractive index of the solutions. These data are available in table 3.1. For what it concerns x and y directions, the samples are maintained into two different configurations: a floating one and a fixed one. In the floating mode the stage performs a spiral trajectory in order to have homogeneous ablation of the target and not to have a localized consumption. Planarity and flatness of target surface is thus maintained. The fixed one, used in the second part of the work in which PE_func_Ag is used as SERS enhancer, the samples are maintained fixed in a specific position. This is due to the particular configuration with the functionalized pellet attached on the internal wall of the glass vial. The movement of the stage must be stopped to avoid ablation laser to hit the pellet.

3.2.2 Raman spectroscopy

Raman vibrational spectroscopy gives information about polyynes presence in solutions as well as in films. In the present work it is applied as a qualitative technique since it provides information about the presence of polyynes but no information about the concentration and abundance. Anyway, for the purpose of this work, determination of polyynes presence is sufficient. The instrument set up is shown in fig. 3.7.

The instrument used to acquire Raman spectra is a Renishaw inVia Raman microscope with a diode-pumped solid-state laser. Once the laser is produced, a system of lens, mirrors and shutters deviates it on the sample; hence before been

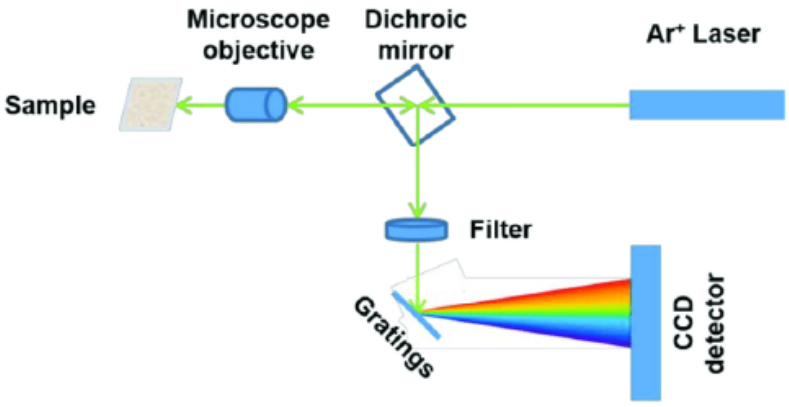

Figure 3.7: *Raman spectrophotometer components.*

received and processed by the charge-couple-detector (CCD) the signal is filtered. Only the non elastic component emitted by the sample is considered. The samples can be investigated with different wavelength lasers: the solid state system provides laser in the green (532 nm) and red region (660 nm). Another Renishaw instrument, available in laboratory with an Argon$^+$ laser source, provides also blue light (457 nm). Blue wavelength is in principle the best to investigate samples in which SERS effect is exploited via SPR of Ag NPs, located around 400 nm; however on samples synthesized in this work green light turns out to have the best performance. Indeed, an attempt was made with blue light but luminescence effects hinder polyynes detection.

Spectra acquisitions have been made with a camera lens with 20x magnification. Energy, exposition and acquisition time are tuned according to the different samples in order to minimize the exposure to laser beam and to prevent material degradation. Acquisitions can be performed into two different modes: static and extended. Static mode consents to have faster acquisition but on a limited range of wavelength while extended mode is slower but on a wider range. Films are analyzed in the so called *ex situ* configuration. Laser probe is fixed on a holder and laser impinges vertically the samples. The position of the stage, on which the sample leans, can be adjusted thanks to a micrometric controller. This allows to focus precisely the laser beam on a desired spot. The remote control of the stage can be also exploited to perform mapping of the film. The instrument software allows to track a defined region on the sample on which subsequent acquisitions are performed, spaced by a user-defined step. This provides a statistical description of the sample. This technique has been applied in this work to few samples due to the time needed to perform it. For the majority of the specimens only spot acquisitions are acquired.

In situ configuration

In situ configuration deserves a separated section to be described. This technique exploits the same instrument described previously. The substantial difference is the spatial configuration. The laser probe in this case is mounted on a movable tripod; this allows to perform analysis on solutions. This configuration indeed is used to acquire Raman spectra during ablation process. The idea behind this technique is

to observe polyynes production evolution while ablation is ongoing. According to the different SERS enhancer used, the *in situ* configuration changes slightly. Raman laser beam is focused inside the liquid medium when physical Ag NPs and aqueous colloid are dispersed in solution. This is possible since the focal length of the 20x camera lens is longer than the vial walls thickness. In this configuration the sample is kept in movement during ablation and only at the Raman acquisition moment is brought into Raman position, defined by software. A different configuration occurs when PE_func_Ag SERS enhancer is used. In this case Raman laser must be focused on the PE pellet to acquire SERS signal; focusing process requires high precision and no remote control on the tripod is present hence all the process is manually made. The samples is then kept fixed while ablation proceeds. When Raman analysis is performed, ablation continues but energy levels must be considered. It has been experimentally tested that laser ablation energy can reach 90 mJ without causing damages to the Raman laser CCD. For higher energy levels a command is set that lowers laser energy to at least 90 mJ.

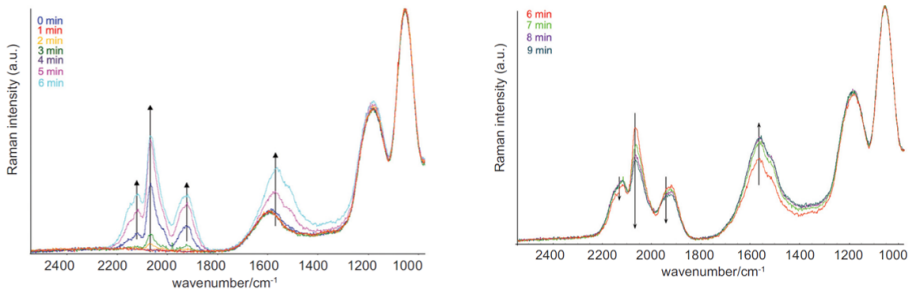

(a) (b)

Figure 3.8: *Polyynes signal evolution during (a) first five minutes and (b) up to nine minutes of arc discharge process in water [48].*

With the *in situ* acquisition of SERS signal, it is expected to observe the growth in time of the polyynic signal. Only one work is present in literature that exploits the in situ analysis and it is provided by Lucotti et al. [48]. In their work, an immersion probe, whose surface is functionalized with Ag NPs, is inserted in the system of arch discharge process while polyynes are produced in water. As shown in fig. 3.8a polyynes signal grows in time together with the sp^2 signal. It has been observed that polyynes signal grows for the first 5 minutes of ablation and decreases for prolonged arcing, as depicted in fig. 3.8b; the sp^2 signal keeps growing in time. Through this experiment, polyynes production mechanism can be better understood in order to optimize the production parameters and to deepen the knowledge on polyynes formation mechanism. However it needs once more to be specified that polyynes signal acquired via SERS technique gives a qualitative information about polyynes presence and it is affected by the Ag-polyynes interactions. These aspects are of crucial significance when results are interpreted.

3.2.3 UV-Vis spectroscopy

UV-Vis spectroscopy analysis are performed thanks to a Shimadzu UV-1800 spectrophotometer. The constituent parts are shown in fig. 3.9.

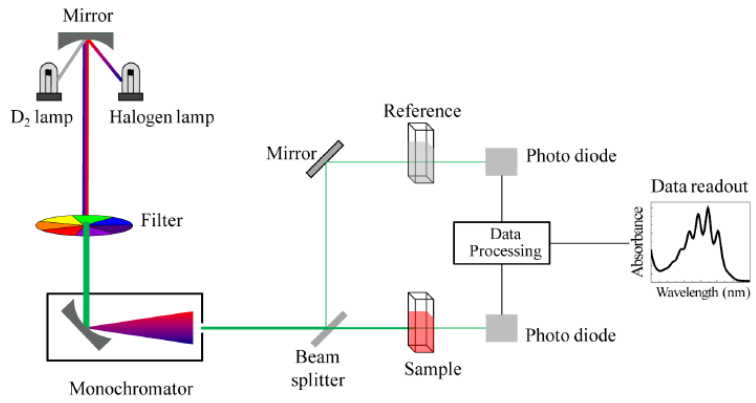

Figure 3.9: *UV-vis spectrophotometer components.*

Two lamps are used as sources of light: a deuterium and a halogen lamp. The light beam, once produced, passes through a filter and a monochromator. Hence it is split in two different beams that will investigate respectively a reference and the real sample. The sample to be investigated can be in liquid state or in solid state. The liquid specimens are collected inside a glass cuvette with transparent surface and a 10 mm thickness and they are investigated in absorbance mode. Solid state samples are mounted directly on a specific support and analyzed in transmittance mode. In the present work only liquid samples are analyzed. Before the acquisition, a reference baseline is recorded in the wavelength range of interest. The instrument allows to record from 190 nm to 1000 nm. For this work UV-Vis spectroscopy is used to investigate metal nanoparticles features, so the wavelength region is limited from 190 nm to 600 nm for Ag NPs and to 700 nm for Au NPs. The final data obtained is a UV-Vis absorption profile where absorbance vs wavelength is plotted.

Chapter 4

Experimental results

In this chapter experimental results are presented. The work is organized into three main sections. The first one deals with ablations performed in PMMA/ACN solutions. This portion of work helped into assessing the laser parameters that will be maintained then for the subsequent ablations. In the second part, ablations in PVA/organic solvent solutions are described and compared. The purpose is to define if a general behaviour occurs for polyynes production in organic solvents when polymer content is varied. Realization of nanocomposite films is then realized and characterized by SERS analysis. The last section concerns application of the new configuration for *in situ* SERS analysis exploiting PE_func_Ag technique. In this part ablations are performed in PVA/water solutions with increasing PVA percentages and evolution of polyynes SERS signal is observed.

4.1 Laser ablations in PMMA/ACN solutions

The first polymeric solution used as liquid medium is PMMA/ACN. The ablations described hereafter are performed to tune laser parameters. The aim is to optimize the production process of metal nanoparticles, crucial elements to perform SERS acquisitions. To assess production performances, UV-Vis absorption spectra are acquired after ablations and metal nanoparticles peak is studied. Absorbance levels, peak position and broadening, are all elements taken in account for this evaluation. Both silver and gold targets are ablated; for Ag NPs, absorption peak is located around 400 nm even though peak shift can happens when NPs average size varies or aggregation phenomena occur; while Au NPs show absorption peak around 500 nm. First ablations are performed on Ag target kept at 140 mm of lens-target distance. Laser energy is set at 150 mJ and ablations are conducted for 15 minutes in 2 mL of solvent. These parameters are applied in solutions with PMMA at 1, 2 and 3 wt.%. The results, in terms of UV-Vis spectra, are shown in fig. 4.1a. Ag NPs show absorption peaks with very low absorbance values. Even though absorbance increases with polymer content, showing a better peak for PMMA at 3 wt.%, SERS spectra acquired during ablation process do not show polyynes signal. This happens with every concentration of PMMA tested. Results are reported in figure 4.1b regarding PMMA 3wt.%. SERS spectra reported are acquired every 5 minutes of ablation, with laser ablation on. Acquisitions are performed thanks to in situ configuration, with Raman laser focused at middle height of solvent. The absence of polyynes signal can be caused by absence of polyynes or by failure of SERS effect due to low

efficiency of Ag NPs.

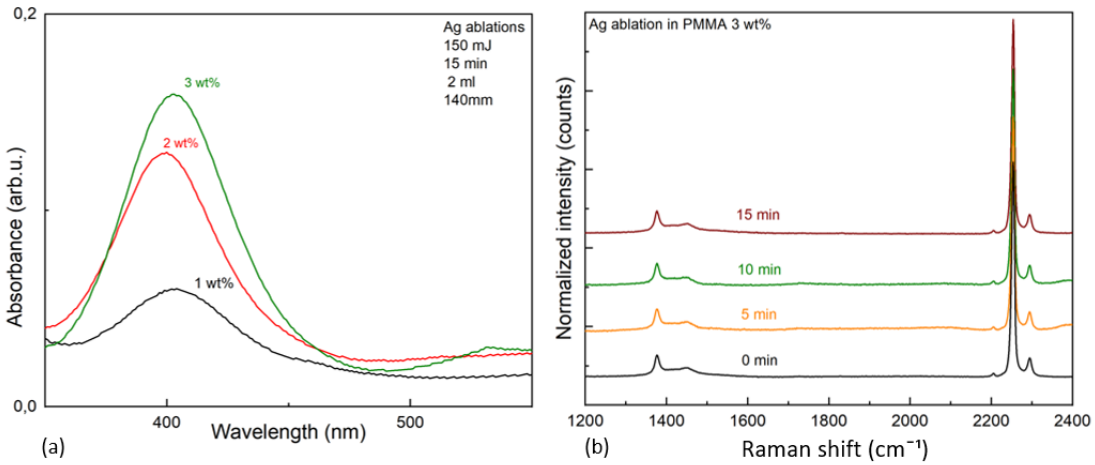

Figure 4.1: *(a) UV-vis spectra of Ag NPs after 15 minutes ablation of Ag target in ACN/PMMA solutions with increasing PMMA content and (b) SERS spectra acquired every 5 minutes during Ag ablation in ACN/PMMA 3 wt% solution. Raman spectra are normalized on ACN C≡N stretching peak around 2250 cm^{-1}.*

The second aspect is firstly investigated. Several ablations are performed varying laser parameters: solvent volume is decreased since in lower volumes Ag NPs production should increase, laser energy is decreased and target is placed at focal distance; this is done to have high fluences on target surface. This condition is presented in literature as the optimum for metal nanoparticles generation. Change of target is also performed. This has been made to verify if a different metal, in this case gold, will show higher performances. The results with gold are not as good as expected. Ablations of Au target are performed both in pure ACN and ACN/PMMA 3wt.%. PMMA percentage of 3 wt.% is chosen since it showed the best Ag NPs UV-Vis absorption profile; however both experiments result to be not promising. Au NPs peak show lower absorption with respect to Ag NPs and no polyynic SERS signal is detected during ablation. In light of this and given the cheapness of Ag target, ablation optimization is conducted on Ag NPs and Au is discarded. After several attempts and studies of literature works, optima laser parameters are defined: energy 30 mJ, lens-target distance equivalent to focal length of 200 mm, 1.5 mL of solvent and 15 minutes of ablation. Moreover it is observed that, by adding a quantity of water in the solution, absorption peak of Ag NPs produced in ACN is improved together with their stabilization in time. This was already proved by existent work that highlights the different stabilities of metal nanoparticles in different solvents [81]. It is once more demonstrated by experimental studies shown in figure 4.2a.

UV-Vis absorption spectra are shown for Ag ablation performed in ACN and ACN:H_2O= 50:50 solution. The latter, given the same conditions of ablation, shows a slightly higher absorption value and a broader peak towards the region of 500 nm. A peak covering this region is desired, being the Raman wavelength used for SERS effect of 532 nm. One last test is performed in order to define the optimum ablation time. Ablations are performed for 5, 10 and 15 minutes. UV-Vis spectra are then compared and, as reported in picture 4.2b, 15 minutes ablation shows the

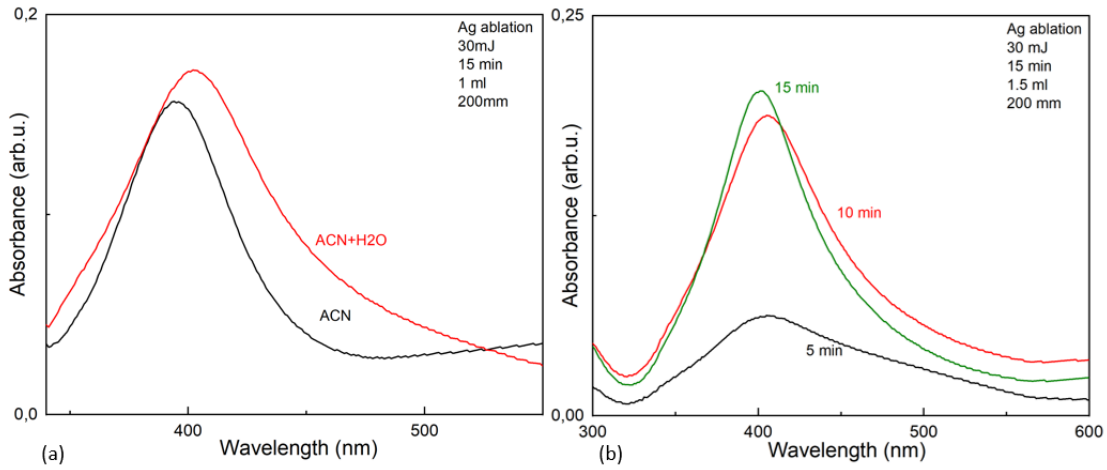

Figure 4.2: *(a) UV-Vis spectra of Ag NPs after 15 minutes ablation of Ag target in ACN and ACN/H_2O and (b) UV-Vis spectra of Ag NPs after different times of ablation.*

best performances in terms of Ag NPs absorption peak.

The addition of water in the system represents though a crucial problem for the polymer here utilized. PMMA is indeed totally incompatible with water that causes its instantaneous aggregation. Being the choice between polymer or Ag NPs stabilization and being the purpose of the work not only the realization of nanocomposite materials but also study of polyynes production process, water is kept in the system and a new polymer is chosen. The choice of the new polymer falls on PVA. Results obtained for ablations in PVA/organic solvents are reported afterward, grouped according to the solvent used. To conclude then, a comparison is made between the different systems.

4.2 Laser ablations in PVA/ACN solutions

With ablations in PVA/ACN solutions, the second part of the work begins. From now on ablations are performed applying the parameters defined in the previous section. An additional step has been herein made to investigate the ongoing polyynes process formation: SERS signal of solutions is acquired, not only during ablation, but also once the ablation laser is shut down. This brings to a turning point for the research.

4.2.1 UV-vis analysis at different PVA percentages

Ablations are performed in solutions with different PVA content and UV-Vis spectra are recorded right after the process. Absorption curves are reported in fig. 4.3. It can be observed that absorption increases with polymer content up to 2 wt.% and then decreases for PVA at 3 wt.%; the latter percentage is then discarded for following experimental tests. Peak shift is present between the different curves even if a general trend can not be defined. Peak values are reported in table 4.1. One other feature noteworthy is the broadening of the peaks towards the 500 nm region. This effect

is more pronounced for PVA at 0, 1 and 2 wt.%. These are also the percentages at which best polyynes SERS signal is detected, as shown in the following section.

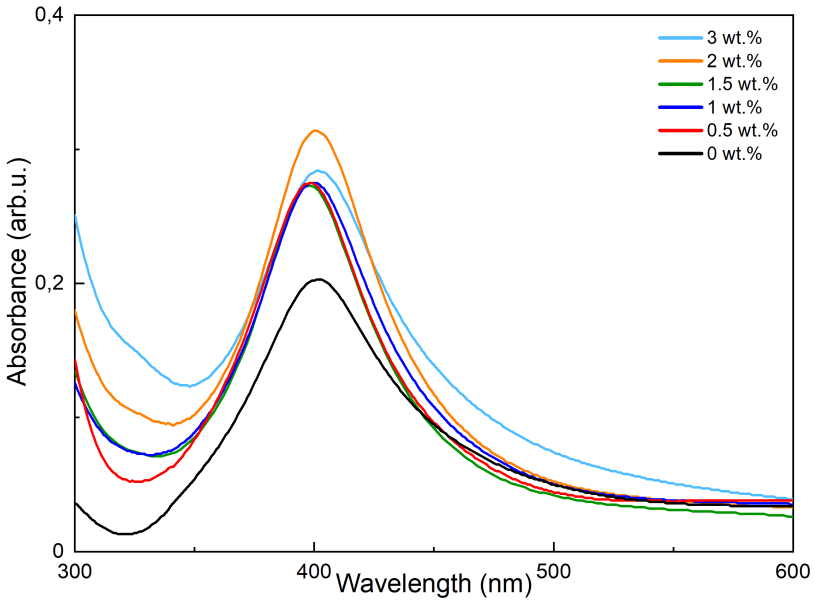

Figure 4.3: *UV-Vis absorption spectra of Ag NPs after ablations in PVA/ACN solutions at different PVA percentages.*

PVA (wt.%)	Ag NPs peak (nm)
0	401.5
0.5	398
1	400
1.5	398
2	400.5
3	402

Table 4.1: *Peak values of Ag NPs UV-Vis absorption spectra reported in fig. 4.3, referred to ablations of Ag target in PVA/ACN solutions.*

4.2.2 In situ SERS during and after PLAL process

Focusing on SERS signal of polyynes, spectra are acquired during ablation, as seen for PMMA/ACN solutions: every five minutes of ablation a spectrum is captured while laser ablation is ongoing. The results are still not promising. Polyynes SERS signal does not appear in any of the solutions. SERS spectra are reported in fig. 4.4a for ablation performed in ACN and PVA 0 wt.%. It is observed that in the polyynic region no signal is growing. All the spectra are normalized on C≡N stretching peak located around 2250 cm^{-1} and baselines have been subtracted. It is noted that SERS spectrum acquired at 15 minutes of ablation shows higher noise to the ones acquired at previous times. The reason behind this effect is to be ascribed to a

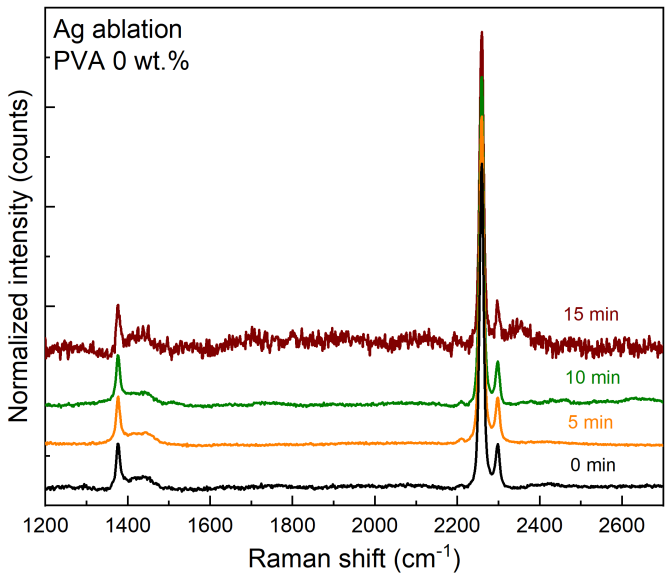

Figure 4.4: *SERS spectra acquired every five minutes during ablation of Ag target in ACN solution. Spectra are normalized on C≡N stretching peak located around 2250 cm^{-1}.*

technical problem most probably slight movement of the glass vial that has caused loss of Raman laser focus.

A different result is observed when SERS acquisitions are performed after ablation process. Right after shutting down ablation laser, SERS acquisitions are performed every minute up to five minutes. The results obtained are shown in fig. 4.5. SERS spectra reported refer to ablation performed in ACN and they are normalized on C≡N stretching peak. Polyynic SERS signal is visible: it appears at the first minute and then it grows in intensity up to five minutes. In the inset of fig. 4.5 a zoom is made on polyynic region (1800-2200 cm^{-1}) to better visualize the variation of the signal. The region from 2000 to 2200 cm^{-1} is interested by short polyynes contribution; in the range 1800-2000 cm^{-1}, where higher variation of signal is detected, contributions come from long polyynes α and β modes, polyynes-Ag NPs interactions and also β mode of short polyynes; this last contribution is actually neglected since cross section of α mode of long chains is predominant [77]. The different trend between the two regions, verified by integration of the underlying areas, highlights that in the system both long and short polyynes are generated.

Same behaviour is observed for systems with PVA. Signal appears only when laser ablation is turned off. SERS spectra acquired after ablations in systems with increasing PVA content, from 0.5 to 2 wt.%, are reported in fig. 4.6. All spectra are normalized on C≡N stretching peak and then only polyynic region is reported. It is noted that, with respect to the system without PVA, the linear growth of signal in time is lost, for every PVA percentage. It is not present anymore a trend in the growth of the signal and its evolution is random. It is however noticed that polyynic signal for 1 and 2 wt.% PVA is more intense compared to 0.5 and 1.5 wt.% PVA.

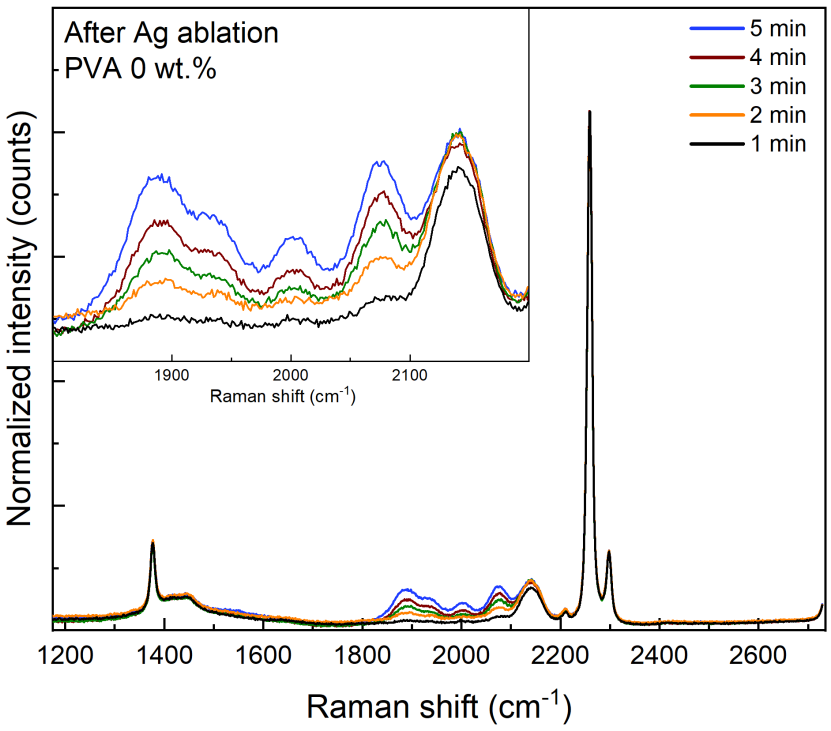

Figure 4.5: *SERS spectra acquired every minute up to 5 minutes after ablation of Ag target in ACN solution. In the inset zoom on polyynic region. Spectra are normalized on C≡N stretching peak around 2250 cm^{-1}.*

It is interesting to notice that better polyynes signal is shown by the percentages which had the broader Ag NPs UV-Vis absorption peak, as reported in fig. 4.3. Observing then again the areas of the two regions of interest, 1800-2000 and 2000-2200 cm^{-1}, it is noted again that they show a different trend of variation in time; indeed, when the ratio between the areas values of the two regions is calculated, it is not constant. This means once again that a different growth is present for the two regions. The ratio values are plotted in fig. 4.7 for the different PVA percentages: for 0 wt.% it decreases in time indeed higher variation was seen in the 1800 region; for other PVA percentages the ratio is less varying but still a trend of decrease is noted. From this behaviour one can assume that both long and short carbon chains are produced but there is no evident connection with the increasing amount of PVA.

The other aspect that need further investigations is the absence of polyynic signal when ablation is ongoing and its following appearance when laser ablation is shut down. Several assumptions are made to explain this phenomenon. The first hypothesis deals with polyynes production and the possibility that they are not present during ablation. This theory is quickly discarded since polyynes signal appears right after the extinction of laser ablation. Furthermore it is well known that ACN has a good polyynes production yield and it is not reasonable to assume that after 15 minutes of ablation they are not formed yet. One other speculation deals with diffusivity issues: it is supposed that laser ablation acts mechanically on

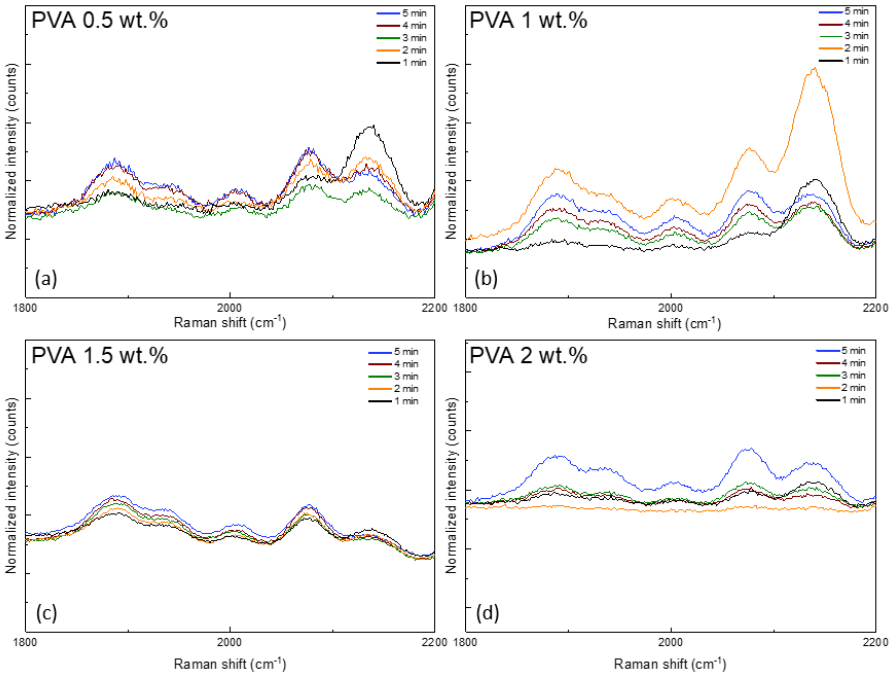

Figure 4.6: *SERS spectra acquired every five minutes after ablation of Ag target in ACN solution with increasing PVA content.*

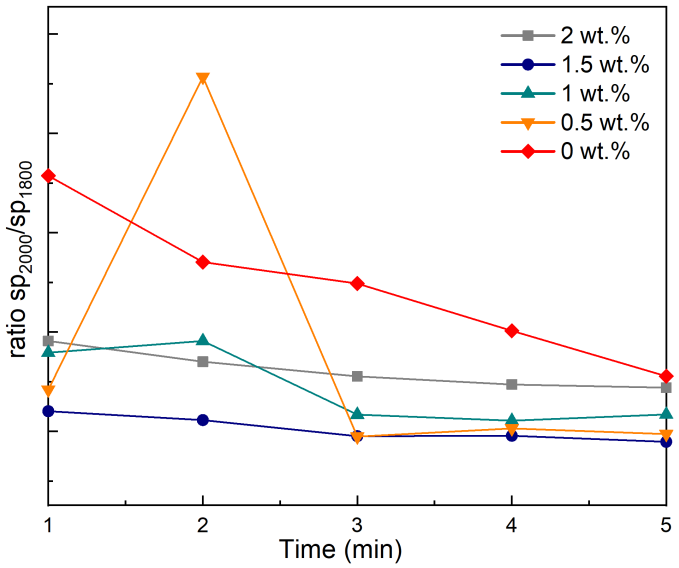

Figure 4.7: sp_{2000}/sp_{1800} *ratio between area values calculated in the two regions: 2000-2200 and 1800-2000* cm^{-1}.

polyynes and Ag NPs, pushing them to the bottom of the vial; being Raman laser focused in the middle of the solvent height, polyynes signal are not visible because they are not present in the investigated region. Even this second thesis is confuted by experimental tests. SERS acquisitions are performed in solutions every 5 minutes of ablation but after giving a resting time to the system. During resting time ablation laser is shut down. This is done to give time to polyynes and Ag NPs to diffuse and interact. After rest period, ablation laser is turned on and SERS spectrum acquired but polyynic signal is still not visible. It is clear then that the problem is given by the presence of the laser ablation that somehow interferes with polyynes detection. The last assumptions and for now, more accredited, is that ablation laser acts on Ag NPs just formed and hinders their interaction with polyynes; thus, SERS effect is not happening and polyynic SERS signal is not detected. The hypothesis considers that continuous action of laser on Ag NPs causes a fragmentation of NPs and prevent the combination with polyynes. Once the laser is removed, NPs reaggregate and SERS effect is obtained. With the aim of better understanding evolution in time of Ag NPs after ablation process and investigate if aggregation phenomena are actually happening, a parallel UV-Vis/SERS analysis is conducted. It is described in detail in the following section.

4.2.3 Parallel analysis of UV-Vis spectra and SERS signal evolution

The analysis hereafter described is implemented in order to study polyynes SERS signal evolution concurrently with Ag NPs UV-Vis spectrum variation. The experiment consists into performing a standard ablation of 15 minutes on Ag target; after that the solution is parted and half collected in a UV-Vis glass cuvette, half kept in the ablation vial. The cuvette is then subjected to UV-Vis analysis while the vial solution undergoes SERS acquisitions. This test is performed on two different systems: PVA 0 wt.% and 1.5 wt.% in ACN solutions. Results are reported in fig. 4.8 for the system without polymer.

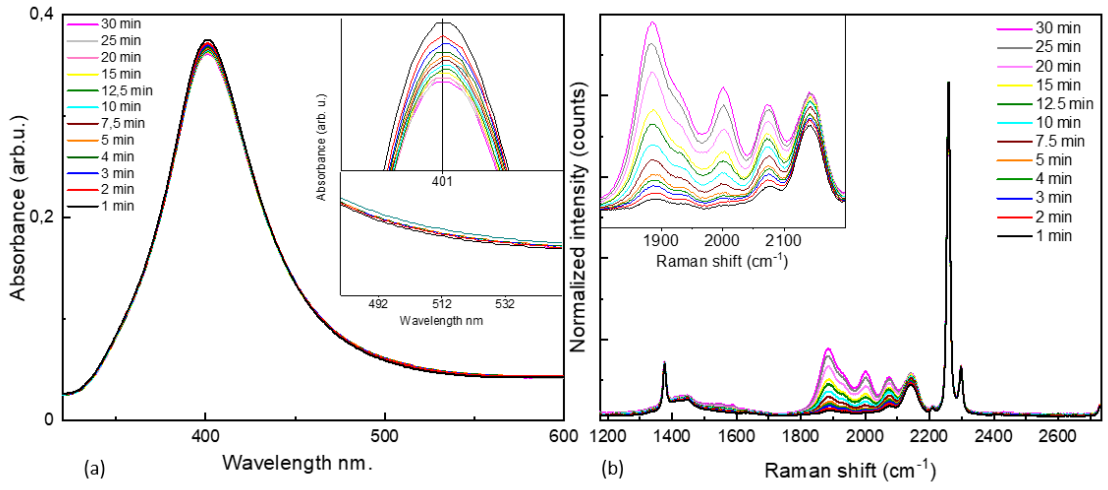

Figure 4.8: *(a) Ag NPs UV-Vis absorption spectra from 1 to 30 minutes after Ag ablation in ACN solution. In the insets zoom on peak and tail around 500 nm. (b) SERS spectra acquired concurrently to UV-Vis spectra, in the inset zoom on polyynic region.*

In fig. 4.8a UV-Vis spectra evolution is reported and in the insets zooms on peak and tail around 500 nm are reported. It is noted that a broadening of the peak is happening together with decreasing of the absorbance and widening of the tail towards higher wavelength. No peak shift is recorded. This variation in UV-Vis absorption curves are accompanied with evolution in time of SERS signal. As already seen in fig. 4.5 for the first five minutes, polyynes SERS signal shows a continuous growth in time up to 30 minutes. SERS spectra are reported in fig. 4.8b. They are normalized on C≡N stretching peak and in the inset a zoom on polyynic region is reported. For the other system investigated, with 1.5 wt.% PVA, a similar behaviour is shown for UV-Vis spectra of Ag NPs. Broadening of the peak is again present and even a peak red shift of 2 nm is pointed out. For SERS signal it is still valid what was seen in fig. 4.6c. PVA at 1.5 wt.% has shown an almost steady polyynic SERS signal and this trend is maintained up to 30 minutes. From the variation of Ag NPs peak it is clear that reaggregation phenomena are occurring and size of particles are varying. It would be interesting to implement an *in situ* UV-Vis absorption technique to detect the difference in NPs when ablation laser is present. This information is not available now and the interpretation of results is limited to the condition without ablation laser.

4.2.4 Ag NPs aqueous colloid application

One other experiment that has been tried involves Ag NPs aqueous colloid. In order to better understand Ag NPs behaviour under laser action, they are added to the investigated system in the form of aqueous colloid. This test is performed on two solutions with 0 and 0.5 wt.% PVA content, respectively. Ag NPs are added to the solution before ablation. UV-Vis spectra are acquired before and after ablation of graphite target; during ablation SERS spectra are acquired every 5 minutes keeping ablation laser on and every minutes when ablation is ended. SERS spectra, once again, do not show any polyynic signal during ablation, but in this case, after ablation, no appearance of SERS polyynic signal is detected. The answer to this behaviour is given by UV-Vis spectra comparison before and after ablations, as reported in fig. 4.9. It appears clearly how the Ag NPs are completly degraded during ablation process. Their peak is indeed totally absent in the UV-Vis spectrum acquired after ablation. For solution with 0.5 wt.% PVA the results are exactly the same and they are not reported. The polymer is then not playing any stabilization effect on Ag NPs since their degradation happens anyway.

4.2.5 Nanocomposite films deposition

Once ablations are performed in the different solutions, films are deposited on Si substrates. Two techniques are applied in first place: spin coating and drop casting.

Spin coating deposition technique

Spin coating deposition technique consists into placing a small quantity of solution on a Si substrate. This substrate is placed on a rotating support handled by an electric engine. The rotation at high speed causes ejection of the solvent and, by only 2 minutes rotation, a dried film is obtained. The film are then analyzed with Raman technique in *ex situ* configuration. It emerges that this deposition technique

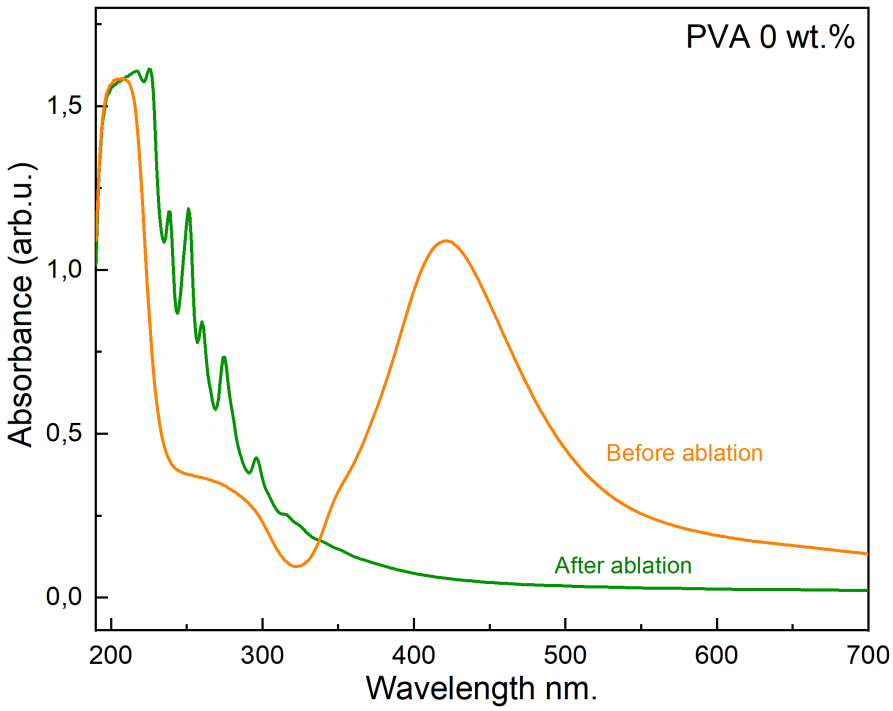

Figure 4.9: *Ag NPs UV-Vis spectra before and after ablation of graphite target in ACN solution with Ag NPs aqueous colloid.*

causes build-up of material at the edges of the film and detection of polyynic signal is really difficult. Moreover, for low concentrations of PVA, Si Raman signal is the predominant one, hindering detection of polyynes. In light of this a different technique is applied.

Drop casting deposition technique

Drop casting technique of deposition is then tested. This method implies deposition of a certain quantity of solution on a Si substrate. The film is then left to dried in order to have solvents evaporation. This allows to obtain a more uniform distribution of material on the substrate. In this case SERS signal of polyynes is detected. The best signal is shown by the film deposited from 1wt.% PVA. This is chosen as representative sample and SERS acquisitions in time are performed to verify stabilization of polyynes. The results are reported in fig. 4.10a. The spectra are normalized on the PVA peak around 2900 cm^{-1}. Reference lines are drawn at 1800 and 2200 cm^{-1} to highlight polyynic region, reported also in the inset. Polyynes signal is visible at least up to 18 days. It appears as a broad band, its shape is varied with respect to the shape detected for solutions. This phenomena was already seen in previous work and ascribed to a different interaction polyynes-Ag NPs when they are fixed in a solid matrix.

For what it concerns stability of polyynes in solution, SERS signal of polyynes

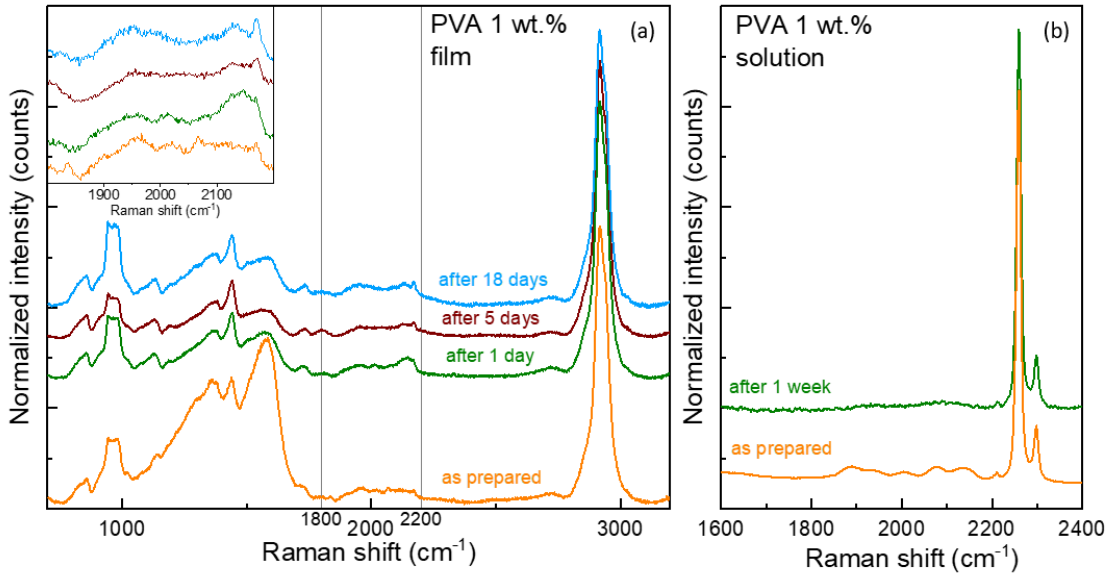

Figure 4.10: *(a) Evolution in time of SERS spectra of 1 wt.% PVA film deposited by drop casting technique after Ag ablation in ACN solution. In the inset zoom on the polyynic region. (b) Evolution in time of SERS spectra of 1 wt.% PVA/ACN solution right after Ag ablation and after 1 week.*

in 1 wt.% PVA/ACN solutions disappears already after one week, as reported in fig. 4.10b. It can be due both to polyynes degradation and Ag NPs reaggregation. Previous studies have demonstrated that polyynes degrade in time when dispersed in solutions but their SERS signal was visible at least up to 3 weeks [69]. In this work already after one week SERS spectrum reveals a flat polyynic region and, in solution, are visible small black flakes, probably due to reaggregation of Ag NPs whose stability was one of the main issues.

The experimental part dealing with PVA/ACN solutions is here terminated. In the following sections, PVA/me-OH solutions first and then PVA/et-OH solutions are presented. The steps followed are more or less the same just analyzed for PVA/ACN solutions hence the analysis will be less long-winded.

4.3 Laser ablations in PVA/me-OH solutions

Results for ablations in PVA/me-OH solutions are hereafter discussed. UV-Vis analysis at different PVA percentages are shown and reviewed together with SERS spectra. Only SERS signals acquired after ablation processes are reported, since it is still not possible to obtain any polyynic SERS signal with ablation laser in action. Then for PVA/me-OH systems, double ablation Ag and C is also performed and results will be discussed. To conclude this section, analysis on films are reported.

4.3.1 UV-Vis analysis at different PVA percentages

UV-Vis analysis are performed right after ablation process at different PVA percentages and they are reported in fig. 4.11. The general trend followed by the curves is a decrease of absorbance levels with increase of polymer content and a red shift of

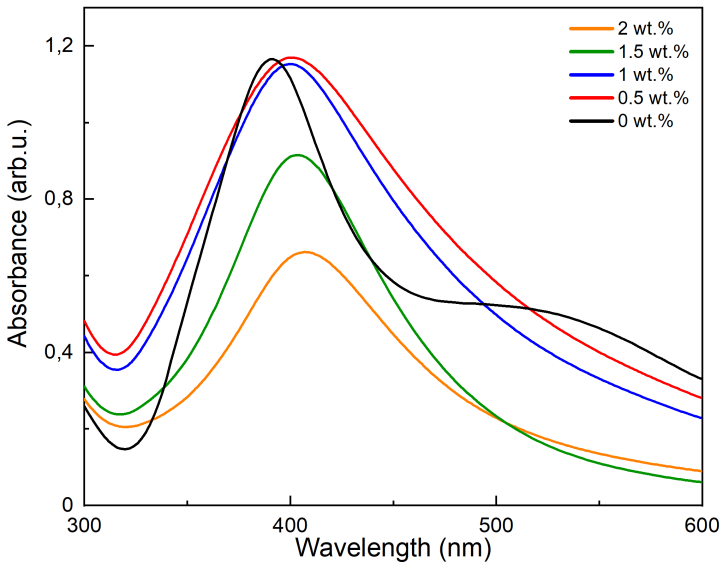

Figure 4.11: *UV-Vis absorption spectra of Ag NPs after ablations in PVA/me-OH solutions at different PVA percentages.*

the peaks. Peak values are reported in table 4.2 to point out the shift. Moreover the addition of polymer causes disappearance of the prominent shoulder visible over 500 nm for 0 wt.% PVA curve. This curve profile is attributed to presence of triangular Ag NPs as reported by [4]. It is not clear why this phenomenon occurs in me-OH solutions and not with other organic solvent and why polymer addition makes it disappears. Moreover it is not clear if the presence of this particular NPs shape will affect SERS effect. Other observations that have been made are that, with respect to PVA/ACN solutions, these spectra provides higher levels of absorbance; this means that yield of Ag NPs production is higher and Ag NPs are more abundant in me-OH systems. Peaks are also broader extending towards 500 nm region. These elements imply, in principle, better performances in terms of SERS effect. In the following section results reported for SERS analysis will show the opposite trend.

PVA (wt.%)	Ag NPs peak (nm)
0	392
0.5	401
1	400
1.5	402
2	407

Table 4.2: *Ag NPs peak values of UV-Vis absorption spectra reported in fig. 4.11 referred to ablations of Ag target in PVA/me-OH solutions.*

4.3.2 In situ SERS after PLAL process

In this section, spectra acquired in the system without polymer are firstly observed. They are reported in fig. 4.12. Spectra are normalized on me-OH peak, located around 1450 cm^{-1}, assigned to CH_3 bending. In the inset of fig. 4.12, zoom on polyynic region is made. The sp signal appears as a broad band, less resolved with respect to the one detected in ACN solutions. Furthermore, it results to be almost steady in time since no growth is detected and it is low variant. It is noted also appearance of a well defined band at 1800 cm^{-1} that is not assigned to polyynes contribution. Indeed it is a signal already seen in previous works, such as Sala's and Peggiani's [72, 69], attributed to C=O stretching vibrational mode; it is probably related to byproducts generated during laser ablation in presence of an oxygen source. It is interesting that this peak appears in me-OH systems while for ACN system it is not present. Probably it must be due to presence of alcohol group coming from the solvent dissociation.

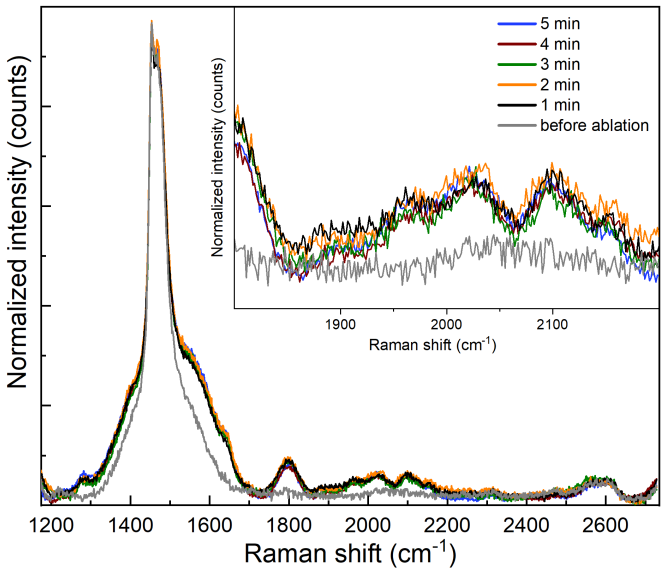

Figure 4.12: *SERS spectra acquired before ablation and every five minutes after ablation of Ag target in me-OH solution. In the inset zoom on sp region.*

For systems with increasing polymer content, SERS polyynic signal totally disappears. Results are reported in fig. 4.13, where spectra in polyynic wavelength range are plotted, normalized on me-OH CH_3 bending peak, not visible in the plots. The absence of sp signal is of difficult interpretation. Ag NPs are supposed to be effective in terms of SERS effect thanks to results provided by UV-Vis absorption curves. Hypothesis are made to explain this behaviour: there can be issues with polyynes production or interference of PVA with SERS effect. It is possible that PVA is surrounding Ag NPs and polyynes, hindering their interaction and preventing SERS enhancement.

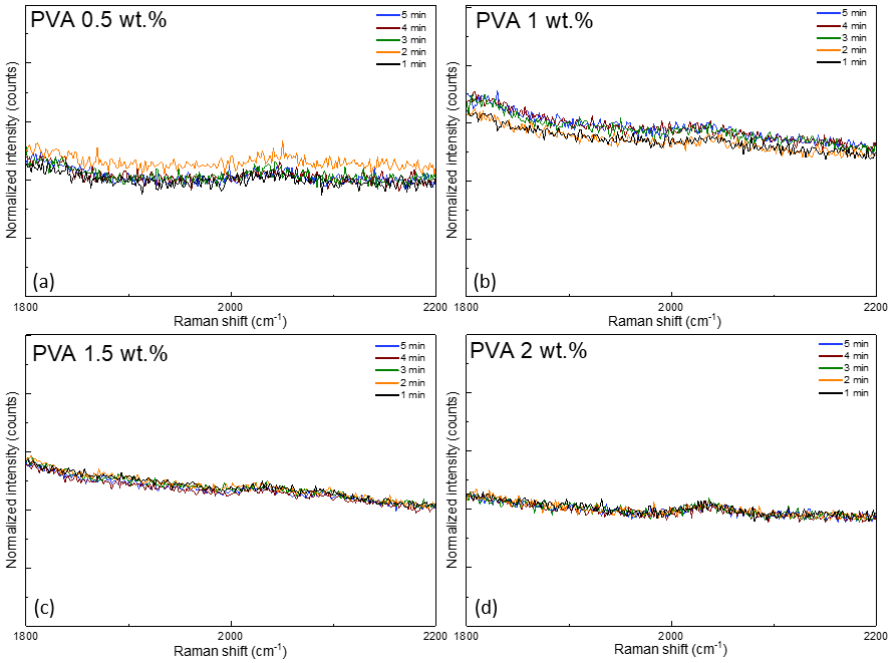

Figure 4.13: *SERS spectra acquired every five minutes after ablation of Ag target in me-OH solutions with increasing PVA content.*

4.3.3 Parallel analysis of UV-Vis spectra and SERS signal evolution

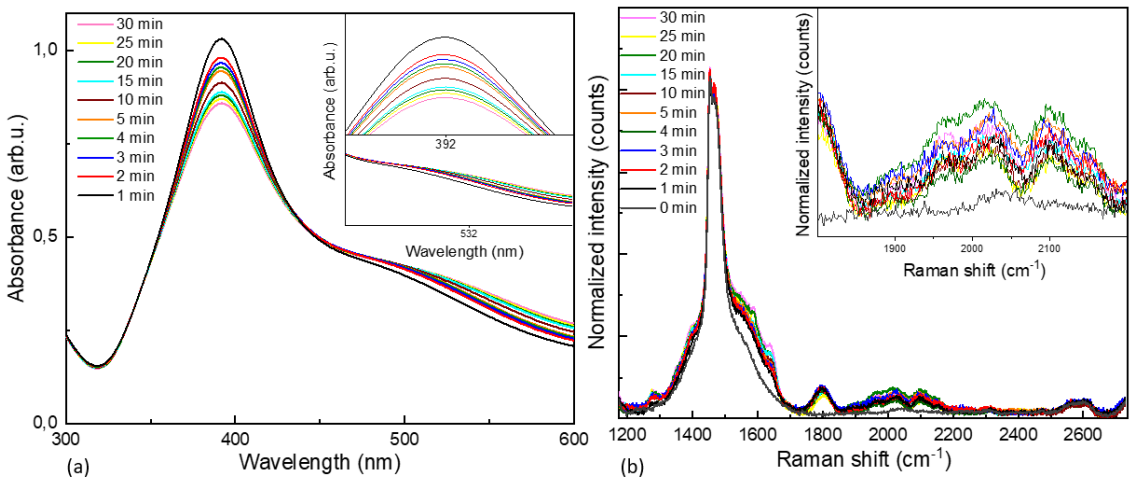

Figure 4.14: *(a) Ag NPs UV-Vis absorption spectra from 1 to 30 minutes after Ag ablation in me-OH solution. In the insets zoom on peak and tail around 500 nm. (b) SERS spectra acquired concurrently to UV-Vis spectra, in the inset zoom on polyynic region.*

For me-OH systems, parallel UV-Vis/SERS analysis is conducted. As seen in ACN system, the experiment is performed on 0 and 1.5 wt.% PVA ablated solutions. Results are reported in fig. 4.14 for ablation performed without PVA; SERS spectra of solution with 1.5 wt.% PVA are completly flat in polyynic region, as already shown in fig. 4.13c. The observations made on these spectra match perfectly with the ones made for ACN solutions. In the system without PVA, Ag NPs absorption

peaks present decrease of absorbance levels and broadening of the peaks, here more pronounced by the shoulder in 500 nm region. No peak shift is recorded while for 1.5 wt. % a 2 nm red shift of the peak is registered. Same value was found in 1.5 wt. % PVA/ACN solutions. SERS spectra are almost steady, no big variation is recorded up to 30 minutes. It can be affirmed then that aggregation phenomenon of particles and their size variation is happening even in me-OH solutions but these information are not enough to explain disappearance of polyynic SERS signal when PVA is added.

4.3.4 Ablation of graphite target

As aforementioned, a double ablation is performed in PVA/me-OH solutions with the aim of assuring polyynes presence and investigate whether polyynic SERS signal is then detectable in systems with PVA. The approach followed is the same already seen for previous ablations. In each solutions Ag target in ablated for 15 minutes, after that vial change occurs in order to have graphite target at the bottom of the new one. This process is made as fast as possible in order to let the least amount of time passing between the two ablations; this will avoid variations in the system such as NPs aggregation and will reduce environmental contaminations. Graphite target is then ablated for 15 minutes. UV-Vis absorption spectra are acquired after the double ablation for each solution and they are displayed in fig. 4.15.

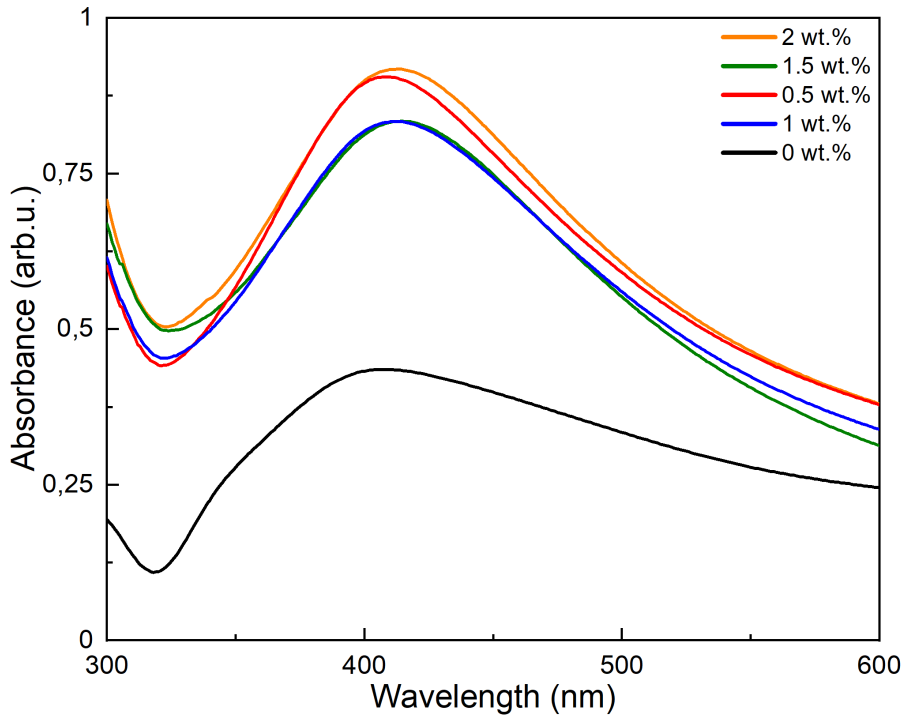

Figure 4.15: *UV-Vis spectra acquired after Ag and C ablation in me-OH solutions with increasing PVA content.*

All the curves show lower absorption values with respect to the same systems after Ag target ablation only. This is reasonable since the prolonged ablation may cause fragmentation of Ag NPs. For 0 wt.% PVA it is not present anymore the shoulder around 500 nm while a broadening of the peak is visible for the tail at lower wavelength. This means that Ag NPs have a widespread dimensions. One other observation is that when PVA is present in the system, Ag NPs seem to be more preserved under laser action, being absorbance values for these systems higher; however this behaviour is not linear with polymer content. Indeed the trend is casual and higher absorbances are detected for 2 and 0.5 wt.%, lower for 1 and 1.5 wt.%. The curves are also all red shifted if compared to Ag ablation only. Peak values are reported in table 4.3.

PVA (wt.%)	Ag NPs peak (nm)
0	408
0.5	407
1	412
1.5	415
2	413

Table 4.3: *Ag NPs peaks of UV-Vis absorption spectra reported in fig. 4.15 referred to ablations of Ag and C target in PVA/me-OH solutions.*

SERS signals are acquired after graphite ablation, from 1 to 5 minutes of rest. Plots of SERS spectra are shown in fig. 4.16. Only zooms in polyynic region are shown for increasing PVA percentage. All the spectra are normalized on me-OH CH_3 bending peak, not visible in the pictures. Even if a net increase on polyynic signal is detected for the solution without PVA, addition of polymer to the solutions implies disappearance of SERS sp signal. Only for 0.5 and 2 wt.% PVA a weak SERS sp signal is detected. These are the solutions with better Ag NPs absorption.

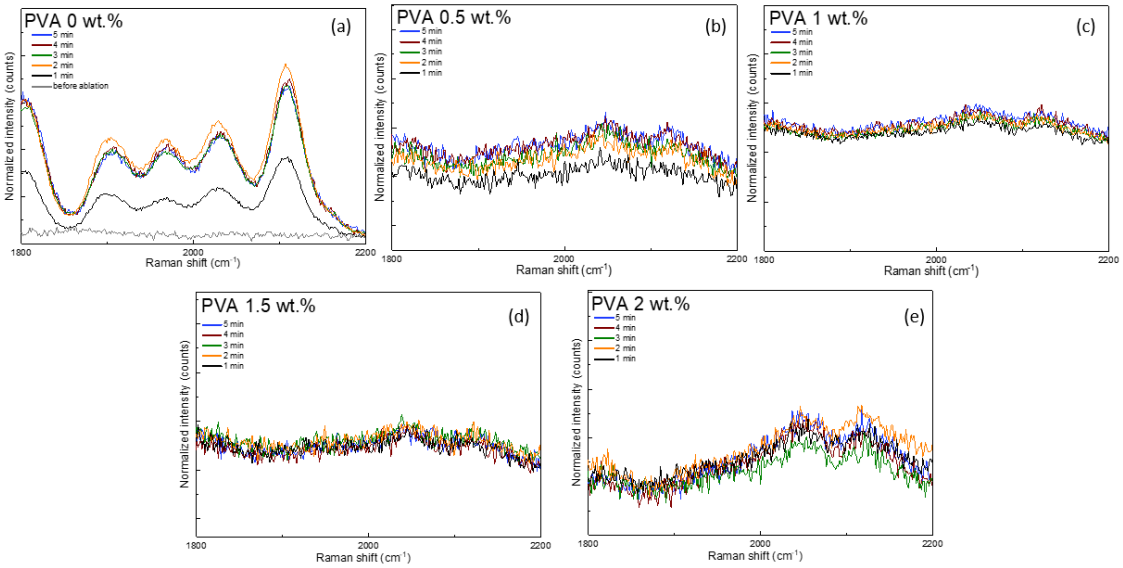

Figure 4.16: *SERS spectra acquired every five minutes after ablation of Ag and C target in me-OH solutions with increasing PVA content.*

4.3.5 Nanocomposite films by drop casting deposition

After ablations in PVA/me-OH solutions, films are deposited by drop casting technique. Films are deposited from solutions where Ag target only is ablated and also from solutions where double ablation is applied. All films have shown presence of polyynic SERS signal, even if in solution it was not detected; the hypothesis that polyynes were not produced is then discarded by this experimental evidence. In fig. 4.17 spectra acquired on 1 wt.% PVA films are reported. In fig. 4.17a film from Ag ablation is analyzed while in fig. 4.17b spectra concern film deposited after double ablation. Each spectrum is normalized on PVA C-H stretching peak around 2900 cm^{-1}.

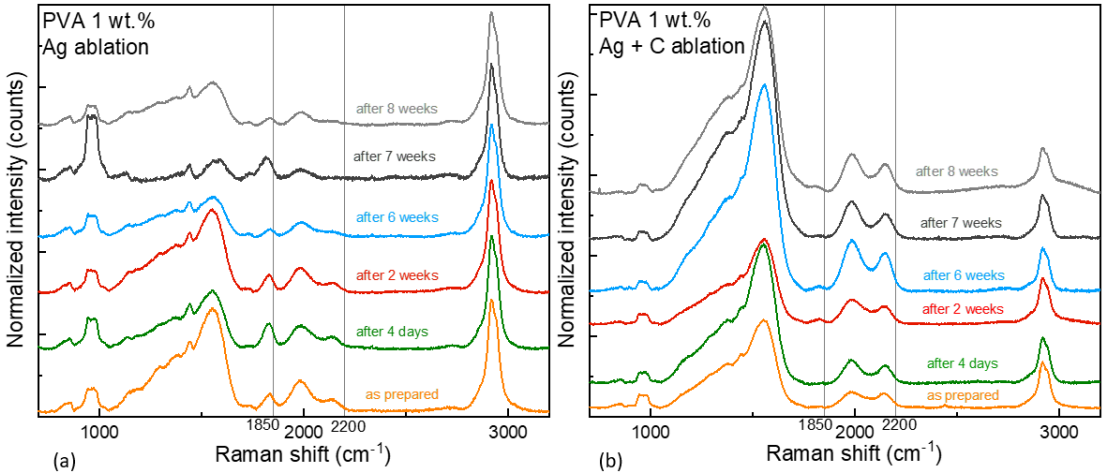

Figure 4.17: *Evolution in time of SERS spectra of 1 wt.% PVA films deposited by drop casting technique after (a) Ag and (b) Ag + C ablation in me-OH solution.*

It is noted that polyynes signal is still visible in both cases up to 18 weeks. In the sample where only Ag target ablation is performed, a weaker polyynic signal is visible, decreasing in time. For specimen with double ablation, polyynes signal is more intense and stable in time. In this samples it is recorded also a stronger sp^2 signal. Vertical reference lines are drawn on both plots in correspondence of 1850 and 2200 cm^{-1}. This is made in order to delimit polyynic region cutting out the band located at 1800 cm^{-1}, described previously. This band is not present in the film where double ablation is performed.

4.4 Laser ablations in PVA/et-OH solutions

Last organic solvent involved in polymeric solutions is ethanol. Hereafter the results for ablations performed in PVA/et-OH systems are discussed. The steps followed are the same as PVA/me-OH, with the exception of the UV-Vis/SERS parallel analysis here not performed since the general behaviour of aggregation encountered by Ag NPs is already been assessed

4.4.1 UV-Vis analysis at different PVA percentages

Absorption spectra of Ag NPs after 15 minutes ablation are reported in fig. 4.18 and peak values are listed in table 4.4. For ACN and me-OH solutions absorption values followed a trend with PVA variation, here no trend is detected. The absorbance values are randomly varying with PVA content and 1 wt.% shows the best absorption level. Even peak shift does not follow a specific trend.

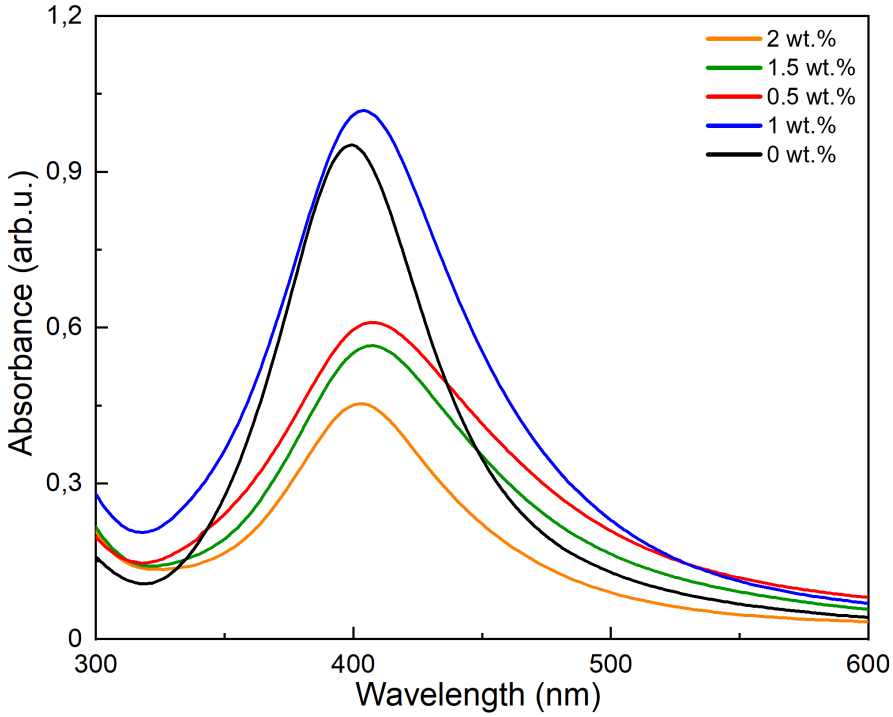

Figure 4.18: *UV-Vis spectra acquired after Ag ablation in et-OH solutions with increasing PVA content.*

PVA (wt.%)	Ag NPs peak (nm)
0	399
0.5	407
1	404
1.5	407
2	402

Table 4.4: *Ag NPs peaks of UV-Vis absorption spectra reported in fig. 4.18 referred to ablations of Ag target in PVA/et-OH solutions.*

4.4.2 In situ SERS after PLAL process

Interpretation of SERS signals is even more difficult. As it is shown in fig. 4.19, after Ag ablation in et-OH solution, no signal is detected in sp region. Spectra have

been normalized on et-OH CH_3 bending peak located around 1450 cm^{-1} and in the inset a zoom in the polyynic region is made to highlight that nothing is visible up to 5 minutes.

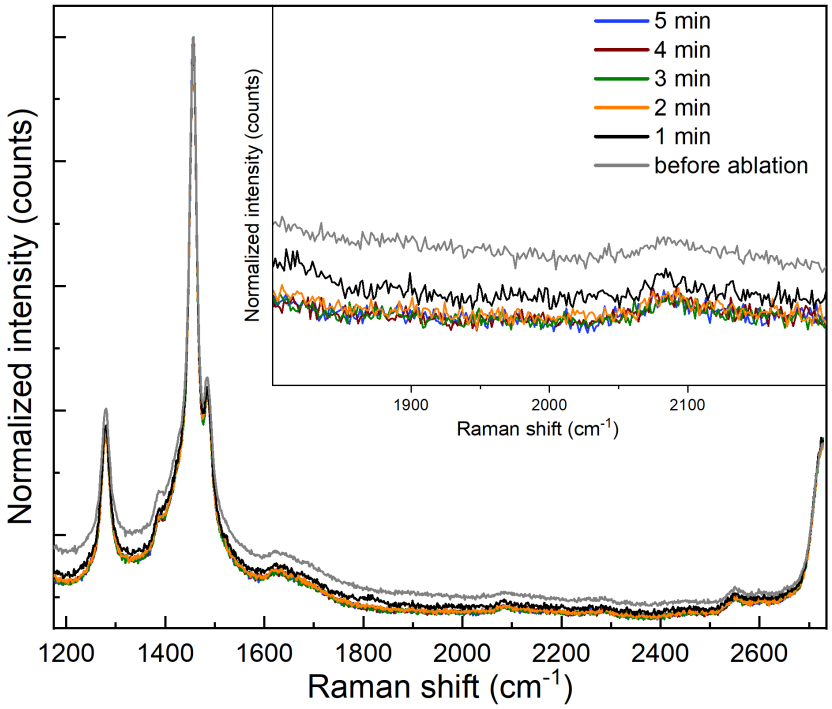

Figure 4.19: *SERS spectra acquired before ablation and every five minutes after ablation of Ag target in et-OH solution with increasing PVA content. In the inset, zoom on polyynic region.*

Similar spectra are reported once PVA is added to the ablation liquid. SERS spectra are reported in fig. 4.20 for increasing PVA content. Only polyynic range is visible and data have been normalized on et-OH peak. It is clear that no polyynes signal is present for 0.5 and 1 wt.% PVA; for 1.5 and 2 wt.% a slight appearance of sp signal is detected.

In order to shed light on the behaviour of et-OH/PVA solutions, the road of double ablation is followed; indeed the absence of polyynic signal in et-OH solution suggests that rate of polyynes production is low. Comparing the different volume fraction of the organic solvents involved in this work, et-OH is present in solutions as 50%vol., lower than me-OH (75%vol.) and almost equal to ACN (42%vol.) but being less efficient as carbon source [70], it is reasonable that the problem into detection of polyynes is their absence.

4.4.3 Ablation of graphite target

Results given by double ablation process are here discussed. The process applied is the same already described for me-OH solutions. UV-Vis spectra acquired after graphite ablation are plotted in fig. 4.21.

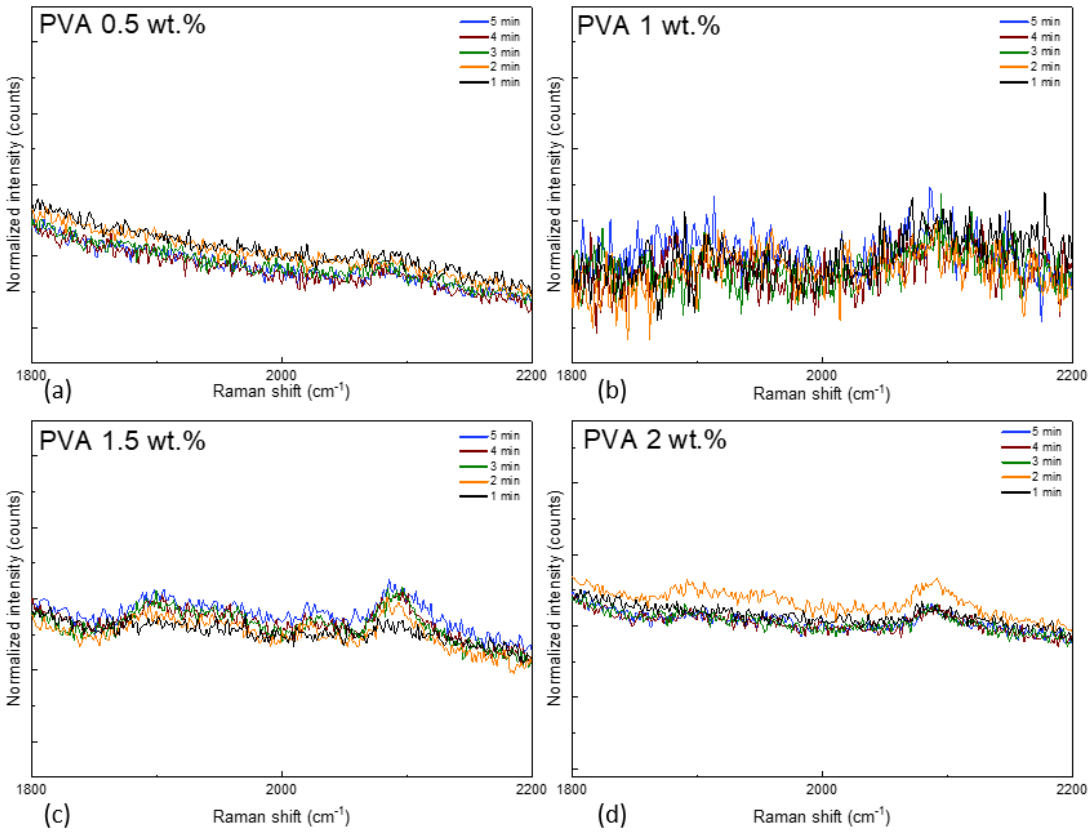

Figure 4.20: *SERS spectra acquired every five minutes after ablation of Ag target in et-OH solutions with increasing PVA content.*

Absorbance levels are overall decreased with respect to the systems where Ag target only is ablated. Shifts of the peaks, whose values are reported in table 4.5 are occurring but without a defined trend. Levels of absorbance do not follow a defined trend with PVA content variation; anyhow it is noted that, as seen for ablation in me-OH, solutions with PVA maintain higher levels of absorbance as if polymer is preserving Ag NPs during prolonged ablation. However a general trend with polymer content is not defined even if it is noted that 1 wt. % PVA shows again the highest level of absorbance.

Results obtained via SERS acquisitions are then studied. Spectra, inherent to the systems at different PVA content, are reported in fig. 4.22. Only polyynic regions are shown for increasing PVA content and data have been normalized on

PVA (wt.%)	Ag NPs peak (nm)
0	407
0.5	404
1	405
1.5	406
2	424

Table 4.5: *Ag NPs peak values of UV-Vis absorption spectra reported in fig. 4.21 referred to ablations of Ag and C target in PVA/et-OH solutions.*

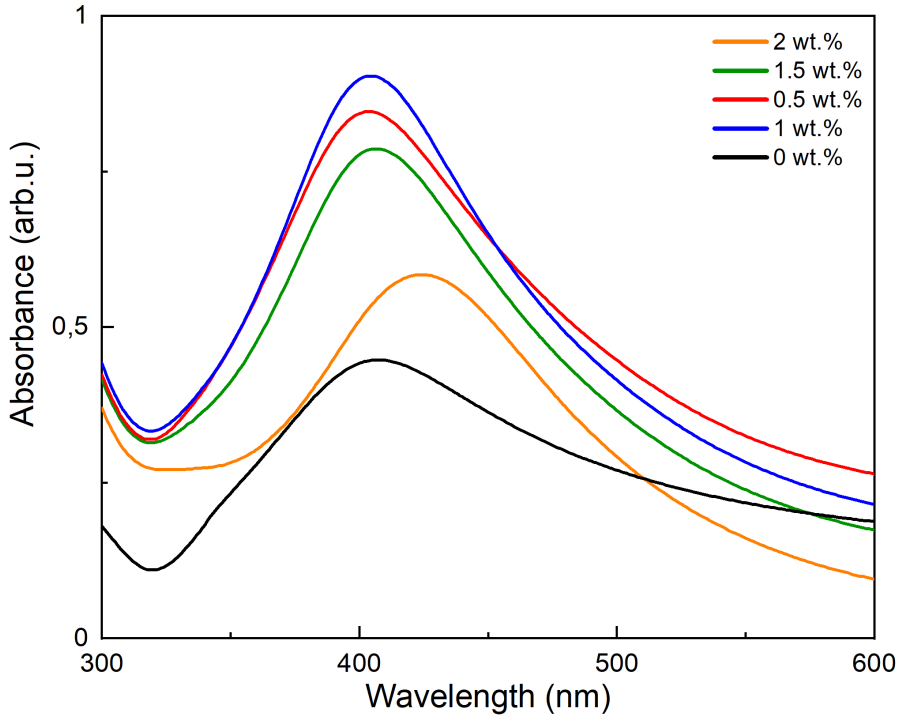

Figure 4.21: *UV-Vis spectra acquired after Ag and C ablation in et-OH solutions with increasing PVA content.*

et-OH peak. A well defined SERS sp signal is now present for solution without PVA. The shape of the peak is broad-band like, less resolved with respect to the one seen for me-OH solution. For increasing content of PVA a net decrease of sp signal is registered if compared to the system with no polymer. However polyynic signal is still visible even if very weak, especially for PVA 2 wt.%. Polymeric solution with 1 wt.% PVA shows the more intense SERS signal and as observed before, it shows also the highest Ag NPs absorption level.

4.4.4 Nanocomposite films by drop casting deposition

Films are deposited from et-OH solutions at different PVA percentages after both Ag ablation only and Ag and C ablation. Drop casting technique is used and films are deposited on Si substrate. Their SERS signals are then acquired in time to verify stabilization of polyynes. Hereafter, in fig. 4.23, SERS spectra are shown. All spectra are normalized on PVA peak around 2900 cm^{-1}. Only film deposited from 1wt.% PVA solutions are studied in time. In fig. 4.23a SERS spectra are reported referred to film from Ag target ablation while on fig. 4.23b film from double ablation is studied. Reference lines at 1850 and 2200 cm^{-1} are given to limit polyynic region. In both pictures, band at 1800 cm^{-1} is detected. This peak was not visible in SERS acquisition of solutions with PVA. Conversely, it appears more pronounced in the case of films obtained after the ablation of only Ag target.

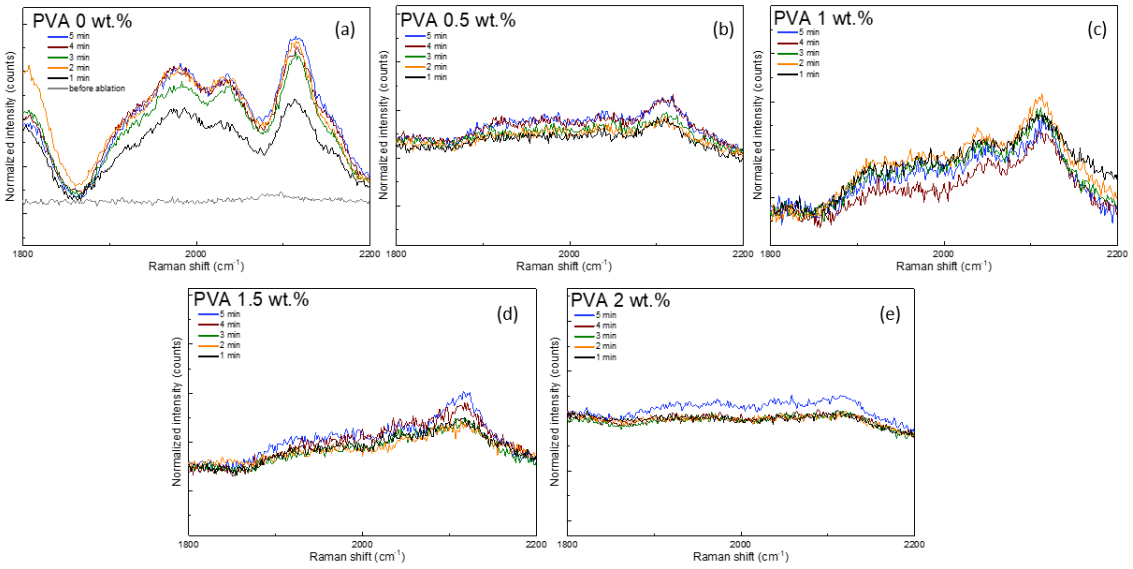

Figure 4.22: *SERS spectra acquired every five minutes after ablation of Ag and C target in et-OH solutions with increasing PVA content.*

It is observed that after Ag target ablation only, polyynes signal is not well defined up to 2 weeks while it becomes stronger after 3 weeks and then remains stable up to 7 weeks. Probably, being the analysis performed on randoms spots, the first acquisitions in time were performed in non optima locations while, the lasts has caught better spots. Film deposited after double ablation shows a polyynic signal more defined and more stable in time, as seen for me-OH solutions.

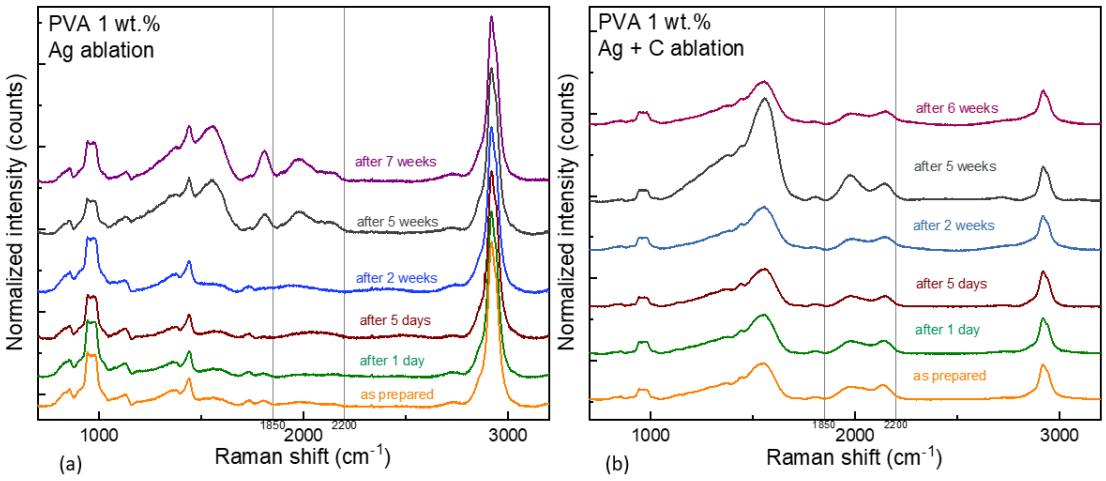

Figure 4.23: *Evolution in time of SERS spectra of 1 wt.% PVA films deposited by drop casting technique after (a) Ag ablation and (b) Ag + C ablation in et-OH solution.*

4.5 Comparison of polymeric solutions

The data acquired from the different systems are many and of difficult interpretation. A general comparison between the systems is desirable but hindered by variation of lot of parameters from one system to the other. In the following section schematic

summary is made in order to shed light on possible connection between detection of polyynic SERS signal and systems parameters.

4.5.1 Evaluation of parameters changing between systems

A list of all the varying parameters is made hereafter and then a schematic table, reported in fig. 4.24, is filled to summarize and make data more clear.

These are the parameters changing in the different polymeric solutions:

Carbon content. Different amount of carbon for polyynes production is available according to organic solvent involved and its volume fraction, content of PVA and target ablated. Anyway the analyses performed in this work are not focused on quantitative production of polyynes but only on their SERS detection that could be affected by several factors, not dealing with concentration of polyynes. Indeed in systems with higher C content SERS signal is not visible.

Water content, calculated as volume fraction. It confers stability to Ag NPs even if it emerges that better Ag NPs absorption does not necessarily implies better polyynic SERS signal.

Viscosity. It is calculated for systems at 0 wt.% PVA. Determination of viscosity for solutions with polymer content requires experimental parameters [60]. To simplify the matter, viscosity values are given for system without polymer, considering that for PVA increase, density will increase. The behaviour followed by the three different systems seems not to be connected with viscosity. Observing the table in fig. 4.24, it is noted that ACN systems show always a good polyynic signal even with increase of viscosity, me-OH systems see disappearance of polyynic signal when viscosity is increased while et-OH shows a light improvement in polyynes detection with increase of viscosity but with values significantly higher with respect to the other systems. Hence, it is not possible to define a limit to viscosity values above or under which polyynes detection is guaranteed.

Compatibility with Ag NPs. According to the organic solvent involved, a different behaviour in Ag NPs absorption peak has been observed. It is highlighted that me-OH and et-OH show higher compatibility with Ag NPs but, ACN systems are the best in terms of SERS polyynes detection. Even this parameter seems to be not determining in order to define the overall behaviour.

Polyynes production. Even if in this work no information about polyynes concentration is detected, it is known, from Peggiani's work [69], that organic solvents have different rate of polyynes production. Among the ones employed in this work ACN shows the best yield of polyynes production followed by et-OH and me-OH.

Polarity. The three different solvents have a different polarity: ACN shows the lowest polarity, it increases then for et-OH and me-OH. PVA is also a polar molecule and its structure has an alcohol group, similar to et-OH and me-OH. It was highlighted that production of polyynes, non polar structures,

was higher for non polar solvent and then decrease by increasing polarity. Once PVA is added to solution, polarity is increased. Hence, polarity issues can be also responsibles of difficult SERS signal detection.

	Ag NPs comp	Polyynes prod	H_2O (%vol.)	Visc (mPa·s)	PVA (wt.%) 0		0.5		1		1.5		2	
					Ag	Ag+C	Ag	Ag+C	Ag	Ag+C	Ag	Ag+C	Ag	Ag+C
ACN	B	VG	58	0.794	●		●		●		●		●	
Me-OH	VG	G-	25	0.735	●	●	●	●	●	●	●	●	●	●
Et-OH	G	G+	50	1.035	●	●	●	●	●	●	●	●	●	●

Figure 4.24: *Summarizing properties for the three different organic solvent systems. Ag NPs compatibility is given in terms of B=bad, VG=very good, G=good affinity with solvent; polyynes production performances are given according to the work of Peggiani et al. [69]; colored dots indicates quality of polyynes SERS signal detected, green for good, yellow for discrete and red for bad/none.*

4.5.2 Equalization of water content and comparison

In order to perform a better comparison between the three different systems, equalization of water content is performed. Me-OH and et-OH volume fractions are reduced to 42 %vol. in order to be equal to ACN volume. This means that for me-OH solutions a decrease of 33%vol. of organic solvent is happening while for et-OH only 8%vol. These tests are conducted on solutions with 0 and 1 wt.% PVA. The synthesis and characterization methods are the same followed in the previous ablations. Ablation are performed both on Ag target only and Ag followed by C target. In fig. 4.25 parameters for the new systems are summarized and performances in terms of SERS signal detected are given by colored spots assignment.

	Ag NPs comp	Polyynes prod	H_2O (%vol.)	Visc (mPa·s)	PVA (wt.%) 0		1	
					Ag	Ag+C	Ag	Ag+C
ACN	B	VG	58	0.794	●		●	
Me-OH	VG	G-	58	0.799	●	●	●	●
Et-OH	G	G+	58	1.050	●	●	●	●

Figure 4.25: *Summarizing properties for the three different organic solvent with equalized water content. Ag NPs compatibility is given in terms of B=bad, VG=very good, G=good affinity with solvent; polyynes production performances are given according to the work of Peggiani et al. [69]; colored dots indicates quality of polyynes SERS signal detected, green for good, yellow for discrete and red for bad/none.*

For et-OH solutions no big differences are detected. UV-Vis absorption spectra of Ag NPs show a slight increase on absorption values as expected due to higher content of water that stabilizes metal nanoparticles. In terms of SERS signals no differences are registered when PVA is in solution and when only Ag is ablated; while, for double ablation without PVA, a net increase of SERS polyynic signal is detected. Moreover increase and decrease of signal is visualized. It seems that variation in water content has caused a variation in dynamic of signal evolution.

For me-OH solutions, the increase of water content is remarkable. In UV-Vis spectra, higher values of absorbance are registered. SERS signals, on the other hand, are not improved as expected. For ablations with PVA, only a weak sp SERS signal is detected after double ablation, not present at lower content of water, as seen in fig. 4.16c; while, as seen for et-OH, after double ablation without polymer, a net increase of sp SERS signal is detected and its variation in time is faster. Indeed both increase and decrease are observed.

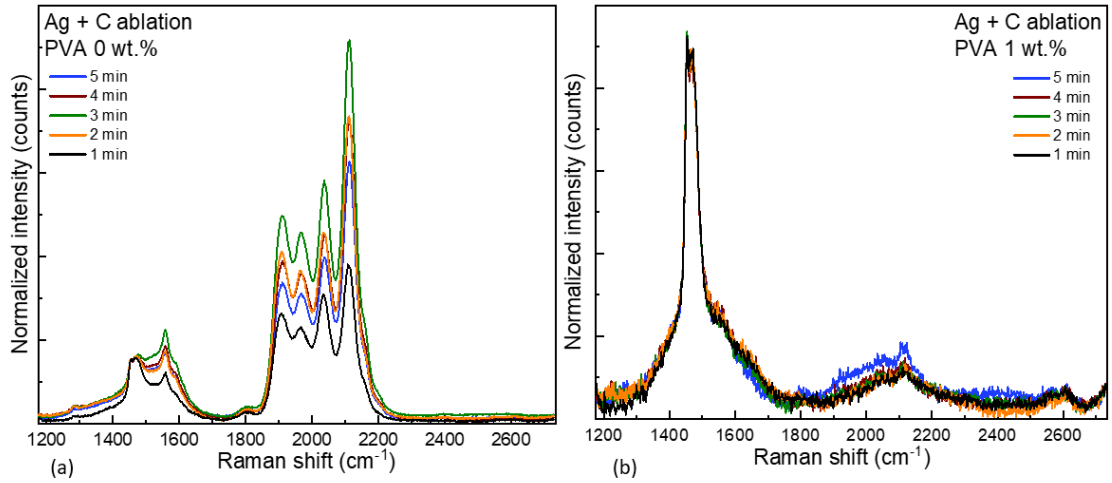

Figure 4.26: *SERS spectra after Ag and C ablation in me-OH solutions with increased water content and (a) without PVA and with (b) PVA content.*

In fig.4.26, SERS spectra acquired after double ablation (a) without and (b) with PVA are reported. All signals are normalized on me-OH CH_3 bending peak around 1450 cm^{-1}. These spectra highlight how the addition of polymer decrees high variation in polyynic SERS signal: heavy decrease is registered together with broadening of the peaks that appear as a whole band when PVA is present. This is the same change observed between SERS signal in solutions and in films. A variation is detected also in sp^2 region, around 1550 cm^{-1}. Without polymer an increase of signal is recorded while with polymer it disappears.

As last comparison, UV-Vis and SERS spectra of the three different systems are plotted together, as shown in fig. 4.27. SERS signals acquired after 5 minutes of rest post Ag ablation are plotted, in fig. 4.27a for 0 wt.% PVA and in fig. 4.27b for 1 wt.% PVA. In the insets, relative UV-Vis absorption spectra are plotted. It is interesting to notice that ACN solutions that show the worst behaviour in terms of Ag NPs absorption peak, are the only ones showing, in these conditions, SERS polyynic signal. Probably, polarity and yield of polyynes production are more crucial elements for polyynes detection.

4.6 PE_func_Ag configuration

Last part of the work deals with different solutions and a different configuration for polyynes characterization. This has been made because a new method to perform *in*

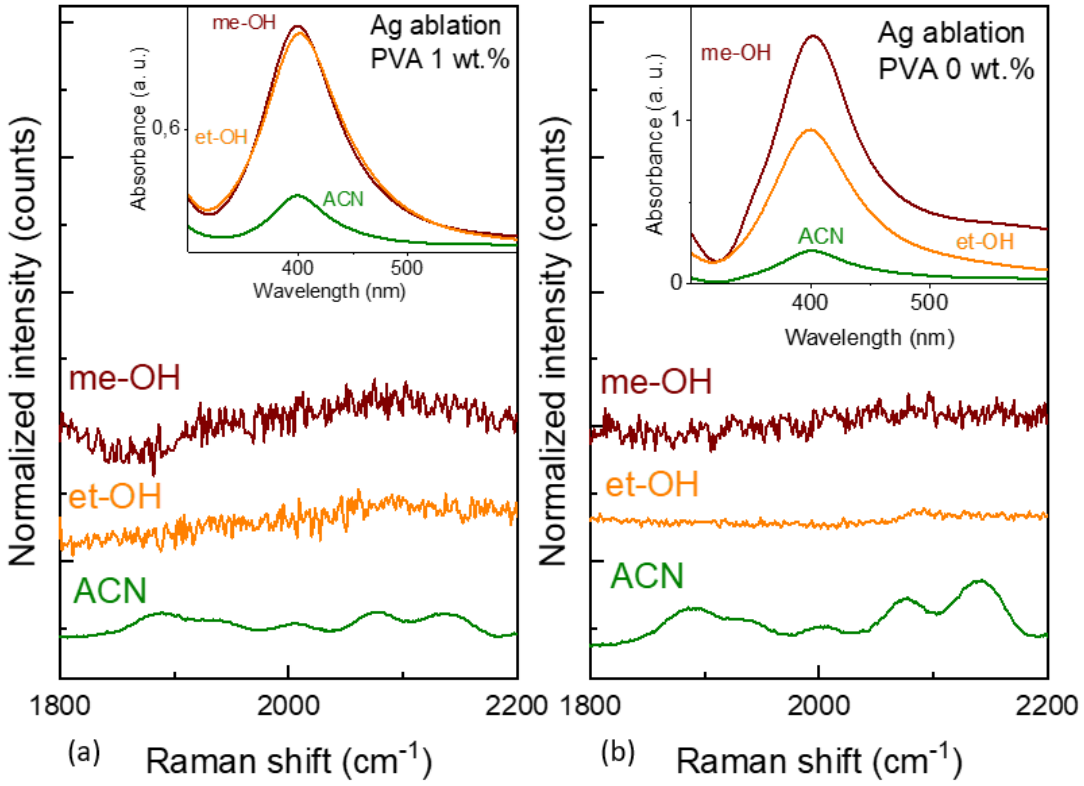

Figure 4.27: *SERS spectra acquired after 5 minutes rest in the different systems after Ag ablation (a) without and (b) with PVA content. In the insets the relative UV-Vis spectra are reported.*

situ SERS analysis has been implemented. Its description has been made in chapter 3 and it is referred to as PE_func_Ag configuration. This new configuration avoids Ag NPs participation to the ablation process. In this way all the issues concerning their fragmentation and mechanical deviation are not present anymore and SERS polyynic signal is indeed detected while ablation laser is on.

Ablations performed with this new configuration deal with PVA/water solutions, with PVA at 0, 0.5, 1, 1.5 and 2 wt.%. Graphite target is ablated and SERS signals acquired while ablation is ongoing. Two ways have been applied to analyze these systems. The first one is a standard ablation of 30 minutes and SERS acquisitions every minute. The second one foresees SERS acquisitions after single laser shots. SERS signal are then acquired while laser is not working. This is done for 200 shots. Hereafter results for both the experiments are discussed.

4.6.1 Standard ablation

First experiment conducted with this new configuration deals with ablation of graphite target in water. Ablation is run for 30 minutes and every minute a SERS spectrum is acquired. Signals detected are plotted in fig. 4.28a and 4.28b.

All the ablations performed with this configuration have been successful in terms of polyynic SERS signal detection. To compare results obtained from ablations in solutions with increasing PVA content, integration of the areas in the polyynic region has been made. A distinction has been made between the two regions: 1800-2000

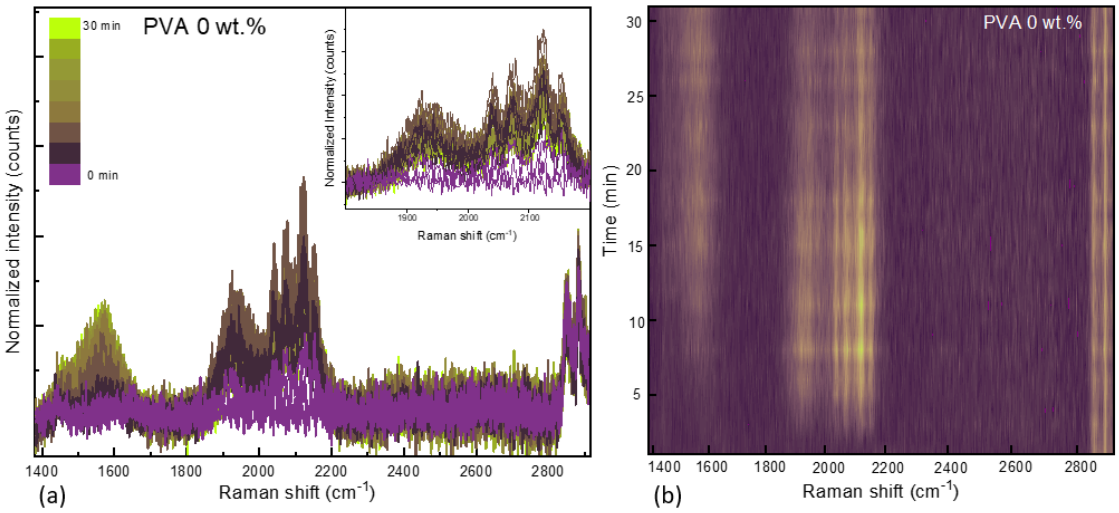

Figure 4.28: *(a) 2D plot for SERS spectra acquired during 30 min ablation of graphite target in water. Cromatographic scale goes from purple to yellow for increasing time. In the inset zoom on polyynic region. (b) 3D plot of the same data seen in (a), cromatographic scale goes from purple to yellow for increasing intensity of the signal. Both set of data are normalized on PE peak around 1880 cm^{-1}.*

and 2000-2200 cm^{-1}. This is done in order to verify if only short polyynes are produced as expected in water, and if PVA addition implies long chains appearance. It is been observed that for every PVA percentage, the trend followed by 1800-2000 and 2000-2200 region areas was the same. This means that only short polyynes are produced and PVA addition does not vary the behaviour.

In order then to compare the different solutions and verify if addition of polymer affects polyynes SERS signal evolution, the trends followed by the areas in the 2000-2200 cm^{-1} region vs time are plotted. The curves are shown in fig. 4.29. Considerations made by observation of these data are that with increasing content of PVA, a slower variation of SERS signal is detected. With 0 wt.% PVA faster growth and then decrease of signal is observed; for increasing content of PVA a slower growth is detected and for 1.5 and 2 wt.% decrease of signal is not visible anymore in the investigated time interval. It is then assumed that polymer is hindering attachment of polyynes on the PE pellet. This can be due to higher solution viscosity that hinders polyynes mobility in solutions as well as attachment of the polymer itself on PE pellet. All the considerations here made concern efficiency of polyynes detection. No consideration can be made on their production rate and concentration. Other analyses should be done to verify active role of polymer in this sense.

4.6.2 Shots ablation

Shots ablations are performed on PVA/water solutions with PVA at 0 and 0.5 wt.%. Laser parameters are the same already seen in all the previous tests. SERS acquisitions are made after every shots, for a total of 200 acquisitions. Ideally this test wants to analyze what is happening in the first period of ablation. Being laser frequency at 10 Hz, the first 200 shots will represent the first 20 second of ablation. Actually there is a resting time after each shot, while SERS acquisition is performed, so diffusion phenomena can happen; furthermore discontinuity of laser

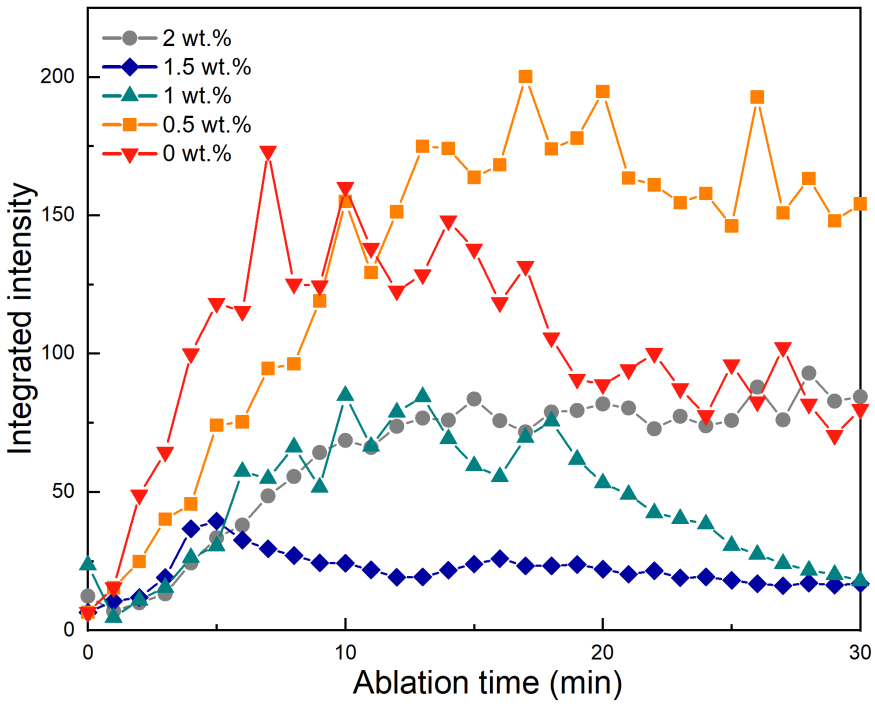

Figure 4.29: *Trend of integrated areas in the 2000-2200 cm^{-1} region for ablations in water at different PVA percentages.*

action implies less degradation phenomena and less thermalization. All this elements help in understanding why results obtained through this experiment seem to be in disagreement with what has been described for standard ablation.

In fig. 4.30a and 4.30b, 3D plots are reported for SERS signals acquired during shots ablation for the solutions with and without PVA. Data are plotted in a number of shots vs. wavelength 2D plot and intensities of signals are given by the cromatographic scale that goes from purple to yellow with intensity increase. All the spectra are normalized on PE peak located around 2880 cm^{-1}. It is noted that with PVA in solution polyynic signal appears sooner and it is more intense.

Observations made on 3D plot are confirmed when areas in polyynic region are integrated; in fig. 4.31 the trend of integrated areas in the two polyynic regions, 1800-2000 and 2000-2200 cm^{-1}, are plotted. It is clear that polyynic signal grows faster when PVA is present. This seems in disagreement with what has been described previously but this can be credited to the different configuration of ablation present when shot test is run. Moreover it is clear once again that the growth in the two regions is the same, meaning that only short chains are detected. PVA even in this experiment seems not to be involved in polyynes production or at lest, it do not provide formation of long chains. In order to confirm a faster growth and more intense polyynic signal when polymer is added to the system, more data are needed with increasing content of PVA.

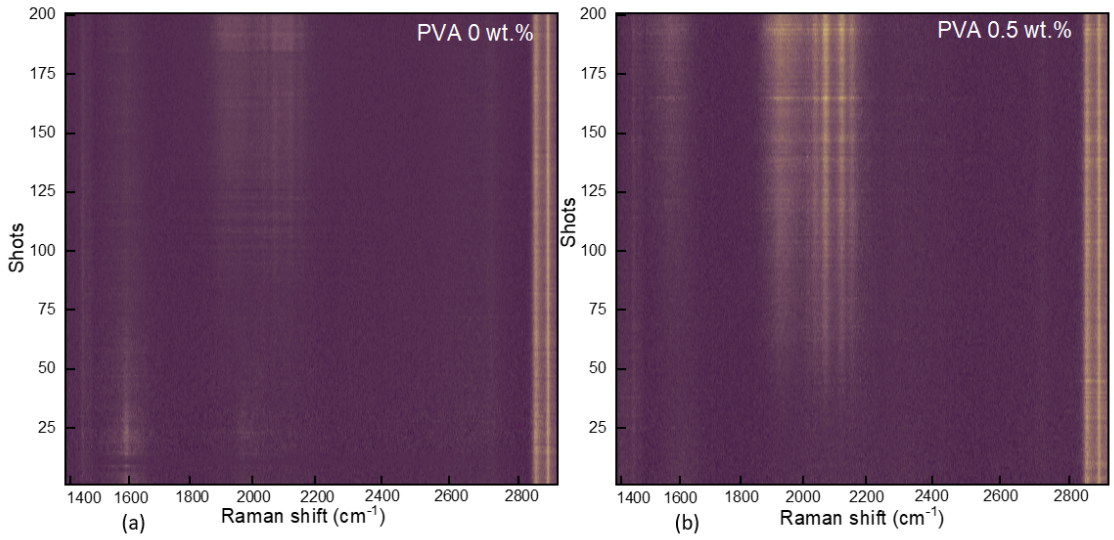

Figure 4.30: *3D plots of SERS signals acquired during shots ablations in (a) water and (b) water/PVA 0.5 wt.%. Cromatographic scale goes form purple to yellow with increasing intensity of signal. All spectra are normalized on PE peak at 2880 cm^{-1}.*

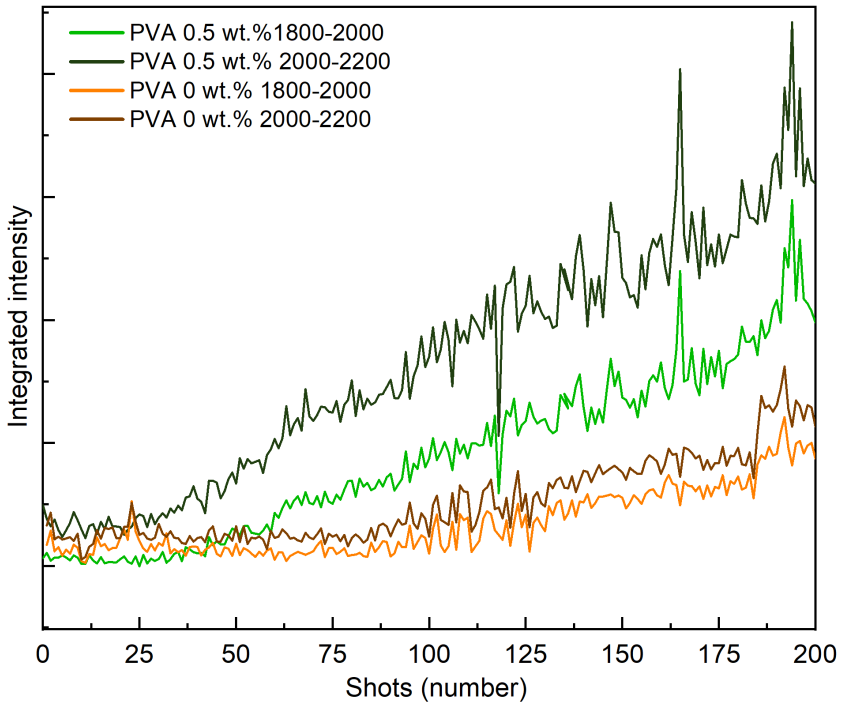

Figure 4.31: *Trend of integrated areas in the 1800-2000 and 2000-2200 cm^{-1} Raman regions for 200 shots on graphite target in water and water/PVA 0.5 wt.%.*

Conclusions and perspectives

The purposes of this experimental project were:

- realization of CAWs-polymer nanocomposite material to stabilize carbon linear chains in time;
- development of a single step production process where, by ablation of a metal target in a polymeric solution, both Ag NPs and polyynes are produced directly in a polymer matrix;
- implementation of an *in situ* SERS analysis to study polyynes signal evolution in time while ablation process is ongoing;
- understanding polymer role during polyynes production.

Realization of nanocomposites films has been fulfilled and, no matter the composition of the polymeric solution involved, CAWs are detected in the deposited film by SERS analysis. Single step PLAL of a metal target in polymeric solutions has demonstrated to be a valid technique for CAWs production even if carbon source is given by the polymeric solution only. Moreover, the initial steps of optimization of laser parameters result to be effective in obtaining SERS active Ag NPs in the deposited films. If the single step process results to be effective to obtain the final nanocomposite materials, it is not the best process to perform *in situ* SERS analysis. Indeed, the presence of Ag NPs in the ablation liquid does not allow to acquire SERS signal of polyynes while the production process is ongoing. This is ascribed to modification of NPs by laser action and hindrance of Ag NPs-polyynes interaction. On light of this, data are available only after production process. Analysis of these data highlighted that PVA seems to hinder SERS effect; whenever it is present, a decrease/ disappearance of polyynes SERS signal is detected. It is assumed that PVA affects Ag NPs-polyynes interaction by shielding and surrounding the nanostructures just formed. Information by an active role of polymer to polyynes formation has not been demonstrated for PVA/organic solvent systems. Quantitative analyses should be performed to understand if, varying PVA content, polyynes concentration is varied as well. A general comparison between the different PVA/organic solvents systems is then performed, even if very challenging since the amount of varying parameters. The main observation is that having better Ag NPs does not imply better SERS effect. Other elements seem to be predominant indeed, when dealing with polyynes SERS signal: polarity of the materials involved, polyynes production rate of the solvents, viscosity of solutions are all considered. Proper choice of materials result once again to be a fundamental step. Turning point to the research is given by the implementation of a new *in situ* SERS configuration via a polymer pellet functionalized with Ag NPs (PE_func_Ag pellet); making Ag NPs external to the liquid

ablation allows to detect polyynes SERS signal, realizing a real *in situ* technique. Ablations with this particular configuration are performed in PVA/water solutions. Organic solvents are not present anymore. The results obtained thanks to this analysis highlight that increasing PVA, evolution of SERS signal is slow down; this is assumed to be caused by reduced mobility of polyynes in more viscous solutions. On the other hand, PVA presence does not imply formation of long carbon chain: only short chains are produced in water and this does not change when PVA is added. Further steps should be made in order to understand if polymer is playing an active role into polyynes formation, by implementing a quantitative analysis technique. Quantitative analysis can be made by UV-Vis absorption technique or combining HPLC/UV-Vis method to have information on size selected polyynes concentration; however these methods are not applicable to polymer solutions due to incompatibility of HPLC columns-polymer and since the polymer absorption is covering the polyynic region in UV-Vis range. Other techniques are then to be investigated in order to obtain these information. These analyses can be useful into understanding if it is worthy to perform single step production process. Further studies on films are also needed: till now the majority of studies on CAWs-polymeric films was focused on assessing polyynes stabilization; however properties of these new materials are still to be investigated and this is certainly a limitation towards real applications. Mechanical and transport properties have been modeled and they seem to be very promising but there is still lack of experimental tests. It could be interesting to perform mechanical tests on nanocomposites films to see if the theoretical values are satisfied and polymer mechanical performances are improved. The same can be done for transport properties in order to develop conducting nanocomposites or increase conductivity of already conducting polymers such as PEDOT. Alignment of wires in the films could be also an interesting aspect to explore, developing a method to realize the alignment and analyzing then if and how performances are improved by aligned nanostructures in a matrix. The idea is then to focus on characterization of the nanocomposite materials and not only on process optimization in order to implement real devices and test-on-field their properties.

Bibliography

[1] N. R. Agarwal et al. "Structure and chain polarization of long polyynes investigated with infrared and Raman spectroscopy". In: *Journal of Raman Spectroscopy* 44.10 (2013), pp. 1398–1410. DOI: https://doi.org/10.1002/jrs.4300. eprint: https://analyticalsciencejournals.onlinelibrary.wiley.com/doi/pdf/10.1002/jrs.4300. URL: https://analyticalsciencejournals.onlinelibrary.wiley.com/doi/abs/10.1002/jrs.4300.

[2] Vincenzo Amendola and Moreno Meneghetti. "What controls the composition and the structure of nanomaterials generated by laser ablation in liquid solution?" In: *Physical chemistry chemical physics : PCCP* 15 (Nov. 2012). DOI: 10.1039/c2cp42895d.

[3] Kang An et al. "Stability improvement of C8H2 and C10H2 embedded in poly(vinyl alcohol) films with adsorption on gold nanoparticles". In: *Chemical Physics Letters* 637 (Aug. 2015). DOI: 10.1016/j.cplett.2015.07.051.

[4] Kadir Aslan, Joseph R. Lakowicz, and Chris D. Geddes. "Rapid Deposition of Triangular Silver Nanoplates on Planar Surfaces: Application to Metal-Enhanced Fluorescence". In: *The Journal of Physical Chemistry B* 109.13 (2005). PMID: 16851692, pp. 6247–6251. DOI: 10.1021/jp044235z. eprint: https://doi.org/10.1021/jp044235z. URL: https://doi.org/10.1021/jp044235z.

[5] F. Banhart. "Chains of carbon atoms: A vision or a new nanomaterial?" In: *Beilstein Journal of Nanotechnology* 6 (2015), pp. 559–569.

[6] Laurent Berthe et al. "Wavelength dependent of laser shock-wave generation in the water-confinement regime". In: *Journal of Applied Physics* 85 (June 1999), pp. 7552–7555. DOI: 10.1063/1.370553.

[7] C. S. Casari et al. "Stabilization of linear carbon structures in a solid Ag nanoparticle assembly". In: *Applied Physics Letters* 90.1 (2007), p. 013111. DOI: 10.1063/1.2430676. eprint: https://doi.org/10.1063/1.2430676. URL: https://doi.org/10.1063/1.2430676.

[8] Carlo Casari et al. "Carbon-atom wires: 1-D systems with tunable properties". In: *Nanoscale* 8 (Nov. 2015). DOI: 10.1039/C5NR06175J.

[9] A. H. Castro Neto et al. "The electronic properties of graphene". In: *Rev. Mod. Phys.* 81 (1 Jan. 2009), pp. 109–162. DOI: 10.1103/RevModPhys.81.109. URL: https://link.aps.org/doi/10.1103/RevModPhys.81.109.

[10] Franco Cataldo. "Simple generation and detection of polyynes in an arc discharge between graphite electrodes submerged in various solvents". In: *Carbon* 41 (Dec. 2003), pp. 2671–2674. DOI: 10.1016/S0008-6223(03)00345-2.

[11] Franco Cataldo et al. “Simple Synthesis of ,-Diarylpolyynes Part 1: Diphenylpolyynes”. In: *Journal of Macromolecular Science, Part A* 47.8 (2010), pp. 739–746. DOI: 10.1080/10601325.2010.491749. eprint: https://doi.org/10.1080/10601325.2010.491749. URL: https://doi.org/10.1080/10601325.2010.491749.

[12] Tykwinski RR Chalifoux WA. “Synthesis of polyynes to model the sp-carbon allotrope carbyne”. In: *Nat Chem* 2.11 (2010), pp. 967–71.

[13] Viacheslav Danilenko. “On the history of the discovery of nanodiamond synthesis”. In: *Physics of the Solid State* 46 (Apr. 2004), pp. 595–599. DOI: 10.1134/1.1711431.

[14] B. L. Dasari et al. “Graphene and derivatives ? Synthesis techniques, properties and their energy applications”. In: *Energy* 140.1 (Dec. 2017). © 2017. This manuscript version is made available under the CC-BY-NC-ND 4.0 license http://creativecommons.org/licenses/by-nc-nd/4.0/, pp. 766–778. DOI: 10.1016/j.energy.2017.08.048. URL: https://openaccess.city.ac.uk/id/eprint/18333/.

[15] M.S. Dresselhaus, G. Dresselhaus, and P.C. Eklund. “Chapter 19 - C60-Related Tubules and Spherules”. In: *Science of Fullerenes and Carbon Nanotubes*. Ed. by M.S. Dresselhaus, G. Dresselhaus, and P.C. Eklund. San Diego: Academic Press, 1996, pp. 756–869. ISBN: 978-0-12-221820-0. DOI: https://doi.org/10.1016/B978-012221820-0/50019-8. URL: https://www.sciencedirect.com/science/article/pii/B9780122218200500198.

[16] Khaled A. Elsayed et al. “Effect of focusing conditions and laser parameters on the fabrication of gold nanoparticles via laser ablation in liquid”. In: *Optics Laser Technology* 45 (2013), pp. 495–502. ISSN: 0030-3992. DOI: https://doi.org/10.1016/j.optlastec.2012.06.004. URL: https://www.sciencedirect.com/science/article/pii/S0030399212002721.

[17] F. J. Baltá-Calleja G. H. Michler. *Mechanical Properties of Polymers based on Nanostructure and Morphology*. 2005.

[18] Rupali Gangopadhyay and Amitabha De. “Conducting Polymer Nanocomposites: A Brief Overview”. In: *Chemistry of Materials* 12.3 (2000), pp. 608–622. DOI: 10.1021/cm990537f. eprint: https://doi.org/10.1021/cm990537f. URL: https://doi.org/10.1021/cm990537f.

[19] Guanghua Gao, Tahir Çagin, and William A Goddard. “Energetics, structure, mechanical and vibrational properties of single-walled carbon nanotubes”. In: *Nanotechnology* 9.3 (Sept. 1998), pp. 184–191. DOI: 10.1088/0957-4484/9/3/007. URL: https://doi.org/10.1088/0957-4484/9/3/007.

[20] A. Geim and K.S. Novoselov. “The Rise of Graphene”. In: *Nature materials* 6 (Apr. 2007), pp. 183–91. DOI: 10.1038/nmat1849.

[21] A. El Goresy and G. Donnay. “A New Allotropic Form of Carbon from the Ries Crater”. In: *Science* 161.3839 (1968), pp. 363–364. ISSN: 0036-8075. DOI: 10.1126/science.161.3839.363. eprint: https://science.sciencemag.org/content/161/3839/363.full.pdf. URL: https://science.sciencemag.org/content/161/3839/363.

[22] Kotaro Hanada. “Detonation nanodiamond: Perspective and Applications”. In: *Surface Engineering* 25.7 (2009), pp. 487–489. DOI: 10.1179/174329409X433939. eprint: https://doi.org/10.1179/174329409X433939. URL: https://doi.org/10.1179/174329409X433939.

[23] Y Herbani et al. “Pulse laser ablation of Au, Ag, and Cu metal targets in liquid for nanoparticle production”. In: *Journal of Physics: Conference Series* 985 (Mar. 2018), p. 012005. DOI: 10.1088/1742-6596/985/1/012005. URL: https://doi.org/10.1088/1742-6596/985/1/012005.

[24] J. Hone et al. “Thermal conductivity of single-walled carbon nanotubes”. In: *Phys. Rev. B* 59 (4 Jan. 1999), R2514–R2516. DOI: 10.1103/PhysRevB.59.R2514. URL: https://link.aps.org/doi/10.1103/PhysRevB.59.R2514.

[25] A. Hu et al. “Spectroscopic characterization of carbon chains in nanostructured tetrahedral carbon films synthesized by femtosecond pulsed laser deposition”. In: *The Journal of Chemical Physics* 126.15 (2007), p. 154705. DOI: 10.1063/1.2727450. eprint: https://doi.org/10.1063/1.2727450. URL: https://doi.org/10.1063/1.2727450.

[26] Khalid Saeed Ibrahim. “Carbon Nanotubes-Properties and Applications: A Review.” In: *Carbon Letters 14* 3 (July 2013), pp. 131–44. DOI: doi:10.5714/CL.2013.14.3.131.

[27] Sumio Iijima. “Helical microtubules of graphitic carbon”. In: *Nature* 354 (Nov. 1991), pp. 56–58. DOI: 10.1038/354056a0.

[28] Francesco Innocenti, Alberto Milani, and Chiara Castiglioni. “Can Raman spectroscopy detect cumulenic structures of linear carbon chains?” In: *Journal of Raman Spectroscopy* 41.2 (2010), pp. 226–236. DOI: https://doi.org/10.1002/jrs.2413. eprint: https://analyticalsciencejournals.onlinelibrary.wiley.com/doi/pdf/10.1002/jrs.2413. URL: https://analyticalsciencejournals.onlinelibrary.wiley.com/doi/abs/10.1002/jrs.2413.

[29] Johanna Januszewski and Rik Tykwinski. “Synthesis and properties of long [n] cumulenes (n ¿= 5)”. In: *Chemical Society reviews* 43 (Mar. 2014). DOI: 10.1039/c4cs00022f.

[30] Johanna A. Januszewski et al. “Synthesis and Structure of Tetraarylcumulenes: Characterization of Bond-Length Alternation versus Molecule Length”. In: *Angewandte Chemie International Edition* 52.6 (2013), pp. 1817–1821. DOI: https://doi.org/10.1002/anie.201208058. eprint: https://onlinelibrary.wiley.com/doi/pdf/10.1002/anie.201208058. URL: https://onlinelibrary.wiley.com/doi/abs/10.1002/anie.201208058.

[31] Martyn Jevric and Mogens Brøndsted Nielsen. “Synthetic Strategies for Oligoynes”. In: *Asian Journal of Organic Chemistry* 4.4 (2015), pp. 286–295. DOI: https://doi.org/10.1002/ajoc.201402261. eprint: https://onlinelibrary.wiley.com/doi/pdf/10.1002/ajoc.201402261. URL: https://onlinelibrary.wiley.com/doi/abs/10.1002/ajoc.201402261.

[32] Chuanhong Jin et al. “Deriving Carbon Atomic Chains from Graphene”. In: *Phys. Rev. Lett.* 102 (20 May 2009), p. 205501. DOI: 10.1103/PhysRevLett.102.205501. URL: https://link.aps.org/doi/10.1103/PhysRevLett.102.205501.

[33] Maria Kalyva et al. “Tuning of the characteristics of Au nanoparticles produced by solid target laser ablation into water by changing the irradiation parameters”. In: *Microscopy Research and Technique* 73.10 (2010), pp. 937–943. DOI: https://doi.org/10.1002/jemt.20868. eprint: https://analyticalsciencejournals.onlinelibrary.wiley.com/doi/pdf/10.1002/jemt.20868. URL: https://analyticalsciencejournals.onlinelibrary.wiley.com/doi/abs/10.1002/jemt.20868.

[34] Rajwant Kaur. “Carbon Nanotubes: A Review Article”. In: *International Journal for Research in Applied Science and Engineering Technology* 6 (Apr. 2018), pp. 5075–5079. DOI: 10.22214/ijraset.2018.4827.

[35] Ayesha Kausar. “Polymer/carbon-based quantum dot nanocomposite: forthcoming materials for technical application”. In: *Journal of Macromolecular Science, Part A* 56.4 (2019), pp. 341–356. DOI: 10.1080/10601325.2019.1578614. eprint: https://doi.org/10.1080/10601325.2019.1578614. URL: https://doi.org/10.1080/10601325.2019.1578614.

[36] Hyoung Seop Kim. “On the rule of mixtures for the hardness of particle reinforced composites”. In: *Materials Science and Engineering: A* 289.1 (2000), pp. 30–33. ISSN: 0921-5093. DOI: https://doi.org/10.1016/S0921-5093(00)00909-6. URL: https://www.sciencedirect.com/science/article/pii/S0921509300009096.

[37] Hyoung Seop Kim, Sun Ig Hong, and Sun Jae Kim. “On the rule of mixtures for predicting the mechanical properties of composites with homogeneously distributed soft and hard particles”. In: *Journal of Materials Processing Technology* 112.1 (2001), pp. 109–113. ISSN: 0924-0136. DOI: https://doi.org/10.1016/S0924-0136(01)00565-9. URL: https://www.sciencedirect.com/science/article/pii/S0924013601005659.

[38] Sanghee Kim. “Synthesis and Structural Analysis of One-Dimensional sp-Hybridized Carbon Chain Molecules”. In: *Angewandte Chemie International Edition* 48.42 (2009), pp. 7740–7743. DOI: https://doi.org/10.1002/anie.200904145. eprint: https://onlinelibrary.wiley.com/doi/pdf/10.1002/anie.200904145. URL: https://onlinelibrary.wiley.com/doi/abs/10.1002/anie.200904145.

[39] Hemant Pandey Kiran Pulidindi. “Polymer Nanocomposites Market Size By Polymer (Epoxy Resin, Polyamide, Polyethylene, Polypropylene), By Nanomaterials (Nanoclays, Carbon Nanotubes, Nanofibers, Nano-oxides), By End-user Industry (Automotive Aerospace, Electrical Electronics, Packaging, Biomedical, Paints Coatings), Industry Analysis Report, Regional Outlook, Growth Potential, Price Trends, Competitive Market Share Forecast, 2019 – 2025”. In: (2019).

[40] H. W. Kroto, A. W. Allaf, and S. P. Balm. “C60: Buckminsterfullerene”. In: *Chemical Reviews* 91.6 (1991), pp. 1213–1235. DOI: 10.1021/cr00006a005. eprint: https://doi.org/10.1021/cr00006a005. URL: https://doi.org/10.1021/cr00006a005.

[41] Yu. P. Kudryavtsev, R. Heimann, and S. Evsyukov. “Carbynes: Advances in the field of linear carbon chain compounds”. In: *Journal of Materials Science* 31 (1996), pp. 5557–5571.

[42] B. Kumanek and Dawid Janas. “Thermal conductivity of carbon nanotube networks: a review”. In: *Journal of Materials Science* 54 (2019), pp. 7397–7427.

[43] Changgu Lee et al. “Measurement of the Elastic Properties and Intrinsic Strength of Monolayer Graphene”. In: *Science* 321.5887 (2008), pp. 385–388. ISSN: 0036-8075. DOI: 10.1126/science.1157996. eprint: https://science.sciencemag.org/content/321/5887/385.full.pdf. URL: https://science.sciencemag.org/content/321/5887/385.

[44] P. C. Lee and D. Meisel. “Adsorption and surface-enhanced Raman of dyes on silver and gold sols”. In: *The Journal of Physical Chemistry* 86.17 (1982), pp. 3391–3395. DOI: 10.1021/j100214a025. eprint: https://doi.org/10.1021/j100214a025. URL: https://doi.org/10.1021/j100214a025.

[45] Xin Jiat Lee et al. “Review on graphene and its derivatives: Synthesis methods and potential industrial implementation”. In: *Journal of the Taiwan Institute of Chemical Engineers* 98 (2019). Microreactor: Fundamentals and Applications in Chemical Engineering, pp. 163–180. ISSN: 1876-1070. DOI: https://doi.org/10.1016/j.jtice.2018.10.028. URL: https://www.sciencedirect.com/science/article/pii/S1876107018306060.

[46] Mingjie Liu et al. “Carbyne from First Principles: Chain of C Atoms, a Nanorod or a Nanorope”. In: *ACS Nano* 7.11 (2013). PMID: 24093753, pp. 10075–10082. DOI: 10.1021/nn404177r. eprint: https://doi.org/10.1021/nn404177r. URL: https://doi.org/10.1021/nn404177r.

[47] Tao Liu and Alessandro Troisi. “What Makes Fullerene Acceptors Special as Electron Acceptors in Organic Solar Cells and How to Replace Them”. In: *Advanced Materials* 25.7 (2013), pp. 1038–1041. DOI: https://doi.org/10.1002/adma.201203486. eprint: https://onlinelibrary.wiley.com/doi/pdf/10.1002/adma.201203486. URL: https://onlinelibrary.wiley.com/doi/abs/10.1002/adma.201203486.

[48] Andrea Lucotti, Michele Casella, and Matteo Tommasini. “Surface-Enhanced Multipurpose Nanosensing with Microneedle-Shaped Fiber Optics”. In: Oct. 2015, pp. 283–305. ISBN: 978-981-4613-32-3. DOI: 10.1201/b19175-9.

[49] Peng-Cheng Ma et al. “Dispersion and functionalization of carbon nanotubes for polymer-based nanocomposites: A review”. In: *Composites Part A: Applied Science and Manufacturing* 41.10 (2010), pp. 1345–1367. ISSN: 1359-835X. DOI: https://doi.org/10.1016/j.compositesa.2010.07.003. URL: https://www.sciencedirect.com/science/article/pii/S1359835X10002009.

[50] Kany Mahmood et al. “Light ScatteRing studies of poly(methyl methaerylate) (PMMA) in different solvents”. In: *Journal of the Chemical Society of Pakistan* 27 (Feb. 2005), pp. 1–5.

[51] L. M. Malard et al. “Resonance Raman study of polyynes encapsulated in single-wall carbon nanotubes”. In: *Phys. Rev. B* 76 (23 Dec. 2007), p. 233412. DOI: 10.1103/PhysRevB.76.233412. URL: https://link.aps.org/doi/10.1103/PhysRevB.76.233412.

[52] Ryutaro Matsutani et al. “Preparation of polyynes up to C22H2 by liquid-phase laser ablation and their immobilization into SiO2 gel”. In: *Carbon* 47.7 (2009), pp. 1659–1663. ISSN: 0008-6223. DOI: https://doi.org/10.1016/j.carbon.2009.02.026. URL: https://www.sciencedirect.com/science/article/pii/S0008622309000967.

[53] Ryutaro Matsutani et al. “Wavelength dependence of polyyne preparation by liquid-phase laser ablation using pellet targets.” In: *Chemical communications* 47 20 (2011), pp. 5840–2.

[54] Alberto Milani, Matteo Tommasini, and Giuseppe Zerbi. “Connection among Raman wavenumbers, bond length alternation and energy gap in polyynes”. In: *Journal of Raman Spectroscopy* 40.12 (2009), pp. 1931–1934. DOI: https://doi.org/10.1002/jrs.2342. eprint: https://analyticalsciencejournals.onlinelibrary.wiley.com/doi/pdf/10.1002/jrs.2342. URL: https://analyticalsciencejournals.onlinelibrary.wiley.com/doi/abs/10.1002/jrs.2342.

[55] Alberto Milani, Matteo Tommasini, and Giuseppe Zerbi. “Connection among Raman wavenumbers, bond length alternation and energy gap in polyynes”. In: *Journal of Raman Spectroscopy* 40.12 (2009), pp. 1931–1934. DOI: https://doi.org/10.1002/jrs.2342. eprint: https://analyticalsciencejournals.onlinelibrary.wiley.com/doi/pdf/10.1002/jrs.2342. URL: https://analyticalsciencejournals.onlinelibrary.wiley.com/doi/abs/10.1002/jrs.2342.

[56] Alberto Milani et al. “Carbon nanowires: Phonon and π-electron confinement”. In: *Phys. Rev. B* 74 (15 Oct. 2006), p. 153418. DOI: 10.1103/PhysRevB.74.153418. URL: https://link.aps.org/doi/10.1103/PhysRevB.74.153418.

[57] Alberto Milani et al. “Raman spectroscopy as a tool to investigate the structure and electronic properties of carbon-atom wires”. In: *Beilstein J. Nanotechnol* 6 (Feb. 2015), pp. 480–491. DOI: 10.3762/bjnano.6.49.

[58] Alberto Milani et al. “Structure modulated charge transfer in carbon atomic wires”. In: *Scientific Reports* 9 (Feb. 2019), p. 1648. DOI: 10.1038/s41598-018-38367-9.

[59] A. Mioltello and R. Kelly. “Laser-induced phase explosion: new physical problems when a condensed phase approaches the thermodynamic critical temperature”. In: *Appl Phys* (1999), s67–s673. DOI: 10.1007/s003399900296.

[60] M. Mohsen-Nia and Hamid Modarress. “Viscometric study of aqueous poly(vinyl alcohol) (PVA) solutions as a binder in adhesive formulations”. In: *Journal of Adhesion Science and Technology - J ADHES SCI TECHNOL* 20 (Jan. 2006), pp. 1273–1280. DOI: 10.1163/156856106778456636.

[61] Mohammad Moniruzzaman and Karen I. Winey. "Polymer Nanocomposites Containing Carbon Nanotubes". In: *Macromolecules* 39.16 (2006), pp. 5194–5205. DOI: 10.1021/ma060733p. eprint: https://doi.org/10.1021/ma060733p. URL: https://doi.org/10.1021/ma060733p.

[62] Roey Nadiv et al. "Optimal nanomaterial concentration: harnessing percolation theory to enhance polymer nanocomposite performance". In: *Nanotechnology* 28.30 (July 2017), p. 305701. DOI: 10.1088/1361-6528/aa793e. URL: https://doi.org/10.1088/1361-6528/aa793e.

[63] William Nichols, Takeshi Sasaki, and Naoto Koshizaki. "Laser ablation of a platinum target in water. III. Laser-induced reactions". In: *Journal of Applied Physics* 100 (Dec. 2006), pp. 114913–114913. DOI: 10.1063/1.2390642.

[64] Teri Wang Odom et al. "Structure and Electronic Properties of Carbon Nanotubes". In: *The Journal of Physical Chemistry B* 104.13 (2000), pp. 2794–2809. DOI: 10.1021/jp993592k. eprint: https://doi.org/10.1021/jp993592k. URL: https://doi.org/10.1021/jp993592k.

[65] Shu Okada, Minoru Fujii, and Shinji Hayashi. "Immobilization of polyynes adsorbed on Ag nanoparticle aggregates into poly(vinyl alcohol) films". In: *Carbon* 49.14 (2011), pp. 4704–4709. ISSN: 0008-6223. DOI: https://doi.org/10.1016/j.carbon.2011.06.074. URL: https://www.sciencedirect.com/science/article/pii/S0008622311005215.

[66] Jimoh Oladunni et al. "A comprehensive review on recently developed carbon based nanocomposites for capacitive deionization: From theory to practice". In: *Separation and Purification Technology* 207 (2018), pp. 291–320. ISSN: 1383-5866. DOI: https://doi.org/10.1016/j.seppur.2018.06.046. URL: https://www.sciencedirect.com/science/article/pii/S1383586618309705.

[67] Dimitrios G. Papageorgiou, Ian A. Kinloch, and Robert J. Young. "Mechanical properties of graphene and graphene-based nanocomposites". In: *Progress in Materials Science* 90 (2017), pp. 75–127. ISSN: 0079-6425. DOI: https://doi.org/10.1016/j.pmatsci.2017.07.004. URL: https://www.sciencedirect.com/science/article/pii/S0079642517300968.

[68] Young Eun Park, Seung Keun Shin, and Seung Min Park. In: *Bulletin of the Korean Chemical Society* 34.4 (Apr. 2013), pp. 1039–1042.

[69] Sonia Peggiani et al. "In situ synthesis of polyynes in a polymer matrix via pulsed laser ablation in a liquid". In: *Mater. Adv.* 1 (8 2020), pp. 2729–2736. DOI: 10.1039/D0MA00545B. URL: http://dx.doi.org/10.1039/D0MA00545B.

[70] Sonia Peggiani et al. "Solvent-dependent termination, size and stability in polyynes synthesized via laser ablation in liquids". In: *Phys. Chem. Chem. Phys.* 22 (45 2020), pp. 26312–26321. DOI: 10.1039/D0CP04132G. URL: http://dx.doi.org/10.1039/D0CP04132G.

[71] R. Peierls. *Quantum Theory of Solids*. 2001.

[72] Sala S. "Linear sp carbon chains-polymer nanocomposites by pulsed laser ablation in liquid". In: *Master thesis at Politecnico di Milano* (2020).

[73] R. Sata et al. “UV-polarizing linear polyyne molecules aligned in PVA”. In: *Chinese Journal of Chemical Physics* 32.2 (2019), pp. 175–181. DOI: 10.1063/1674-0068/cjcp1812273. eprint: https://doi.org/10.1063/1674-0068/cjcp1812273. URL: https://doi.org/10.1063/1674-0068/cjcp1812273.

[74] A.G. El-Shamy, W. Attia, and K.M. Abd El-Kader. “The optical and mechanical properties of PVA-Ag nanocomposite films”. In: *Journal of Alloys and Compounds* 590 (2014), pp. 309–312. ISSN: 0925-8388. DOI: https://doi.org/10.1016/j.jallcom.2013.11.203. URL: https://www.sciencedirect.com/science/article/pii/S0925838813029459.

[75] Shiv Shukla. *Polymer Nanocomposites Market by Type (Carbon Nanotubes, Nanoclays, Metal Oxide, Ceramics), Application (Construction, Automotive, Electrical Electronics, Packaging) - Global Opportunity Analysis and Industry Forecast, 2014-2022*. 2016.

[76] Chandan Adhikary Sibananda Sana. “Synthesis And Entrapment of Polyynes Inside Nano-Pores of Anodized Alumina Membrane:A Linear Allotrope of Carbon”. In: *IJSART* 3.9 (2017), pp. 400–406.

[77] Hiroshi Tabata et al. “Raman and surface-enhanced Raman scattering of a series of size-separated polyynes”. In: *Carbon* 44 (Dec. 2006), pp. 3168–3176. DOI: 10.1016/j.carbon.2006.07.004.

[78] Masaharu Tsuji et al. “Formation of hydrogen-capped polyynes by laser ablation of C60 particles suspended in solution”. In: *Carbon* 41.11 (2003), pp. 2141–2148. ISSN: 0008-6223. DOI: https://doi.org/10.1016/S0008-6223(03)00241-0. URL: https://www.sciencedirect.com/science/article/pii/S0008622303002410.

[79] Masaharu Tsuji et al. “Formation of hydrogen-capped polyynes by laser ablation of graphite particles suspended in solution”. English. In: *Chemical Physics Letters* 355.1-2 (Mar. 2002), pp. 101–108. ISSN: 0009-2614. DOI: 10.1016/S0009-2614(02)00192-6.

[80] Masaharu Tsuji et al. “Formation of hydrogen-capped polyynes by laser ablation of graphite particles suspended in solution”. In: *Chemical Physics Letters* 355.1 (2002), pp. 101–108. ISSN: 0009-2614. DOI: https://doi.org/10.1016/S0009-2614(02)00192-6. URL: https://www.sciencedirect.com/science/article/pii/S0009261402001926.

[81] Bozhena Tsyupa. “Synthesis of Silver Nanoparticles via Ablation in Liquid for Surface Enhanced Raman Spectroscopy”. In: *Master thesis at Politecnico di Milano* (2019).

[82] J. Turkevich, P. Stevenson, and J. Hillier. “A study of the nucleation and growth processes in the synthesis of colloidal gold”. In: *Discussions of The Faraday Society* 11 (1951), pp. 55–75.

[83] Hai-dou Wang. “Graphite Solid Lubrication Materials”. In: *Encyclopedia of Tribology*. Ed. by Q. Jane Wang and Yip-Wah Chung. Boston, MA: Springer US, 2013, pp. 1550–1555. ISBN: 978-0-387-92897-5. DOI: 10.1007/978-0-387-92897-5_1261. URL: https://doi.org/10.1007/978-0-387-92897-5_1261.

[84] Xin Wang et al. “In situ polymerization of graphene nanosheets and polyurethane with enhanced mechanical and thermal properties”. In: *J. Mater. Chem.* 21 (12 2011), pp. 4222–4227. DOI: 10.1039/C0JM03710A. URL: http://dx.doi.org/10.1039/C0JM03710A.

[85] Zhen Xu and Chao Gao. “In situ Polymerization Approach to Graphene-Reinforced Nylon-6 Composites”. In: *Macromolecules* 43.16 (2010), pp. 6716–6723. DOI: 10.1021/ma1009337. eprint: https://doi.org/10.1021/ma1009337. URL: https://doi.org/10.1021/ma1009337.

[86] Bal Yadav and Ritesh Kumar. “Structure, properties and applications of fullerene”. In: *International Journal of Nanotechnology and Applications* 1 (Nov. 2008), pp. 15–24.

[87] Shujiang Yang and Miklos Kertesz. “Bond Length Alternation and Energy Band Gap of Polyyne”. In: *The Journal of Physical Chemistry A* 110.31 (2006). PMID: 16884210, pp. 9771–9774. DOI: 10.1021/jp062701+. eprint: https://doi.org/10.1021/jp062701+. URL: https://doi.org/10.1021/jp062701+.

[88] Yasser Zare and Kyong Yop Rhee. “A multistep methodology for calculation of the tensile modulus in polymer/carbon nanotube nanocomposites above the percolation threshold based on the modified rule of mixtures”. In: *RSC Adv.* 8 (54 2018), pp. 30986–30993. DOI: 10.1039/C8RA04992K. URL: http://dx.doi.org/10.1039/C8RA04992K.

[89] Junwei Zhao et al. “Synthesis of polyynes by intense femtosecond laser irradiation of SWCNTs suspended in methanol”. In: *Chemical Physics Letters* 682 (2017), pp. 96–100. ISSN: 0009-2614. DOI: https://doi.org/10.1016/j.cplett.2017.05.063. URL: https://www.sciencedirect.com/science/article/pii/S0009261417305109.

[90] Leonid V. Zhigilei, Zhibin Lin, and Dmitriy S. Ivanov. “Atomistic Modeling of Short Pulse Laser Ablation of Metals: Connections between Melting, Spallation, and Phase Explosion”. In: *The Journal of Physical Chemistry C* 113.27 (2009), pp. 11892–11906. DOI: 10.1021/jp902294m. eprint: https://doi.org/10.1021/jp902294m. URL: https://doi.org/10.1021/jp902294m.